Edit Mátyus

# Universal variational approaches to the quantum nuclear motion problem

Supervisor:
Prof. Dr. Attila G. Császár
Laboratory of Molecular Spectroscopy, Institute of Chemistry
Eötvös University

Chemistry Doctoral School
Head of the doctoral school: Prof. Dr. György Inzelt
Theoretical and Physical Chemistry, Structural Chemistry Doctoral Programme
Head of the doctoral programme: Prof. Dr. Péter Surján

Eötvös University
Budapest, 2009

# Acknowledgments

First of all, I would like to thank my supervisor, Professor Attila G. Császár, for his help and support.

I thank Dr. Gábor Czakó for his help especially during the first half of my doctoral research. Our later scientific discussions were especially valuable too.

I enjoyed the collaboration with Professor Brian T. Sutcliffe. I learned a lot from him especially on different coordinate systems and their transformations.

I thank Jan Šimunek for his work on iterative eigensolver techniques. Dr. Tibor Furtenbacher's initial help on the Lanczos eigensolver is also acknowledged.

I thank Csaba Fábri and Tamás Szidarovszky for reading this text and for the interesting discussions during the last three years.

I thank Dr. Antal Lopata for providing the source code of the Z-matrix reader developed by Lopata and Kiss.

I thank Professor Tucker Carrington for providing the T8 potential of methane with permission of Professor David Schwenke.

The PES of ammonia provided to me by Dr. Sergei Yurchenko is gratefully acknowledged.

Collaboration with Professor Wesley D. Allen and Professor Peter R. Schreiner is gratefully acknowledged.

Finally, I am grateful to my family for the help and support during the weekdays. I thank my father, László Mátyus, for his invaluable help in computer science. I also thank Ádám Masát for his support and continuous encouragement during my doctoral research.

# Contents

# Chapter 1

# Introduction

The Born–Oppenheimer (BO) approximation[1,2] allows to decouple the total electron-nuclear Schrödinger equation into separate equations for the electronic and nuclear motions, thus defining two fields of research for computational quantum chemistry, namely electronic structure and nuclear motion theories.

The nuclear Schrödinger equation consists of a kinetic energy operator (KEO) corresponding to the motion of the nuclei which can always be made exact, and an approximate potential energy surface (PES) containing the electronic and the potential energy of nuclear repulsion, all terms depending only on the nuclear coordinates. The value of the potential energy surface at each nuclear configuration is provided by electronic structure computations.

In principle, having an appropriate representation of the PES and the masses of the nuclei at hand, the nuclear Hamiltonian is completely defined. However, in practice, the nuclear KEO is not expressed in terms of Cartesian coordinates, as it is common for the electronic kinetic energy operator, but in specific coordinates more or less adapted to the different kinds of motions of the nuclei. After the separation of the translational motion, rotational and specific internal coordinates are defined. As a result of these choices, the form of the nuclear Hamiltonian can be very different for molecules of different size and bonding arrangements.

The first class of approaches of the nuclear motion problem, based on tailor-made analytic kinetic energy operators[3,4,5] and codes utilizing them, proved to be especially useful for certain tri-, tetra-, and pentatomic species.[6,7,8,9,10,11,12,13] Within this

class, almost without exception, separate codes had to be developed for molecules of different size and bonding arrangements. Obviously, there have been initiatives to develop universal variational nuclear motion protocols and codes.

The traditional type of such universal codes uses the Eckart–Watson Hamiltonian(s)[14,15] expressed in the Eckart frame and built upon rectilinear internal coordinates. We are aware of several computer codes based on the Eckart–Watson Hamiltonians capable of yielding variationally computed vibrational spectra for polyatomic systems,[16,17,18,19,20,21,22,23,24,25] although seemingly only the code developed during my doctoral research,[25] and presented in Chapter 4, has at present the capability to perform a numerically exact computation of (ro)vibrational eigenpairs corresponding to a given PES for molecules with more than four nuclei. The principal advantage of these codes is their universality while their most important shortcoming is connected with the rectilinear nature of normal coordinates and the use of the Eckart frame. As a result, floppy molecular systems having PESs with multiple minima cannot be treated straightforwardly within this approach.

There have also been attempts to use arbitrarily chosen body-fixed frames and curvilinear internal coordinates,[26,27,28] for example by Luckhaus *et al.*,[29,30] Lauvergnat *et al.*,[31,32] and Yurchenko *et al.*[33] This class of approaches seems to be the only one which offers the possibility of a true black-box-type algorithm to compute rovibrational spectra of complex and floppy molecules, similar to the widely appreciated black-box approaches of electronic structure theory. Nevertheless, as it is also shown in Chapter 5, practical realization of such a universal algorithm for nuclear motion computations is far from being straightforward,[34] and numerical accuracy and stability must be carefully tested.

In nuclear motion computations rovibrational energy levels and wave functions (and properties based on them) are computed. Often, however, only the rotationless vibrational levels (and transition wavenumbers) are required, which are obtained by the solution of a Hamiltonian constrained to zero total angular momentum ($J = 0$, where $J$ is the quantum number of the overall molecular rotation). Furthermore, adding the capability of the computation of rotational-vibrational states to an existing vibrations-only code is straightforward. Thus, it is deemed to be sufficient to

concentrate during my doctoral research mainly on the constrained, $J = 0$, vibrational problem.

During my doctoral research I have considered a variety of nuclear KEOs. I have developed possible universal algorithms and implemented these algorithms for the treatment of the nuclear motion problem. These algorithms and implementations pose inherent restrictions neither on the number of nuclei nor on the bonding arrangement of the molecular system studied. The main goal of my research was the production of numerically exact vibrational energy levels and wave function for a given PES within this universal context.

Due to recent developments in electronic structure techniques and fitting algorithms, highly accurate representations of the PES[9,35] can be constructed for small to medium-sized molecules. Thus, the numerically exact solution of the nuclear motion problem using such accurate (semi-)global PESs, rovibrational energy levels can be computed which may approach spectroscopic accuracy. The main application of variational nuclear motion methods in molecular spectroscopy points toward the computation of a complete rotational-vibrational spectrum. Experimental measurement of complete spectra under different physical conditions is unfeasible; thus, in certain ranges a complete but imprecise theoretical spectrum can supplement the incomplete but precise experimental data. Computation of (nearly) complete rovibrational spectra of medium-sized molecules is still an extremely challenging task requiring sophisticated algorithms and their efficient implementation.

The main results of my doctoral research are discussed in the next Chapters 1–10, which are organized as follows. Following this brief Introduction, in Chapter 1, the most important physical and chemical notions related to computational molecular spectroscopy, such as the coordinate systems used in molecular Hamiltonians, the representation of the PES, the discrete variable representation (DVR), and iterative eigensolver techniques used throughout this work are discussed.

In Chapter 3, quantum rovibrational Hamiltonians are derived in a general framework by separating the translational coordinates and using a body-fixed frame, Euler angles and internal coordinates.

In Chapter 4, the Eckart–Watson[14,15] forms of the rovibrational Hamiltonian are used, which correspond to Watson's rectilinear orthogonal internal coordinates and the Eckart frame. Implementation of the Eckart–Watson Hamiltonian in a computer code, called DEWE,[25,36] is presented, which does not contain any inherent limitations on the number of nuclei in the molecule. Advantages and limitations of the DEWE protocol and program are discussed.

In order to go beyond the limitations of the DEWE algorithm, in Chapter 5, the restrictions resulting from the use of the Eckart frame and Watson's rectilinear coordinates are removed. An algorithm and computer code, called GENIUSH,[34] is presented, which allows, in principle, the use of a variety of body-fixed frames and internal coordinates without posing any inherent limitations for the number of nuclei. Additionally, in the GENIUSH protocol constraints can be introduced on the nuclear motion straightforwardly, leading to reduced-dimensional models, thus reducing the overall computational effort. This feature is especially important for the investigation of larger molecular systems.

Sophisticated eigensolver algorithms are discussed in Chapter 6. In order to make feasible the computation of a large number of eigenvalues and eigenvectors of (ro)vibrational Hamiltonian matrices appearing in the approaches presented in Chapters 4 and 5 consideration and implementation of efficient eigensolver techniques are essential. As a result of these improvements, a large number of well-converged energy levels and wave functions were computed for the five-atomic $CH_4$ and $CH_2D_2$ molecules. These are discussed in Chapter 7.

The problem of the assignment of computed energy levels through the analysis of the vibrational wave functions is addressed in Chapter 8.

It is important to emphasize that besides the computation of (ro)vibrational eigenvalues and eigenvectors and the corresponding spectra, the techniques developed here can be utilized in many other fields of computational chemistry. Some of those fields are considered in Chapter 9 where I had acquired some experience during my doctoral research and fruitful further applications are expected. These include, for instance, accurate thermochemistry and reaction dynamics. This thesis is ended with a summary of the results and conclusions in Chapter 10.

# Chapter 2

# Variational techniques

## 2.1 Coordinate systems

Let us consider a molecule with $N$ nuclei, whose positions are specified by $3N$ rectilinear Cartesian coordinates, $X_{i\alpha},\ i = 1, \ldots, N \quad (\alpha = X, Y, Z)$, in the laboratory-fixed frame, and $m_i$ $(i = 1, \ldots, N)$ masses are associated to them. In anticipation of a computationally more efficient representation, the $3N$ rectilinear Cartesian coordinates are replaced[27,37,38,39,40] by coordinates of the center of mass of the nuclei (NCM), $(X_X^{\mathrm{NCM}}, X_Y^{\mathrm{NCM}}, X_Z^{\mathrm{NCM}})$, which describe the translational motion of the system; the Euler angles, $(\phi, \theta, \chi)$, which specify the instantaneous orientation of a body-fixed frame with respect to the laboratory-fixed frame; and $3N - 6$ coordinates describing the internal motion of the system. Several choices of body-fixed frames (also called embeddings) and internal coordinates are possible. Here some of the most common coordinates are introduced which are used also in my work. In what follows, Cartesian coordinates of the $i$th nucleus in the body-fixed frame are denoted by $x_{ia}$ $(a = x, y, z)$ or by $\mathbf{x}_i$.

### 2.1.1 Body-fixed frames

In general, a frame is fixed to the molecule by defining six constraints on the Cartesian coordinates. There are three translational and three orientational constraints.

**Scattering (xxy) frame** This body-fixed frame is defined by fixing certain coordinates of three atoms, A, B, and C of the molecule. The conditions are $x_{\mathrm{A}x} = x_{\mathrm{A}y} = x_{\mathrm{A}z} = x_{\mathrm{B}y} = x_{\mathrm{B}z} = x_{\mathrm{C}z} = 0$.[27] In this work a modified version of this scattering frame is defined whose origin is shifted to the NCM. This body-fixed frame becomes undefined, also called singular, if the three atoms used for its definition lie along a line.

**Principal axis frame** For fixing a principal axis frame to the molecule the translational conditions are

$$\sum_{i=1}^{N} m_i \mathbf{x}_i = 0. \tag{2.1}$$

The rotational conditions require that the off-diagonal elements of the (symmetric) instantaneous inertia tensor vanish,

$$\sum_{i=1}^{N} \sum_{\beta\gamma=x,y,z} e^2_{\alpha\beta\gamma} m_i x_{i\beta} x_{i\gamma} = 0, \quad \alpha = x, y, z, \tag{2.2}$$

where $e_{\alpha\beta\gamma}$ is the Lévi-Cività symbol. Although this body-fixed frame is well-known in molecular spectroscopy, it is not used in this work as it becomes singular at symmetric top instantaneous structures.[27,37]

**Eckart frame** The Eckart frame,[41] one of the most commonly used embedding in molecular spectroscopy is defined by three translational,

$$\sum_{i=1}^{N} m_i \mathbf{x}_i = \mathbf{0}, \tag{2.3}$$

and three rotational,

$$\sum_{i=1}^{N} m_i \mathbf{c}_i \times \mathbf{x_i} = \mathbf{0}, \tag{2.4}$$

conditions, where $\mathbf{c}_i$ contains the coordinates of a chosen nonlinear reference structure. The reference structure can be arbitrarily specified, but in practice it is often

chosen to be the equilibrium structure minimizing the actually used PES. In general, the Eckart frame is defined if $m_i$ and $\mathbf{c}_i$ $(i = 1, \ldots, N)$ are specified.

### 2.1.2 Internal coordinates

A set of internal coordinates is used to characterize the relative positions of nuclei in the KEO and also in the representations of PESs.

**Watson's rectilinear coordinates, normal coordinates** Following common practice, Watson introduced[14] $3N-6$ internal coordinates defined in terms of Cartesian coordinates corresponding to the Eckart frame as

$$Q_k = \sum_{i=1}^{N} \sum_{\alpha} \sqrt{m_i} l_{iak} \left( x_{ia} - c_{ia} \right) = \sum_{i=1}^{N} \sqrt{m_i} \mathbf{l}_{ik}^{\mathrm{T}} \left( \mathbf{x}_i - \mathbf{c}_i \right) \tag{2.5}$$
$$Q_k \in (-\infty, +\infty) \quad k = 1, 2, \ldots, 3N-6,$$

requiring for the elements of $\mathbf{l} \in \mathcal{R}^{N \times 3 \times (3N-6)}$ that

$$\sum_{i=1}^{N} \mathbf{l}_{ij}^{\mathrm{T}} \mathbf{l}_{ik} = \delta_{jk}, \quad \sum_{i=1}^{N} \sqrt{m_i}\, \mathbf{l}_{ik} = \mathbf{0}, \quad \text{and} \quad \sum_{i=1}^{N} \sqrt{m_i}\, \mathbf{c}_i \times \mathbf{l}_{ik} = \mathbf{0} \tag{2.6}$$
$$j, k = 1, 2, \ldots, 3N-6.$$

The $\mathbf{Q}$ coordinates are often called rectilinear and orthogonal internal coordinates, in reference to their linear relationship to the body-fixed Cartesian coordinates, given in Eq. (2.5), and the orthogonality requirement imposed on the elements on the $\mathbf{l}$ matrix in the sense given in Eq. (2.6).

Eqs. (2.6) form an underdetermined system of equations for the elements of $\mathbf{l}$. The well-known normal coordinates can be regarded as a special case of the coordinates introduced by requiring that the set of $Q_k$s diagonalize both the kinetic and the harmonic potential energy matrix, as well as that Eqs. (2.6) are fulfilled. In general, however, one can build a set of orthogonal, rectilinear coordinates describing the internal motion of a molecule satisfying Eqs. (2.6) which are independent of the actual PES.

Due to the introduction of $Q_k$s in Eqs. (2.5)–(2.6), Eq. (2.5) can be inverted to express the Cartesian coordinates in the Eckart frame in terms of $Q_k$s as

$$\mathbf{x}_i = \mathbf{c}_i + \frac{1}{\sqrt{m_i}} \sum_{k=1}^{3N-6} \mathbf{l}_{ik} Q_k, \quad i = 1, \ldots, N. \tag{2.7}$$

**Valence coordinates** Valence or internal coordinates were used in this work both in the KEOs and also in the PESs. In the KEOs the standard[42] stretching, bending, and torsional coordinates and their symmetry-adapted combinations were used. Body-fixed Cartesian coordinates were expressed in terms of primitive valence coordinates by means of the Z-matrix reader program developed by Lopata and Kiss.[43] In a force field representation of the PES (see Section 2.2), the well-known stretching (STRE, SPF),[44] bending (BEND), torsional (TORS), linear bending (LINX, LINY), and out-of-plane bending (OUT) coordinates and their symmetry adapted combinations were used as defined in the INTDER2000 program.[45,46,47]

**Jacobi coordinates** For triatomic molecules Jacobi coordinates[48] were used, which are defined as follows, if the three nuclei are denoted by A, B, and C

$$r_{1\mathrm{j}} = r(\mathrm{A} - \mathrm{B}) \in [0, \infty) \tag{2.8}$$

$$r_{2\mathrm{j}} = r(\mathrm{NCM_{AB}} - \mathrm{C}) \in [0, \infty) \tag{2.9}$$

$$\theta_{\mathrm{j}} = \angle(B - \mathrm{NCM_{AB}} - C) \in [0, \pi], \tag{2.10}$$

where $\mathrm{NCM_{AB}}$ stands for the center of mass of the A and B nuclei.

**Internuclear coordinates** For triatomic molecules, ABC, the three internuclear distances $r(\mathrm{A} - \mathrm{B})$, $r(\mathrm{B} - \mathrm{C})$, and $r(\mathrm{A} - \mathrm{C})$, were used, requiring of course that the three distances fulfill the triangle inequality.

## 2.2 Potential energy surfaces

Single-point electronic structure computations provide electronic energies at given configurations of the nuclei. In nuclear motion computations the "total" electronic

energy, containing also the potential energy of nuclear repulsion, could be computed on-the-fly whenever it is required.[24] However, this is rather time consuming and usually cannot be done at a level of electronic structure theory required to obtain accurate results. In contrast to this strategy, in this work a function expressed in terms of appropriately chosen internal coordinates is used to represent the part of the PES required.

A force field can be constructed by expanding the PES around a reference structure, usually its minimum point, into a fourth- (or sixth- or eighth-) order Taylor polynomial. This representation is reliable for lower-lying energy levels and small amplitude vibrational motions. The convergence of the force field with respect to the order of expansion can be improved for the stretching-type motions, if instead of primitive bond distances the Simons-Parr-Finlan (SPF)[44] coordinates are used.[6] Transformation of force fields between different sets of coordinate systems was carried out by using the INTDER2000 program.[45]

A more accurate and a more generally applicable (semi-)global representation of the PES is achievable by fitting appropriately chosen functions to the data provided by electronic structure computations corresponding to specific nuclear geometries. In this work such (semi-)global surfaces were used for water (CVRQD PESs)[9,35] and ammonia.[49]

## 2.3 Discrete variable representation

In what follows the discrete variable representation (DVR)[50,51] is presented which is used exclusively in my work to construct the matrix representation of operators.

In nuclear motion theory normalized, standard orthogonal polynomials (such as Hermite, Laguerre, Legendre, and Chebyshev), $\phi_j(q)$, can be employed to construct a basis. Instead of using spectral functions, a DVR basis,[52] a kind of grid basis, can also be employed. In order to build a DVR, the coordinate matrix of dimension $N_k^0 \times N_k^0$ is constructed having the elements $(\mathbf{q}_k)_{ij} = \langle \phi_i(q_k) | q_k | \phi_j(q_k) \rangle$ for each active vibrational degree of freedom, $k = 1, 2, \ldots, D$. For the $k$th vibrational degree of freedom the quadrature points, $\xi_{k,n_k}$, are the eigenvalues of the $k$th co-

ordinate matrix, and the DVR basis is defined as $\Phi_{n_k}(q_k) = \sum_{j=0}^{N_k^0-1} (\mathbf{T}_k)_{n_k,j}\, \phi_j(q_k)$, where columns of $\mathbf{T}_k$ are the eigenvectors of $\mathfrak{q}_k$. In the case of standard orthogonal polynomials it is also known[53] that

$$\mathbf{T}_k = \mathcal{F}_k, \tag{2.11}$$

and

$$(\mathcal{F}_k)_{ni} = w_{k,i_k}^{1/2} \phi_{k,n_k}^*(\xi_{k,i_k}), \tag{2.12}$$

where $\{\xi_{k,i_k}, w_{k,i_k}\}_{i_k=1}^{N_k}$ are the Gaussian quadrature points and weights corresponding to the $k$th vibrational degree of freedom. In practice, $\mathbf{T}_k$ is often constructed by diagonalizing the coordinate matrix, $\mathfrak{q}_k$. The normalized eigenvectors are undetermined up to a factor of $(-1)$. To be consistent with the DVR construction, the sign of eigenvectors must be chosen so that the constructed $\mathbf{T}_k$ matrix is consistent with Eqs. (2.11) and (2.12). For instance, if a Hermite-DVR is constructed, the first element of each eigenvector, $(\mathbf{T}_k)_{0i_k}$ $(i_k = 1, \ldots, N_k^0)$, must be positive to be consistent with as $(\mathcal{F}_k)_{0i_k} = w_{k,i_k}^{1/2} H_{k,0}^*(\xi_{k,i_k}) = w_{k,i_k}^{1/2} \geq 0$.

Matrices of the $\frac{\partial}{\partial q_k}$ and $\frac{\partial^2}{\partial q_k^2}$ differential operators can be first determined in the spectral basis, yielding $\mathcal{D}_k^{[1]}$ and $\mathcal{D}_k^{[2]}$, respectively. Then, they can be transformed to DVR by means of the transformation method,[50]

$$\mathbf{D}_k^{[1]} = \mathbf{T}_k^{\mathrm{T}} \mathcal{D}_k^{[1]} \mathbf{T}_k \quad \text{and} \quad \mathbf{D}_k^{[2]} = \mathbf{T}_k^{\mathrm{T}} \mathcal{D}_k^{[2]} \mathbf{T}_k. \tag{2.13}$$

For a system with $D$ degrees of freedom a DVR direct-product basis and grid is constructed as $\left\{\prod_{k=1}^{D} \Phi_{n_k}(q_k)\right\}_{n_1=1,n_2=1,\ldots,n_D=1}^{N_1^0,N_2^0,\ldots,N_D^0}$, $\{(\xi_{1,n_1}, \ldots, \xi_{D,n_D})\}_{n_1=1,n_2=1,\ldots,n_D=1}^{N_1^0,N_2^0,\ldots,N_D^0}$. The size of the direct-product basis and grid is $\mathcal{N} = N_1^0 N_2^0 \cdot \ldots \cdot N_D^0$.

### Potential-optimized DVR

It is desirable to employ as compact of a representation of the Hamiltonian as possible. A step toward this goal is to optimize the primitive DVR grid employ-

ing a suitable one-dimensional (1D) model Hamiltonian. In the present work the potential-optimized (PO) DVR approach[53,54,55] was utilized. In the PO-DVR approach 1-dimensional $\hat{h}_k^{1\mathrm{D}}(q_k)$ $(k = 1, \ldots, D)$ operators are used to preoptimize the grid points. Eigenvalues and eigenvectors corresponding to $\hat{h}_k^{1\mathrm{D}}(q_k)$ are then evaluated using a large number of primitive grid points, $N_k^0$, distributed on a wide interval of the $k$th coordinate.

Next, the first few eigenvectors, $N_k^{\mathrm{PO}} \leq N_k^0$, of the one-dimensional problem ordered in a matrix, $\mathbf{u}_k \in \mathcal{R}^{N_k^0 \times N_k^{\mathrm{PO}}}$, are used to construct the $k$th "optimized" coordinate matrix, $\left(\mathfrak{q}_k^{\mathrm{PO}}\right)_{ij} = \sum_{l=1}^{N_k^0} \left(\mathbf{u}_k\right)_{li} \xi_{k,l} \left(\mathbf{u}_k\right)_{lj}$ $(i, j = 1, 2, \ldots, N_k^{\mathrm{PO}})$. The eigenvalues of $\mathfrak{q}_k^{\mathrm{PO}}$ are the PO-DVR quadrature points, $\xi_{k,n_k}^{\mathrm{PO}}$ $(n_k = 1, 2, \ldots, N_k^{\mathrm{PO}})$. The eigenvectors of $\mathfrak{q}_k^{\mathrm{PO}}$ ordered in a matrix, $\mathbf{T}_k^{\mathrm{PO}}$, are used to set up the PO-DVR of the differential operators via the transformation method.[50]

There are several advantages of the use of this optimization method. First, it offers an inexpensive and valuable test of the actual coordinate definition, as it also provides the "energy levels" of a 1-dimensional, but already meaningful, model of the system. Second, it automatically provides an optimized interval for the quadrature points corresponding to each internal coordinate. Third, and this is the main advantage of PO-DVR, due to the optimization a reduced number of grid points is sufficient to obtain eigenpairs with the desired accuracy.

In what follows, $N_k$ denotes the number of grid points corresponding to the $k$th degree of freedom. If PO-DVR is used, $N_k = N_k^{\mathrm{PO}}$, otherwise, $N_k = N_k^0$ $(k = 1, 2, \ldots, D)$. The direct-product grid constructed from these points has the size $\mathcal{N} = \prod_{k=1}^{D} N_k$. In computations a direct-product grid can be used directly, or it can be truncated based on geometrical or energetic requirements, thus resulting in a nondirect-product grid. Due to a simple indexing scheme used in the implementation of the presented programs (Chapters 4 and 5) the matrix-vector multiplication and eigensolver algorithms developed for the direct-product case can be employed also for a reduced (nondirect-product) case.

As a result of the construction of (PO-)DVR, the matrix of the coordinate operator is diagonal. Furthermore, due to the Gaussian quadrature approximation and the special properties of the (PO-)DVR, the matrix representation of operators that de-

pend only on the coordinates is also always diagonal,[53] which is the main advantage of this representation.

## 2.4 Lanczos eigensolver

The Lanczos technique[56,57,58] is a widely used iterative method for the computation of a set of eigenvalues and eigenvectors of large (and often sparse) real, symmetric matrices. Let us denote the matrix in question by $\mathbf{A} \in \mathcal{R}^{n\times n}$, and choose an initial vector $\mathbf{q}_1$ of unity norm. Set $\beta_0 = 0$, $\mathbf{q}_0 = \mathbf{0}$, and then the original Lanczos algorithm (OL) can be described as follows:

**Do** $j = 1, 2, \ldots, m \leq n$

**(a)** $\mathbf{q}_{j+1} = \mathbf{A}\mathbf{q}_j$

**(b)** $\alpha_j = (\mathbf{q}_j, \mathbf{q}_{j+1})$

**(c)** $\mathbf{q}_{j+1} = \mathbf{q}_{j+1} - \alpha_j \mathbf{q}_j - \beta_{j-1}\mathbf{q}_{j-1}$

**(d)** $\beta_j = (\mathbf{q}_{j+1}, \mathbf{q}_{j+1})$ if $\beta_j = 0$ then **Stop**

**(e)** $\mathbf{q}_{j+1} = \mathbf{q}_{j+1}/\beta_j$

**End do**

After step $m$ the following recurrence is valid for the Lanczos vectors

$$\mathbf{A}\mathbf{Q}_m = \mathbf{Q}_m\mathbf{T}_m + \beta_m \mathbf{q}_{m+1}\mathbf{e}_m^{\mathrm{T}}, \tag{2.14}$$

where the columns of $\mathbf{Q}_m$ contain the first $m$ Lanczos vectors, $\mathbf{e}_m$ is the last column of the identity matrix $\mathbf{I}_m$, and $\mathbf{T}_m = \mathbf{Q}_m^{\mathrm{T}}\mathbf{A}\mathbf{Q}_m$ is a tridiagonal matrix,

$$\mathbf{T}_m = \begin{pmatrix} \alpha_1 & \beta_1 & & & 0 \\ \beta_1 & \alpha_2 & & & \\ & \ddots & \ddots & \ddots & \\ & & & \alpha_{m-1} & \beta_{m-1} \\ 0 & & & \beta_{m-1} & \alpha_m \end{pmatrix}. \tag{2.15}$$

The eigenvalues of $\mathbf{T}_m$ are the so-called Ritz values. If the eigenvectors of $\mathbf{T}_m$ are denoted by $\mathbf{y}_i$ $(i = 1, 2, \ldots, m)$, the vectors $\mathbf{v}_i = \mathbf{Q}_m \mathbf{y}_i$ are the Ritz vectors. The Ritz values and vectors are the Rayleigh–Ritz approximations to the eigenvalues and eigenvectors of $\mathbf{A}$ from the subspace spanned by the Lanczos vectors $\mathbf{Q}_m$.

At this point, a couple of important properties of the Lanczos algorithm are worth emphasizing. First, the eigenvalues of $\mathbf{T}_m$ $(m = 1, 2, \ldots \leq n)$ converge to the largest eigenvalues of $\mathbf{A}$. Therefore, instead of introducing $\mathbf{A}$ directly in the Lanczos iteration, a spectral transformation is carried out using a filter function, $\mathbf{A}' = \mathcal{F}(\mathbf{A})$, so that the required eigenvalues of $\mathbf{A}$ are the largest eigenvalues of $\mathbf{A}'$. The required range is often the lowest end of the spectrum. Second, explicit knowledge of the matrix $\mathbf{A}$ is not required. Even if a spectral transformation step is introduced in the algorithm, only the multiplication of $\mathbf{A}$ with a vector is necessary. Third, the Lanczos vectors, $\mathbf{q}_j$, remain orthogonal among each other only if exact arithmetics is used. Due to round-off errors, resulting from the use of finite arithmetics, the orthogonality is satisfied only at the beginning of the iteration. The loss of orthogonality results in copies of eigenvalues and spurious values in the computed spectrum. To avoid the computation of these annoying features, the orthogonality of Lanczos vectors is usually artificially maintained.

# Chapter 3

# Rovibrational Hamiltonians

## 3.1 The classical Hamiltonian in internal coordinates

Lagrangian of an $N$-atomic system expressed in terms of Cartesian coordinates in the laboratory-fixed frame, $X_{i\alpha}$ or $\mathbf{X}_i$, is defined as

$$L = \frac{1}{2}\sum_{i=1}^{N} m_i \dot{\mathbf{X}}_i{}^{\mathrm{T}} \dot{\mathbf{X}}_i - V, \tag{3.1}$$

where dots denote time derivatives, $m_i$ denotes the mass associated to the $i$th nucleus and $V$ is the potential energy depending only on the coordinates of the nuclei. In anticipation of a computationally more efficient representation, the $3N$ rectilinear Cartesian coordinates are replaced by coordinates of the center of mass of the nuclei (NCM), $(X_X^{\mathrm{NCM}}, X_Y^{\mathrm{NCM}}, X_Z^{\mathrm{NCM}})$, which describe the translational motion of the system; the Euler angles, $(\phi, \theta, \chi)$, which specify the instantaneous orientation of a body-fixed frame with respect to the laboratory-fixed frame; and coordinates describing the internal motion of the system, $(q_1, q_2, \ldots, q_D)$, where $D \leq 3N - 6$ (see Section 2.1). In this new set of coordinates the Lagrangian has the form, using the compact notation $\mathbf{q} = (q_1, q_2, \ldots, q_{D+6})$ and $q_{D+1} = \phi$, $q_{D+2} = \theta$, $q_{D+3} = \chi$,

$q_{D+4} = X_X^{\mathrm{NCM}}$, $q_{D+5} = X_Y^{\mathrm{NCM}}$, and $q_{D+6} = X_Z^{\mathrm{NCM}}$,

$$L = \frac{1}{2}\sum_{kl=1}^{D+6}\left(\sum_{i=1}^{N} m_i \frac{\partial \mathbf{X}_i^{\mathrm{T}}}{\partial q_k}\frac{\partial \mathbf{X}_i}{\partial q_l}\right)\dot{q}_k\dot{q}_l - V = \frac{1}{2}\sum_{kl=1}^{D+6}\dot{q}_k g_{kl}^{\mathrm{trv}}\dot{q}_l - V, \tag{3.2}$$

where

$$g_{kl}^{\mathrm{trv}} = \sum_{i=1}^{N} m_i \frac{\partial \mathbf{X}_i^{\mathrm{T}}}{\partial q_k}\frac{\partial \mathbf{X}_i}{\partial q_l}, \quad k,l = 1,2,\ldots,D+6. \tag{3.3}$$

was introduced. The momentum, $p_k$, conjugate to $q_k$, is

$$p_k = \frac{\partial L}{\partial \dot{q}_k} = \sum_{l=1}^{D+6} g_{kl}^{\mathrm{trv}}\dot{q}_l \quad \text{and hence for nonsingular } \mathbf{g}\text{'s,} \quad \dot{\mathbf{q}} = \left(\mathbf{g}^{\mathrm{trv}}\right)^{-1}\mathbf{p}. \tag{3.4}$$

After appropriate rearrangements the classical rotational-vibrational Hamiltonian is written as

$$H^{\mathrm{rv}} = \frac{1}{2}\sum_{kl=1}^{D+3} p_k \left(\mathbf{g}^{-1}\right)_{kl} p_l + V = \frac{1}{2}\sum_{kl=1}^{D+3} p_k G_{kl} p_l + V, \tag{3.5}$$

where the notation $\mathbf{G} = \mathbf{g}^{-1} \in \mathrm{R}^{(D+3)\times(D+3)}$ was introduced. Note that the translational degrees of freedom can be separated exactly, thus in what follows these degrees of freedom are not considered.

## 3.2 The quantum Hamiltonian in internal coordinates

In order to rewrite Eq. (3.5) to its quantum mechanical counterpart, $\hat{H}^{\mathrm{rv}}$, a method advocated by Podolsky[59] can be applied, whereby

$$\hat{H}^{\mathrm{rvP}} = \frac{1}{2}\sum_{kl=1}^{D+3} \tilde{g}^{-1/4}\hat{p}_k^{\dagger} G_{kl}\tilde{g}^{1/2}\hat{p}_l\tilde{g}^{-1/4} + V, \tag{3.6}$$

where $\tilde{g} = \det \mathbf{g}$, and $\hat{p}_k$ has the form

$$\hat{p}_k = -i\hbar \frac{\partial}{\partial q_k}, \quad k = 1, 2, \ldots, D \quad \text{and} \tag{3.7}$$

$$\hat{p}_{D+1} = \hat{J}_x, \quad \hat{p}_{D+2} = \hat{J}_y, \quad \hat{p}_{D+3} = \hat{J}_z, \tag{3.8}$$

if the volume element is (using Wilson's normalization) $\mathrm{d}q_1 \mathrm{d}q_2 \ldots \mathrm{d}q_D \sin\theta \mathrm{d}\theta \mathrm{d}\phi \mathrm{d}\chi$. Elements of $\mathbf{G}$ and $\tilde{g}$ are expressed in terms of the internal coordinates and they are not functions of the Euler angles. Thus an effective vibrational operator can be introduced,

$$\hat{H}^{\mathrm{vP}} = \frac{1}{2} \sum_{kl=1}^{D} \tilde{g}^{-1/4} \hat{p}_k^{\dagger} G_{kl} \tilde{g}^{1/2} \hat{p}_l \tilde{g}^{-1/4} + V. \tag{3.9}$$

From now on this form will be referred to as the Podolsky-form, $\hat{H}^{\mathrm{vP}}$.

The Podolsky-form of the rotation-vibration Hamiltonian given in Eq. (3.6) can be rearranged, and after trivial manipulations it simplifies to

$$\hat{H}^{\mathrm{rvR}} = \frac{1}{2} \sum_{kl=1}^{D+3} \hat{p}_k^{\dagger} G_{kl} \hat{p}_l + U + V, \tag{3.10}$$

and the corresponding effective vibration-only operator is

$$\hat{H}^{\mathrm{vR}} = \frac{1}{2} \sum_{kl=1}^{D} \hat{p}_k^{\dagger} G_{kl} \hat{p}_l + U + V, \tag{3.11}$$

where

$$U = \frac{\hbar^2}{32} \sum_{kl=1}^{D} \left[ \frac{G_{kl}}{\tilde{g}^2} \frac{\partial \tilde{g}}{\partial q_k} \frac{\partial \tilde{g}}{\partial q_l} + 4 \frac{\partial}{\partial q_k} \left( \frac{G_{kl}}{\tilde{g}} \frac{\partial \tilde{g}}{\partial q_l} \right) \right], \tag{3.12}$$

or after a useful rearrangement

$$U = \frac{\hbar^2}{32} \sum_{kl=1}^{D} \left[ \frac{G_{kl}}{\tilde{G}^2} \frac{\partial \tilde{G}}{\partial q_k} \frac{\partial \tilde{G}}{\partial q_l} - 4 \frac{\partial}{\partial q_k} \left( \frac{G_{kl}}{\tilde{G}} \frac{\partial \tilde{G}}{\partial q_l} \right) \right]. \tag{3.13}$$

The form given in Eq. (3.11) will be referred to as the rearranged form of the vibrational Hamiltonian, $\hat{H}^{\mathrm{vR}}$, to distinguish it from the Podolsky-form, $\hat{H}^{\mathrm{vP}}$, given in Eq. (3.9).

The extrapotential term, $U$, is an inherently quantum mechanical term in the Hamiltonian. Both the vibration-only Podolsky-form, Eq. (3.9), and the rearranged form, Eq. (3.11), contain the determinant of the rotational-vibrational $\mathbf{g} \in \mathcal{R}^{(D+3)\times(D+3)}$ matrix (or that of the $\mathbf{G}$ matrix), irrespective whether the full rovibrational or only the effective vibrational problem is solved. Consequently, even if only the vibrations are studied, the choice of the body-fixed frame might affect the convergence rate of the computed vibrational levels, and also, for instance, the singular regions ($\tilde{g} = 0$) of the Hamiltonian.

In practice, the quantum Hamiltonians given in Eqs. (3.9) or (3.11) are further rearranged according to the actually chosen body-fixed frame and internal coordinates.[3,4,5,11,12,13,14,15,60,61,62,63,64]

# Chapter 4

# DEWE: A universal program for semirigid molecules

The Eckart frame,[41] defined in Eqs. (2.3) and (2.4), and the rectilinear coordinates introduced by Watson,[14] given in Eqs. (2.5) and (2.6), correspond to a set of coordinates universally defined for a molecule with $N$ nuclei and an arbitrary bonding arrangement. Thus, by using these coordinates the quantum Hamiltonian, given in Eq. (3.10), can be further simplified to a form first given by Watson.[14] This Hamiltonian has a universal form for an $N$-atomic molecule, thus allowing the construction of a universal variational (ro)vibrational approach.

The Eckart–Watson Hamiltonian[14] has been used extensively in variational nuclear motion computations.[17,19,20,22,23,24,25] Seemingly only the present implementation has at present the capability to perform a numerically exact computation of (ro)vibrational eigenpairs corresponding to a given PES for molecules with more than four nuclei.

The algorithm and computer code detailed here and called DEWE is based on the Discrete variable representation of the Eckart–Watson Hamiltonian with a numerically Exact inclusion of the actual representation of the PES, whose eigenvalues and eigenvectors are computed by using an iterative eigensolver.[25,36] The DEWE program is able to provide numerically exact vibrational energy levels and wave functions (corresponding to a given PES). It does not contain any inherent limita-

tions for the number of nuclei, however, in practice, molecules with maximum six nuclei can be handled on nowadays standard personal computers.

In what follows the main parts of DEWE protocol,[25,36] are described. Important results obtained with the DEWE program are presented in Chapter 7. Further applications of the DEWE program are described in Refs. 25, 65, 66, 67, 36, 68, 69, and 70.

## 4.1 Eckart–Watson Hamiltonian

Upon any choice of **c** and **l** satisfying the requirements given in Eqs. (2.6), the rovibrational Hamiltonian, given in Eq. (3.6) or Eq. (3.10), can be simplified, as was first given by Watson in 1968,[14] to the well-known Eckart–Watson form,

$$\hat{H}^{\mathrm{rv}} = \frac{1}{2}\sum_{\alpha\beta}(\hat{J}_\alpha - \hat{\pi}_\alpha)\mu_{\alpha\beta}(\hat{J}_\beta - \hat{\pi}_\beta) + \frac{1}{2}\sum_{k=1}^{3N-6}\hat{P}_k^2 - \frac{\hbar^2}{8}\sum_\alpha \mu_{\alpha\alpha} + V, \tag{4.1}$$

where

$$\hat{\pi}_\alpha = \sum_{kl=1}^{3N-6}\zeta_{kl}^\alpha Q_k \hat{P}_l, \quad \text{(Coriolis-coupling operator)} \tag{4.2}$$

$$\zeta_{kl}^\alpha = \sum_{i=1}^{N} m_i \left(\mathbf{l}_{ik} \times \mathbf{l}_{il}\right)_\alpha , \tag{4.3}$$

$$\mu_{\alpha\beta} = \sum_{\gamma\delta}\left(\mathbf{I}''^{-1}\right)_{\alpha\gamma} I^0_{\gamma\delta}\left(\mathbf{I}''^{-1}\right)_{\delta\beta}, \quad \text{(generalized inverse inertia tensor)} \tag{4.4}$$

and

$$I''_{\alpha\beta} = I^0_{\alpha\beta} + \frac{1}{2}\sum_{k=1}^{3N-6} a_k^{\alpha\beta} Q_k \quad \text{and} \quad a_k^{\alpha\beta} = 2\sum_{\gamma\delta\varepsilon} e_{\alpha\gamma\varepsilon} e_{\beta\delta\varepsilon} \sum_{i=1}^{N}\sqrt{m_i}\; c_{i\gamma} l_{\delta ik}. \tag{4.5}$$

In the above expressions $\hat{P}_k = -i\hbar\frac{\partial}{\partial Q_k}$ and $\hat{J}_x, \hat{J}_y, \hat{J}_z$ are the angular momentum operators. In what follows the vibration-only, effective operator for $J = 0$, part of

the Eckart–Watson Hamiltonian is used in this work,

$$\hat{H}^{\mathrm{v}} = \frac{1}{2}\sum_{\alpha\beta}\hat{\pi}_\alpha\mu_{\alpha\beta}\hat{\pi}_\beta + \frac{1}{2}\sum_{k=1}^{3N-6}\hat{P}_k^2 - \frac{\hbar^2}{8}\sum_\alpha \mu_{\alpha\alpha} + V. \tag{4.6}$$

## 4.2 DVR of the Eckart–Watson Hamiltonian

Normalized Hermite polynomials, $H_j(q)$, are employed to construct a basis for the representation of the Eckart–Watson Hamiltonian. Instead of using spectral functions, the corresponding DVR functions are employed in DEWE. Construction of the Hermite-DVR grid points and matrices of the derivative operators $\frac{\partial}{\partial Q_k}$, $\frac{\partial}{\partial Q_k^2}$ was discussed in detail in Section 2.3.

Matrix representation of $\hat{H}^{\mathrm{v}}$, given in Eq. (4.6), on a direct-product Hermite-DVR grid can be facilitated by introducing the truncated resolution of identity between $\hat{\pi}_\alpha$ and $\mu_{\alpha\beta}$ and between $\mu_{\alpha\beta}$ and $\hat{\pi}_\beta$ and corresponds to

$$\mathbf{H}^{\mathrm{vib}} = \frac{1}{2}\sum_{\alpha\beta}\boldsymbol{\pi}_\alpha\boldsymbol{\mu}_{\alpha\beta}\boldsymbol{\pi}_\beta + \frac{1}{2}\sum_{k=1}^{3N-6}\mathbf{P}_k^2 - \frac{\hbar^2}{8}\sum_\alpha \boldsymbol{\mu}_{\alpha\alpha} + \mathbf{V}, \tag{4.7}$$

where $\boldsymbol{\mu}_{\alpha\beta}$ $(\alpha,\beta = x,y,z)$ and $\mathbf{V} \in \mathcal{R}^{\mathcal{N}\times\mathcal{N}}$ are diagonal matrices, and $\mathcal{N}$ is the size of the direct-product grid, $\mathcal{N} = \prod_{i=1}^{3N-6} N_i$, where $N_i$ denotes the number of grid points corresponding to the $i$th vibrational degree of freedom.

A representation of a PES is often expressed in terms of a set of valence coordinates. These coordinates can be expressed in terms of Watson's rectilinear internal coordinates, for instance, by means of Eq. (2.7). In DVR this composite function providing the values of the PES in terms of rectilinear internal coordinates used in the KEO is represented by a diagonal matrix whatever complicated the actual form of the potential function is.

In order to compute eigenpairs of the Hamiltonian matrix given in Eq. (4.7) a Lanczos iterative eigensolver was employed.

## 4.3 Multiplication of the Hamiltonian matrix with a vector

One of the prime features making iterative eigensolvers useful in DEWE is the fact that the Hamiltonian matrix of Eq. (4.7) does not have to be constructed explicitly, only its product with a vector is required. In (ro)vibrational computations the Lanczos eigensolver algorithm is the most often used iterative technique. The basic concepts of the Lanczos eigensolver algorithms were discussed in Section 2.4, and more sophisticated Lanczos techniques specifically adapted for the presented (ro)vibrational problems are discussed in Chapter 6. In this section an efficient multiplication algorithm is presented for the multiplication of $\mathbf{H}^{\mathrm{v}}$, given in Eq. (4.7), with a vector $\mathbf{x}$ exploiting the special structure of the matrices contributing to $\mathbf{H}^{\mathrm{v}}$. Such an efficient matrix-vector multiplication algorithm is essential for carrying out large computations, like those presented in Chapters 6 and 7. Details of the algorithm implemented are described in what follows. Thus,

$$\mathbf{y} = \mathbf{H}^{\mathrm{vib}}\mathbf{x} = \frac{1}{2}\sum_{\alpha}\left(\boldsymbol{\pi}_{\boldsymbol{\alpha}}\sum_{\beta}\boldsymbol{\mu}_{\alpha\beta}\left(\boldsymbol{\pi}_{\beta}\mathbf{x}\right)\right) + \left(\frac{1}{2}\sum_{k=1}^{3N-6}\mathbf{P}_k^2\mathbf{x} + \mathbf{V}'\right)\mathbf{x}, \tag{4.8}$$

where the parentheses indicate the order of operations, and

$$\mathbf{V}' = \mathbf{V} - \frac{\hbar^2}{8}\sum_{\alpha}\boldsymbol{\mu}_{\alpha\alpha}, \tag{4.9}$$

$$\mathbf{P}_k = -i\ \mathbf{I}_1 \otimes \mathbf{I}_2 \otimes \ldots \otimes \mathbf{I}_{k-1} \otimes \mathbf{D}_k^{[1]} \otimes \mathbf{I}_{k+1} \otimes \ldots \otimes \mathbf{I}_{3N-6} \in \mathcal{R}^{\mathcal{N}\times\mathcal{N}}, \tag{4.10}$$

$$\mathbf{P}_k^2 = \mathbf{I}_1 \otimes \mathbf{I}_2 \otimes \ldots \otimes \mathbf{I}_{k-1} \otimes \mathbf{D}_k^{[2]} \otimes \mathbf{I}_{k+1} \otimes \ldots \otimes \mathbf{I}_{3N-6} \in \mathcal{R}^{\mathcal{N}\times\mathcal{N}}, \tag{4.11}$$

and $k = 1, 2, \ldots, 3N-6$. $\mathbf{I}_k \in \mathcal{R}^{N_k\times N_k}$ denotes a unit matrix, $\mathbf{D}_k^{[1]}$ and $\mathbf{D}_k^{[2]} \in \mathcal{R}^{N_k\times N_k}$ are the matrices of $\frac{\partial}{\partial Q_k}$ and $\frac{\partial^2}{\partial Q_k^2}$ in DVR. In Hermite-DVR $\mathbf{D}_k^{[1]}$ and $\mathbf{D}_k^{[2]}$ are asymmetric and symmetric matrices, respectively. For convenience, let us introduce the notation $\mathfrak{N}_l = \prod_{j=1}^{l-1} N_j$. It is also useful to introduce a composite index, $r$, that can be expressed as $r = 1+\sum_{k=1}^{3N-6}(r_k-1)\mathfrak{N}_k$ using the subindexes $(r_1, r_2, \ldots, r_{3N-6})$. The matrix-vector multiplication can then be described in detail as follows.

Initialization: $a := 0$, $\mathbf{b} := \mathbf{0}$, $\mathbf{c} := \mathbf{0}$, $\mathbf{y}_\alpha := \mathbf{0}$ $(\alpha = x, y, z)$.

**(a)** Computation of the term $\left(\frac{1}{2}\sum_{k=1}^{3N-6} \mathbf{P}_k^2 + \mathbf{V}'\right)\mathbf{x}$

**Do** $r = 1, \ldots, \mathcal{N}$ $\leftarrow$ OpenMP

$$\mathbf{y}[r] = \mathbf{V}'[r]\ \mathbf{x}[r] + \frac{1}{2}\sum_{k=1}^{3N-6}\sum_{j=1}^{N_k} \mathbf{D}_k^{[2]}[r_k, j]\ \mathbf{x}[r + (j - r_k)\mathfrak{N}_k)]$$

**End do**

**(b)** Computation of the term $\frac{1}{2}\sum_{\alpha\beta} \boldsymbol{\pi}_\alpha \boldsymbol{\mu}_{\alpha\beta} \boldsymbol{\pi}_\beta \mathbf{x}$

**Do** $r = 1, \ldots, \mathcal{N}$ $\leftarrow$ OpenMP

**Do** $l = 1, \ldots, 3N - 6$

$$a = \sum_{j=1}^{N_l} \mathbf{D}_l^{[1]}[r_l, j]\ \mathbf{x}[r + (j - r_l)\mathfrak{N}_l]$$

$$\mathbf{y}_\alpha[r] = \mathbf{y}_\alpha[r] + \left(\sum_{k=1}^{3N-6} \zeta_{kl}^\alpha\ q[k, r_k]\right) a, \quad \alpha = x, y, z$$

**End do**

**End do**

**Do** $r = 1, \ldots, \mathcal{N}$ $\leftarrow$ OpenMP

$a = 0$

**Do** $l = 1, \ldots, 3N - 6$

$$b_{\alpha\beta} = \sum_{j=1}^{N_l} \boldsymbol{\mu}_{\alpha\beta}[r+(j-r_l)\mathfrak{N}_l]\ \mathbf{y}_\beta[r+(j-r_l)\mathfrak{N}_l], \quad \alpha, \beta = x, y, z$$

$$c_\alpha = \sum_{j=1}^{N_l} \mathbf{D}_l^{[1]}[r_l, j]\ (b_{\alpha x} + b_{\alpha y} + b_{\alpha z}), \quad \alpha = x, y, z$$

$$a = a + \sum_\alpha \left(\sum_{k=1}^{3N-6} \zeta_{kl}^\alpha\ q[k, r_k]\right) c_\alpha$$

**End do**

$\mathbf{y}[r] = \mathbf{y}[r] - a/2$

**End do**

where the working variables and arrays $a \in \mathcal{R}$, $\mathbf{b} \in \mathcal{R}^{3\times3}$, $\mathbf{c} \in \mathcal{R}^3$, $\mathbf{y}_\alpha \in \mathcal{R}^{\mathcal{N}}$ $(\alpha = x, y, z)$ were introduced.

This matrix-vector multiplication algorithm requires the storage of $10\mathcal{N}$ 64-bit real numbers. The favorable property of this algorithm is based on the fact that the multiplication with the matrix $\boldsymbol{\pi}_\alpha$ can be carried out only by using

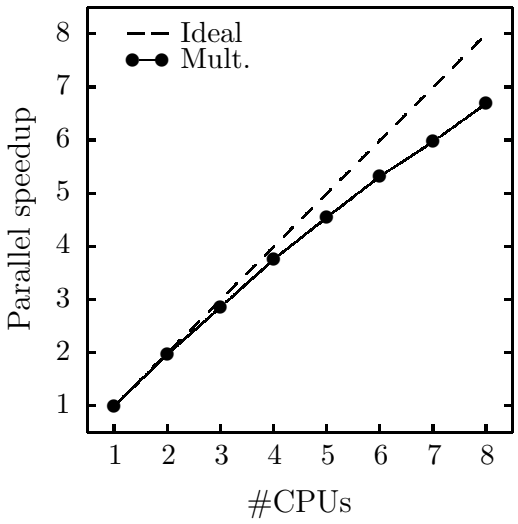


Figure 4.1: Parallel speedup of the multiplication of the Hamiltonian matrix with a vector as implemented in DEWE and using OpenMP.[71] Results are obtained for the case of $CH_4$ using 6 grid points on each vibrational degree of freedom, which corresponds to a Hamiltonian matrix of the size of $10\,077\,696 \times 10\,077\,696$. A Supermicro server equipped with two Intel Quad-Core Xeon 2.0 GHz processors was employed in the computations.

the $\zeta_{kl}^{\alpha}$ elements, the quadrature points, and the $\mathbf{D}_l^{[1]}$ and $\mathbf{D}_k^{[2]}$ matrices, which have negligible storage requirements. The number of multiplicative operations is $(1 + 12D(D+1) + 14DN')\mathcal{N}$, where $D = 3N - 6$, and $N'$ is a representative number for the number of points along a vibrational degree of freedom ($N_1, N_2, \ldots, N_{3N-6}$ can have different values), and $\mathcal{N}$ is the size of the direct-product grid. Lanczos vectors, each of size $\mathcal{N}$, spanning the Krylov subspace (see Section 2.4 and Chapter 6) are stored on the hard disk.

In the matrix-vector multiplication algorithm the main loop is organized for the elements of the product vector, which is thus computed directly (not iteratively). This makes our algorithm straightforwardly parallelizable with OpenMP[71] (as indicated on the sketch of the algorithm). The parallel speed-up on a Supermicro server machine equipped with two quad-core Xeon processors, the largest computer available to me, is presented on Figure 4.1. Up to four cores the speedup is nearly ideal. Above four cores the declination of the curve from the ideal one can be explained by the properties of the architecture.

## 4.4 Advantages and limitations of the DEWE program

Due to the universal form of the Eckart–Watson Hamiltonian,[14] Eq. (4.1), the DEWE protocol can be used to compute eigenpairs of semi-rigid molecules with arbitrary bonding arrangements without the introduction of any kind of numerical approximation. Due to the favorable properties of the DVR, inclusion of the PES expressed in arbitrarily chosen coordinates is numerically exact.

In spite of the fact that DEWE uses a direct-product DVR grid, the ideal combination of the Hermite polynomials used to construct the DVR and normal coordinates used to express the vibrational Hamiltonian allow the computation of many numerically exact eigenvalues and eigenfunctions of small- to medium-sized molecules using sophisticated eigensolver techniques (see Chapter 6) on nowadays standard server machines.

An efficient matrix-vector multiplication scheme specifically developed for the Eckart–Watson Hamiltonian has been presented. Multiplication of the Hamiltonian matrix and a vector is the most CPU-intensive part of variational computations using a direct-product grid and an iterative eigensolver. Therefore, an algorithm parallelized with OpenMP[71] was developed.

The DEWE approach has two serious deficiencies. First, the Eckart–Watson Hamiltonian given in Eqs. (4.1) and (4.6) is singular at linear instantaneous geometries of the molecule. This is due to the fact that as the coordinates approach their values at linear geometries certain elements of the generalized inverse inertia tensor, $\boldsymbol{\mu}$, tend to infinity. This behavior is also related to the fact that for linear geometries the definition of the Eckart frame fails (see Section 2.1.1). In general, this singularity problem could be handled by choosing basis functions which vanish fast enough approaching the singular region.[3] However, Watson's rectilinear coordinates (normal coordinates) are coupled in the singular region, thus it is not straightforward to find an appropriate basis of direct product form. The singularity problem shows up for molecules whose vibrations significantly sample linear configurations,

for instance, most of the triatomics and quasi-linear larger species. In most four or especially in the case of five- and six-atomic molecules, this problem does not arise.

In short, the Eckart–Watson Hamiltonian is an excellent choice for the description of semi-rigid molecules with a single minimum on the PES. However, the rectilinear nature of internal coordinates and the Eckart body-fixed frame, which favors the neighborhood of the chosen reference structure, makes any approach based on the Eckart–Watson Hamiltonian inefficient for the description of molecules having large amplitude internal motions.

In the next Chapter, an algorithm and computer code is presented in which these two deficiencies are eliminated, while keeping the universal context of the treatment.

# Chapter 5

# GENIUSH: Numerical construction of the kinetic energy matrix

The algorithm and computer code presented in this chapter overcomes the main deficiencies of DEWE and any implementation based on the Watson Hamiltonian using the Eckart frame. The main idea of this universal method is that Hamiltonians given in Eqs. (3.9) or (3.11) are not rearranged further, but their matrix representation is inserted directly into an eigensolver dealing explicitly only with the universal $G_{kl}$, $\tilde{g}$, and $U$ quantities. This allows one to write a universal, fully numerical computer code. In each application the $G_{kl}$, $\tilde{g}$, and $U$ quantities, specific for the chosen body-fixed frame and internal coordinates, are determined numerically. Such an algorithm and the corresponding computer code is able to surmount the deficiencies of DEWE discussed in Chapter 4, while trying to keep its advantages, especially the intention of universality and the black-box nature.

In this chapter, I present (a) the theory behind an approach leading toward a black-box-type procedure to compute rovibrational energy levels and wave functions, with special emphasis on the numerical evaluation of the kinetic energy matrix (Section 5.1), (b) a carefully tested implementation of this procedure in a computer code, built upon the use of the discrete variable representation[50,51] and a direct-product

basis, especially useful when a large number of eigenstates is to be computed from the resulting sparse Hamiltonian of special structure (Sections 5.2–5.3), and (c) thorough numerical tests and results on simple model-type molecular systems, water, ammonia, and methane, in order to demonstrate the flexibility and utility of the code (Section 5.4). This algorithm and computer code is called GENIUSH, in reference to its main characteristics: General (ro)vibrational code with Numerical, Internal-coordinate, User-Specified Hamiltonians.[34] Indeed, GENIUSH is able to compute eigenpairs of a (ro)vibrational operator corresponding to any body-fixed frame and internal coordinates defined by the user, either in full or reduced vibrational dimensionality. Furthermore, inclusion of the user-defined representation of the PES is numerically exact.

## 5.1 Theoretical details

The GENIUSH approach is based on the most universal forms of the (ro)vibrational Hamiltonian expressed in internal coordinates which is discussed in detail in Chapter 3. The corresponding vibration-only parts, which are considered here, can be written in the Podolsky-form, $\hat{H}^{\mathrm{vP}}$, given in Eq. (3.9), or in a "rearranged form", $\hat{H}^{\mathrm{vR}}$, given in Eq. (3.11). From a theoretical point of view the Podolsky- and the rearranged forms of the (ro)vibrational Hamiltonian are equivalent; however, their numerical behavior can be quite different.

Both the $\hat{H}^{\mathrm{vP}}$ and $\hat{H}^{\mathrm{vR}}$ forms are valid for any choice of the body-fixed frame and internal coordinates. The actual choice of these coordinates determines the values of the $\mathbf{g}$ or $\mathbf{G}$ matrices. In what follows the possible constructions of this central quantity, $\mathbf{g}$, and the related $\mathbf{G}$, $\tilde{g}$, and $U$ terms are considered.

### 5.1.1 Formulation of the g and G matrices

#### t-vector formalism

The relationship between Cartesian coordinates in the laboratory-fixed frame, $X_{i\alpha}$, and Cartesian coordinates in the body-fixed frame, $x_{ia}$, is given by

$$X_{i\alpha} = X_{\alpha}^{\mathrm{NCM}} + \sum_{a} C_{\alpha a} x_{ia}, \tag{5.1}$$

where $x_{ia}(q_1, q_2, \ldots, q_D)$ denotes the Cartesian coordinates of the $i$th nucleus in the body-fixed frame with the axis $a = x, y, z$, while $\mathbf{C}(\phi, \theta, \chi)$ denotes the (orthogonal) direction cosine matrix between the laboratory-fixed and the body-fixed frames. The so-called **t**-vectors[37,72] are now introduced as

$$t'_{i\alpha k} = \frac{\partial X_{i\alpha}}{\partial q_k} \quad \text{and} \quad t_{iak} = \sum_{\alpha} C_{\alpha a} t'_{i\alpha k}, \quad k = 1, 2, \ldots, D+6. \tag{5.2}$$

$$\tag{5.3}$$

It can be demonstrated[27] that the translational and rotational **t**-vectors are

$$t_{iak+D+3} = \delta_{ak}, \quad \text{and} \quad t_{iak+D} = (\vec{e}_k \times \vec{x}_i)_a, \qquad k = 1(x), 2(y), 3(z), \tag{5.4}$$

where $\delta_{ak}$ is the Kronecker delta symbol, and $\vec{e}_k$ denotes the unit vector pointing along the $k$th axis of the body-fixed frame and the vibrational **t**-vectors can be expressed as

$$t_{iak} = \frac{\partial x_{ia}}{\partial q_k}, \quad k = 1, 2, \ldots, D. \tag{5.5}$$

Elements of the **g** matrix can now be given in terms of the **t**-vectors as

$$g_{kl} = \sum_{i=1}^{N} m_i \sum_{a} t_{iak} t_{ial} = \sum_{i=1}^{N} m_i \mathbf{t}_{ik}^{\mathrm{T}} \mathbf{t}_{il}. \tag{5.6}$$

It follows from Eq. (5.6) that **g** (and also $\mathbf{G} = \mathbf{g}^{-1}$) is specified entirely by the actual values of the internal coordinates and the definition of the body-fixed frame.

**s-vector formalism**

A possible construction of the **G** matrix is offered by its definition introduced below Eq. (3.5) using the **t** vectors. An alternative formulation, based on the chain rule, is often used,

$$G_{kl} = \sum_{i=1}^{N} \frac{1}{m_i} \sum_{\alpha} \frac{\partial q_k}{\partial X_{i\alpha}} \frac{\partial q_l}{\partial X_{i\alpha}}, \tag{5.7}$$

which is the well-known El'yashevich–Wilson[42] **G** matrix. Similarly to the **t** vectors [Eq. (5.2)], the so-called **s** vectors[42] are defined as

$$s'_{i\alpha k} = \frac{\partial q_k}{\partial X_{i\alpha}} \quad \text{and} \quad s_{iak} = \sum_{\alpha} C_{\alpha a} s'_{i\alpha k}, \quad k = 1, 2, \ldots, 3N. \tag{5.8}$$

It can be shown[27] that the vibrational **s** vectors assume the form

$$s_{iak} = \frac{\partial q_k}{\partial x_{ia}}. \tag{5.9}$$

A detailed procedure for the evaluation of translational and rotational **s** vectors can be found in Ref. 27, which relies only on the translational and rotational **t** vectors and the vibrational **s** vectors, but does not assume the knowledge of the vibrational **t** vectors. Finally, the **G** matrix can be written also in terms of the **s** vectors as

$$G_{kl} = \sum_{i=1}^{N} \frac{1}{m_i} \sum_{a} s_{iak} s_{ial} = \sum_{i=1}^{N} \frac{1}{m_i} \mathbf{s}_{ik}^{\mathrm{T}} \mathbf{s}_{il}. \tag{5.10}$$

From a theoretical point of view, the **t**- and **s**-vector formalisms are equivalent, but numerically the computation of either the $\frac{\partial x_{ia}}{\partial q_k}$- or the $\frac{\partial q_k}{\partial x_{ia}}$-type derivatives can be more favorable.

### 5.1.2 Reduced-dimensional vibrational models

In nuclear motion computation of larger systems approximations based on physical considerations must often be introduced, yielding effective Hamiltonians. As inspired

by the given application, certain types of internal coordinates may be decoupled from the rest.

Let us consider $3N-6$ internal coordinates, out of which there are only $D < 3N-6$ active variables $(q_1, q_2, \ldots, q_D)$ in our model, and the rest of the coordinates $(\rho_1, \rho_2, \ldots, \rho_{3N-6-D})$ are fixed at a given value (or are prescribed functions of the active coordinates). In classical mechanics, constraining coordinates $\rho_i$ is equivalent to choosing $\dot{\rho}_i = 0$ $(i = 1, 2, \ldots, 3N-6-D)$. The classical Lagrangian of such a constrained model is already given in Eq. (3.2) with $D < 3N-6$. This is equivalent to deleting rows and columns corresponding to the constrained coordinates in the full $\mathbf{g} \in \mathcal{R}^{(3N-3)\times(3N-3)}$ (reduction in $\mathbf{g}$).

Another possible approximation to the full-dimensional problem can be introduced if those rows and columns of the full dimensional $\mathbf{G} \in \mathcal{R}^{(3N-3)\times(3N-3)}$ matrix are deleted which correspond to the constrained coordinates (reduction in $\mathbf{G}$).

Constrained models constructed by reducing the $\mathbf{g}$ as well as the $\mathbf{G}$ matrices will be presented later. It is perhaps worth pointing out that the two reduction strategies in general provide different models of the system, and thus numerically different results.

## 5.2 DVR of the vibrational Hamiltonian

In what follows the matrix representations of $\hat{H}^{\mathrm{vP}}$ and $\hat{H}^{\mathrm{vR}}$ in DVR are presented and difficulties of the numerical construction of the kinetic energy terms are discussed.

In this work, Hermite-DVR, PO-DVR and Legendre-DVR were used, as described in Section 2.3. To construct PO-DVR, the one-dimensional operator

$$\hat{h}_k^{\mathrm{1D}} = \frac{1}{2}\hat{p}_k^{\dagger} G_{kk}(q_k; \mathbf{q}'_{\mathrm{e}})\hat{p}_k + V(q_k; \mathbf{q}'_{\mathrm{e}}), \quad k = 1, 2, \ldots, D \tag{5.11}$$

was used, as it provides an excellent choice for simplifying the full operator given in Eq. (3.11), where all the coordinates, except the $k$th active mode, are fixed at their equilibrium values. The extrapotential term is left out from this simplified form.

Due to the use of a DVR coupled with a direct-product grid, the resulting Hamiltonian matrix is very sparse but is often of extreme size. To avoid the explicit construction of this large Hamiltonian matrix or even storage of its nonzero elements, a Lanczos iterative eigensolver is used, which requires only the multiplication of the Hamiltonian matrix with a vector. I worked out an efficient matrix-vector multiplication scheme parallelizable with OpenMP.[71] Fundamental concepts of the Lanczos eigensolver were introduced in Section 2.4 and more sophisticated techniques are discussed in detail in Chapter 6.

### 5.2.1 Numerical construction of the kinetic energy

In order to construct the matrix of the kinetic energy operator corresponding to arbitrarily chosen body-fixed frames and internal coordinates, only the numerical values of $\mathbf{G}$, $\tilde{g}$, and $U$ are required at the quadrature points. These quantities are constructed point by point on the DVR grid using directly the (ro)vibrational Hamiltonian operators in the Podolsky-form, Eq. (3.9), or in the rearranged form, Eq. (3.11). The fact that in DVR any quantity depending only on the coordinates can be represented as a diagonal matrix makes the present approach efficient without the need of introducing any approximations in the kinetic energy terms.

**t-vector formalism** The rotational and vibrational $\mathbf{t}$-vectors introduced in Eqs. (5.4) and (5.5) are used to construct $\mathbf{g}$, the central quantity in the present treatment. It is inverted to obtain $\mathbf{G} = \mathbf{g}^{-1} \in \mathcal{R}^{(D+3)\times(D+3)}$. If the vibration-only operator is used, it is sufficient to evaluate the vibrational subblock of the $\mathbf{G}$ matrix.

If the Podolsky-form of the Hamiltonian, Eq. (3.9), is employed, $\tilde{g} = \det \mathbf{g}$ is left to be computed, which is numerically straightforward. Within this formalism only $\frac{\partial \mathbf{x}_i}{\partial q_k}$, the first derivatives of the body-fixed Cartesian coordinates in terms of the internal coordinates, are required. These derivatives can be evaluated either by numerical (using standard double-precision arithmetic) or analytic differentiation.

If the rearranged form of the Hamiltonian, Eq. (3.11), is used, the extrapotential term, $U$, must also be computed. In full-dimensional models or reduced-dimensional models constructed by reduction in $\mathbf{g}$, it is better to use Eq. (3.12) for $U$. In reduced-

dimensional models constructed by reduction in $\mathbf{G}$, it is more straightforward to use the formulation of Eq. (3.13). My numerical tests showed that brute-force numerical differentiation of the formulae in Eqs. (3.12) and (3.13) may introduce numerical instabilities in the treatment. In order to avoid such numerical instabilities each term in Eqs. (3.12) and (3.13) are expressed numerically (not necessarily in a symbolic form) in terms of the first, second and third derivatives of the body-fixed Cartesian coordinates with respect to internal coordinates, $\frac{\partial \mathbf{x}_i}{\partial q_k}$, $\frac{\partial^2 \mathbf{x}_i}{\partial q_k \partial q_l}$, and $\frac{\partial^3 \mathbf{x}_i}{\partial q_k \partial q_l \partial q_m}$, which are evaluated in an accurate procedure. An accuracy of $< 0.01$ cm$^{-1}$ in the eigenvalues can be firmly achieved only if the higher-order derivatives of the body-fixed Cartesian coordinates in terms of internal coordinates are evaluated by analytic differentiation using standard double precision arithmetic (64-bit reals) or by numerical differentiation using increased numerical precision (128-bit reals). Details of the approach are discussed in Appendix A. In the current version of GENIUSH analytic derivatives are available for an arbitrary set of internal coordinates defined with a Z-matrix and an $xxy$ (scattering) body-fixed frame introduced in Section 2.1.1. Any other coordinate definition can be treated by (quadruple precision) numerical derivatives.

**s-vector formalism** The **s**-vector formalism offers an alternative to the **t**-vector formalism toward the numerical use of kinetic energy operators. The extrapotential term, $U$, can be formulated entirely in terms of **s**-vectors, as it was given in Ref. 37. In this expression of $U$ first derivatives of the rotational **s**-vectors and first and second derivatives of the vibrational **s**-vectors in terms of internal coordinates appear.

After having studied the numerical behavior of the different possible formalisms in detail, I prefer to use the **t**-vector formalism over the **s**-vector formalism. In theory, the two representations are equivalent; however, technically the first requires the computation of $\frac{\partial x_{ia}}{\partial q_k}$, $\frac{\partial^2 x_{ia}}{\partial q_l \partial q_k}$, and $\frac{\partial^3 x_{ia}}{\partial q_m \partial q_l \partial q_k}$, whereas the second assumes the knowledge of $\frac{\partial q_k}{\partial x_{ia}}$, $\frac{\partial^2 q_k}{\partial q_l \partial x_{ia}}$, and $\frac{\partial^3 q_k}{\partial q_m \partial q_l \partial x_{ia}}$. To explain this preference, I note that (a) in the **s**-vector formalism, implementation of internal coordinates defined for ammonia in Section 5.4.2 using a dummy atom turned out to be numerically unstable, and (b) introduction of reduced-dimensional models having approximations in the $\mathbf{g}$ matrix is more straightforward in the **t**-vector formalism.

### 5.2.2 Numerical representation of the potential energy

Numerical inclusion of any representation of the PES is straightforward due to the favorable properties of DVR. There is no need to adapt a specific representation of the actual PES (Taylor expansion, $n$-mode representation, etc.). Inclusion of potentials with multiple minima separated by low-energy barriers is numerically exact, which is necessary for a reliable description of a molecular system with large amplitude motions.

### 5.2.3 The vibrational Hamiltonian in DVR

Matrix representations of the vibrational Hamiltonians given in Eqs. (3.9) and (3.11) are constructed on a (PO-)DVR direct-product grid. Matrices of the quantities depending only on the coordinates assume a simple diagonal form, *e.g.*,

$$(\mathbf{V})_{nm} = V(\xi_{1,n_1}, \xi_{2,n_2}, \ldots, \xi_{D,n_D}) \prod_{i=1}^{D} \delta_{n_i,m_i}, \tag{5.12}$$

$n, m = 1, 2, \ldots, \mathcal{N}$. The matrices of $\tilde{g}$, $U$, and $G_{kl}$ $(k, l = 1, 2, \ldots, 3N-3)$ are similarly constructed. Note that an unambiguous correspondence can be established between the index $n$ of the direct product grid and the subindexes $(n_1, n_2, \ldots, n_D)$ of the grid points of each vibrational degree of freedom, for instance $n = (n_1 - 1)\prod_{i=2}^{D} N_i + \ldots + (n_{D-1} - 1)N_D + n_D$.

To make the computation of the matrix elements more feasible, insert the truncated resolution of identity in Eq. (3.9) and in Eq. (3.11), resulting in

$$\mathbf{H}^{\mathrm{vP}} = \frac{1}{2} \sum_{kl=1}^{D} \tilde{\mathbf{g}}^{\mathbf{-1/4}} \mathbf{p}_k^{\dagger} \mathbf{G}_{kl} \tilde{\mathbf{g}}^{\mathbf{1/2}} \mathbf{p}_l \tilde{\mathbf{g}}^{(\mathbf{-1/4})} + \mathbf{V}, \tag{5.13}$$

and

$$\mathbf{H}^{\mathrm{vR}} = \frac{1}{2} \sum_{kl=1}^{D} \mathbf{p}_k^{\dagger} \mathbf{G}_{kl} \mathbf{p}_l + \mathbf{U} + \mathbf{V}, \tag{5.14}$$

where

$$(\mathbf{p}_k)_{nm} = -i \left(\mathbf{D}_k^{[1]}\right)_{n_k,m_k} (1 - \delta_{n_k,m_k}) \prod_{i=1,i\neq k}^{D} \delta_{n_i,m_i}, \tag{5.15}$$

and $\mathbf{D}_k^{[1]} \in \mathcal{R}^{N_k \times N_k}$ is the matrix of the differential operator $\frac{\partial}{\partial q_k}$ in DVR constructed by the transformation method (see Section 2.3).

## 5.3 Multiplication of the Hamiltonian matrix with a vector

In the Lanczos iterative eigensolver the most time-consuming step is the computation of the product of the Hamiltonian matrix with a vector, $\mathbf{y} = \mathbf{H}\mathbf{x}$. Thus, the efficient evaluation of $\mathbf{y}$ is crucial for the efficient computation of eigenpairs. Storage of the whole Hamiltonian matrix or even its non-zero elements in the main memory (or even on the hard disk) would be unfeasible already for a four-atomic application.

An efficient algorithm that avoids the storage of the Hamiltonian matrix and which can be parallelized with OpenMP[71] is based on the following considerations. The matrix-vector multiplication using $\mathbf{H}^{\mathrm{vP}}$ is computed as

$$\mathbf{y} = \mathbf{H}^{\mathrm{vP}}\mathbf{x} = \frac{1}{2}\tilde{\mathbf{g}}^{\mathbf{-1/4}} \sum_{k=1}^{D} \left( \mathbf{p}_k^{\dagger} \sum_{l=1}^{D} \left( \mathbf{G'}_{kl} \left( \mathbf{p}_l \mathbf{x'} \right) \right) \right) + \mathbf{V}\mathbf{x}, \quad \text{where} \tag{5.16}$$

$$\mathbf{G'}_{kl} = \mathbf{G}_{kl}\tilde{\mathbf{g}}^{\mathbf{1/2}} \quad \text{and} \quad \mathbf{x'} = \tilde{\mathbf{g}}^{\mathbf{-1/4}}\mathbf{x}. \tag{5.17}$$

Using $\mathbf{H}^{\mathrm{vR}}$, the multiplication should be done as

$$\mathbf{y} = \mathbf{H}^{\mathrm{vR}}\mathbf{x} = \frac{1}{2} \sum_{k=1}^{D} \left( \mathbf{p}_k^{\dagger} \sum_{l=1}^{D} \left( \mathbf{G}_{kl} \left( \mathbf{p}_l \mathbf{x} \right) \right) \right) + \left( \mathbf{U} + \mathbf{V} \right) \mathbf{x}, \tag{5.18}$$

where $\mathbf{G}_{kl}$ $(k, l = 1, 2, \ldots, D)$, $\tilde{\mathbf{g}}^{\mathbf{-1/4}}$, $\tilde{\mathbf{g}}^{\mathbf{1/2}}$, $\mathbf{U}$, and $\mathbf{V}$ are diagonal matrices. Furthermore, the special structure of $\mathbf{p}_k$, Eq. (5.15), due to the direct-product basis and

grid, can be exploited in the matrix-vector multiplication, $\mathbf{y}_k = \mathbf{p}_k\mathbf{x}$, as

$$\mathbf{y}_k[n + p\mathfrak{N}_k] = \sum_{j=1}^{N_k} \mathbf{D}_k^{[1]}[n_k + p, j] \cdot \mathbf{x}[n + (j - n_k)\mathfrak{N}_k)], \tag{5.19}$$

where $p = -(n_k - 1), \ldots, 0, \ldots, N_k - (n_k - 1)$, and $n = \sum_{k=1}^{D}(n_k - 1)\mathfrak{N}_k + 1$, where $\mathfrak{N}_k = \prod_{j=k+1}^{D} N_j$. Apart from the $\mathbf{x}$ and the product vectors, $\mathbf{y}_k$, only the small $\mathbf{D}_k^{[1]}$ matrices are stored. It is important to point out that using this multiplication scheme the elements of the product vector $\mathbf{y}_k$ are computed directly (not iteratively), which is required for the parallelization of this time-consuming step.

The total memory requirement of the algorithm using $\mathbf{H}^{\mathrm{vR}}$ corresponds to the storage of $\left(\frac{D(D+1)}{2} + D + 5\right)\mathcal{N}$ number of 64-bit reals, which corresponds to the storage of $\mathbf{G}_{kl} = \mathbf{G}_{lk}$ $(k, l = 1, 2, \ldots, D)$, $(\mathbf{U} + \mathbf{V})$, the $\mathbf{y}_l$ $(l = 1, 2, \ldots, D)$ scratch vectors, and further 4 working vectors of the size $\mathcal{N}$. If the Podolsky-form, $\mathbf{H}^{\mathrm{vP}}$, is used, an additional vector of size $\mathcal{N}$ must be stored in the main memory containing the elements of the diagonal $\tilde{\mathbf{g}}^{-\mathbf{1/4}}$ matrix. Lanczos vectors, each of size $\mathcal{N}$, spanning the Krylov subspace (see Section 2.4 and Chapter 6) are stored on the hard disk.

The number of iteration steps required to converge the Lanczos procedure is approximately proportional to the number of required eigenpairs. The scaling of the total CPU time in terms of the size of the direct product grid for $\mathbf{H}^{\mathrm{vR}}$ is $t_{\mathrm{CPU}} \sim$ [No. of required eigenpairs] $\times (1 + 2DN + D^2)\mathcal{N}$. If the Podolsky-form is employed, two additional vector-vector multiplications are required in each matrix-vector multiplication step.

## 5.4 Numerical results

In order to demonstrate the robustness and flexibility of the program GENIUSH, three-, four-, and five-atomic examples, both in full and reduced vibrational dimensionality, and using different sets of internal coordinates, are presented in the next sections. The actual choice of internal coordinates affects the convergence properties of the eigenpairs. In the following examples the rearranged form of the vibrational Hamiltonian, Eq. (3.11), is employed, if it is not otherwise stated.

Before giving details about the computations and their results, let us summarize how the vibrational model can be defined in the current version of the code GENIUSH.

First, Cartesian coordinates expressed in the chosen body-fixed frame must be specified in terms of the chosen set of internal coordinates. This work is helped by a Z-matrix reader implemented in GENIUSH based on the Z-matrix reader program developed by Lopata and Kiss,[43] which allows various definitions of simple internal coordinates. Furthermore, the three interatomic coordinates and the orthogonal Jacobi coordinates have also been implemented for the case of triatomic molecules. In general, any subroutine would be appropriate, which provides the Cartesian coordinates in the body-fixed frame in terms of internal coordinates.

Then, the active and constrained sets of coordinates are specified. An interval must be defined for grid points along each active vibrational coordinate. The position of the grid points can be optimized (PO-DVR). Otherwise, primitive scaled and shifted[7] Hermite-DVR or primitive Legendre-DVR points are used. If there are constrained coordinates, their constrained value also needs to be specified. If there are special mathematical requirements on the range of internal coordinates, *e.g.*, in the case of the three interatomic coordinates the triangle inequality, the range of internal coordinates is automatically tested. After construction of the direct-product grid, those grid points are omitted which do not fulfill the prescribed requirements, *e.g.*, on the ranges of coordinates. Furthermore, not only geometrical restrictions, but also energy (potential energy) requirements can be employed in order to reduce the number of grid points involved in the computation.

Then, the step size for the numerical differentiation is to be defined. If internal coordinates are defined within the framework of a Z-matrix, first, second, and third analytic derivatives are also available.

After appropriate choices have been made for all of the above options, the representation of the kinetic energy part is completely specified. The potential energy is obtained from electronic structure computations, and usually available as a force field or a (semi-)global PES (see Section 2.2) as implemented in a subroutine. In order to call this subroutine a user-supplied interface might be required, which con-

verts the values of the internal coordinates actually defined for the kinetic energy operator to the input coordinates of the potential energy subroutine. If the potential energy subroutine requires the Cartesian coordinates as input parameters, it can be automatically linked to GENIUSH.

### 5.4.1 Testing the accuracy: Full- and reduced-dimensional models of $H_2O$

$H_2{}^{16}O$ was extensively studied during the validation of the code GENIUSH for two reasons. First, accurate benchmark results in full vibrational dimensionality are easily available for this system.[6] Second, as the system is small, full- and reduced-dimensional calculations can be carried out very fast, and numerous internal coordinate choices are possible either in full or reduced dimensionality. It is important to emphasize that GENIUSH allows to perform all these computations within a single code, which constructs automatically the kinetic energy representation once the coordinates are defined. From a technical point of view, it is not straightforward to have a numerically robust implementation of such a universal protocol (Section 5.2.1 and Appendix A), if one is interested in the energy levels with spectroscopic accuracy, $< 0.01$ cm$^{-1}$, which corresponds typically to six or seven significant digits.

In the light of the numerical difficulties discussed, the accuracy and flexibility of the program were carefully tested. The most relevant results are collected in Tables 5.1 and 5.2. In all computations the CVRQD PES[9] and the corresponding nuclear masses were used. 3-dimensional benchmark data were obtained with the DOPI code[6,7] using the same PES and masses.

In Table 5.1 full 3D results obtained with GENIUSH using valence-, Jacobi-, and interatomic coordinates and an $xxy$ body-fixed frame are compared with benchmark data obtained with an independent code, DOPI.[6] To switch between the different sets of coordinates used, only the coordinate definition was changed, the representation of the Hamiltonian was generated automatically by the program.

The numerical results meet the fundamental physical expectation that the converged values of computed vibrational energy levels are independent of the actual

Table 5.1: ZPVE and the first 20 VBOs of $H_2{}^{16}O$, in $cm^{-1}$, obtained with GENIUSH using three different full, 3D models (V: valence coordinates, J: Jacobi coordinates, I: interatomic coordinates) and the CVRQD PES.[9]

| Label | DOPI[a] | $\tilde{\nu}$(3D,V)[b,c] | $\tilde{\nu}$(3D,J)[b,d] | $\tilde{\nu}$(3D,I)[b,e] | |
|---|---|---|---|---|---|
| (0 0 0) | 4638.31 | 4638.31 (0.00) | 4638.31 (0.00) | 4638.31 | (0.00) |
| (0 1 0) | 1595.08 | 1595.08 (0.00) | 1595.08 (0.00) | 1595.0$\underline{7}$ | (0.01) |
| (0 2 0) | 3152.20 | 3152.20 (0.00) | 3152.20 (0.00) | 3152.1$\underline{9}$ | (0.01) |
| (1 0 0) | 3657.05 | 3657.05 (0.00) | 3657.05 (0.00) | 3657.05 | (0.00) |
| (0 0 1) | 3755.73 | 3755.73 (0.00) | 3755.73 (0.00) | 3755.73 | (0.00) |
| (0 3 0) | 4667.57 | 4667.57 (0.00) | 4667.57 (0.00) | 4667.$\underline{47}$ | (0.10) |
| (1 1 0) | 5235.49 | 5235.49 (0.00) | 5235.49 (0.00) | 5235.49 | (0.00) |
| (0 1 1) | 5331.51 | 5331.51 (0.00) | 5331.51 (0.00) | 5331.51 | (0.00) |
| (0 4 0) | 6135.08 | 6135.08 (0.00) | 6135.08 (0.00) | 613$\underline{6.19}$ | (−1.11) |
| (1 2 0) | 6775.96 | 6775.96 (0.00) | 6775.96 (0.00) | 6775.9$\underline{1}$ | (0.05) |
| (0 2 1) | 6872.15 | 6872.15 (0.00) | 6872.15 (0.00) | 6872.1$\underline{4}$ | (0.01) |
| (2 0 0) | 7201.19 | 7201.19 (0.00) | 7201.19 (0.00) | 7201.19 | (0.00) |
| (1 0 1) | 7249.22 | 7249.22 (0.00) | 7249.22 (0.00) | 7249.22 | (0.00) |
| (0 0 2) | 7444.88 | 7444.88 (0.00) | 7444.88 (0.00) | 7444.88 | (0.00) |
| (0 5 0) | 7543.86 | 7543.86 (0.00) | 7543.86 (0.00) | 755$\underline{0.89}$ | (−7.03) |
| (1 3 0) | 8275.08 | 8275.08 (0.00) | 8275.08 (0.00) | 8275.$\underline{39}$ | (−0.31) |
| (0 3 1) | 8374.77 | 8374.77 (0.00) | 8374.77 (0.00) | 8374.75 | (0.02) |
| (2 1 0) | 8761.92 | 8761.92 (0.00) | 8761.92 (0.00) | 8761.93 | (−0.01) |
| (1 1 1) | 8807.03 | 8807.03 (0.00) | 8807.03 (0.00) | 8807.03 | (0.00) |
| (0 6 0) | 8872.17 | 8872.17 (0.00) | 8872.17 (0.00) | 89$\underline{42.88}$ | (−70.71) |
| (0 1 2) | 9000.39 | 9000.39 (0.00) | 9000.39 (0.00) | 9000.40 | (−0.01) |

[a] Converged 3D reference results were obtained with the DOPI algorithm.[6] Exactly the same CVRQD PES and nuclear masses were applied as in the GENIUSH calculations.

[b] Results obtained with GENIUSH. Nuclear masses $m_{\mathrm{H}} = 1.0072765$ u and $m_{\mathrm{O}} = 15.990526$ u, and an $xy$ body-fixed frame were used throughout the calculations. Underlined digits did not converge upon the increase of the basis size due to the singularity of the Hamiltonian. Deviations from results of DOPI are given in parentheses, $(\tilde{\nu}(\mathrm{DOPI}) - \tilde{\nu})$.

[c] The active internal coordinates $r_{1\mathrm{v}}$, $r_{2\mathrm{v}}$, $\cos\theta_{\mathrm{v}}$, and the Podolsky-form of the vibrational Hamiltonian, given in Eq. (3.9), were used. (30,30) PO-DVR grid points, each optimized on a primitive grid of 80 points and the interval $[0.5, 2.5]$ Å were used for the $r_{1\mathrm{v}}$ and $r_{2\mathrm{v}}$ coordinates, and 30 primitive Legendre-DVR grid points were utilized for $\cos\theta_{\mathrm{v}}$.

[d] The active internal coordinates $r_{1\mathrm{j}}$, $r_{2\mathrm{j}}$, $\cos\theta_{\mathrm{j}}$, and the Podolsky-form of the vibrational Hamiltonian, given in Eq. (3.9), were used. (30,30) PO-DVR grid points, each optimized on a primitive grid of 80 points and the interval $[0.5, 2.5]$ Å were used for the $r_{1\mathrm{j}}$ and $r_{2\mathrm{j}}$ coordinates, and 30 primitive Legendre-DVR grid points were utilized for $\cos\theta_{\mathrm{j}}$.

[e] The active internal coordinates were $r_1$, $r_2$, and $r_3$. A (40,40,40) primitive grid was used on $r_1, r_2 \in [0.6, 1.5]$ Å, and $r_3 \in [1.0, 2.5]$ Å intervals.

Table 5.2: ZPVE and VBOs of $H_2{}^{16}O$, in $cm^{-1}$, obtained with GENIUSH using 2D vibrational models (J: Jacobi coordinates, I: interatomic coordinates, **g**: reduction in the **g**-matrix, **G**: reduction in the **G**-matrix) and the CVRQD PES.[9]

| Label | $\tilde{\nu}$(3D)[a] | $\tilde{\nu}$(2D,J,**g**)[b,c,e] | | $\tilde{\nu}$(2D,I,**g**)[b,d,e] | | $\tilde{\nu}$(2D,J,**G**)[b,c,f] | | $\tilde{\nu}$(2D,I,**G**)[b,d,f] | |
|---|---|---|---|---|---|---|---|---|---|
| (0 0 0) | 4638.31 | 2723.50 | – | 2723.50 | – | 2723.50 | – | 3018.0$\underline{4}$ | – |
| (0 1 0) | 1595.08 | 1616.08 | (−21.00) | 1616.08 | (−21.00) | 1616.08 | (−21.00) | 2182.$\underline{56}$ | (−587.48) |
| (0 2 0) | 3152.20 | 3197.45 | (−45.26) | 3197.45 | (−45.26) | 3197.45 | (−45.26) | 3697.43 | (−545.23) |
| (0 0 1) | 3755.73 | 3711.56 | (44.17) | 3711.56 | (44.17) | 3711.56 | (44.17) | 438$\underline{6.53}$ | (−630.80) |
| (0 3 0) | 4667.57 | 4739.03 | (−71.46) | 4739.0$\underline{6}$ | (−71.49) | 4739.03 | (−71.46) | 5830.$\underline{27}$ | (−1162.70) |
| (0 1 1) | 5331.51 | 5309.39 | (22.12) | 5309.39 | (22.12) | 5309.39 | (22.12) | 663$\underline{3.76}$ | (−1302.25) |
| (0 4 0) | 6135.08 | 6232.92 | (−97.84) | 6233.4$\underline{3}$ | (−98.35) | 6232.92 | (−97.84) | 7231.02 | (−1095.94) |
| (0 2 1) | 6872.15 | 6874.32 | (−2.17) | 6874.3$\underline{3}$ | (−2.18) | 6874.32 | (−2.17) | 798$\underline{2.54}$ | (−1110.39) |
| (0 0 2) | 7444.88 | 7257.58 | (187.31) | 7257.58 | (187.31) | 7257.58 | (187.31) | 895$\underline{0.92}$ | (−1506.04) |
| (0 5 0) | 7543.86 | 7665.34 | (−121.49) | 7671.$\underline{84}$ | (−127.98) | 7665.34 | (−121.49) | 9314.$\underline{84}$ | (−1770.99) |
| (0 3 1) | 8374.77 | 8402.03 | (−27.26) | 8402.1$\underline{4}$ | (−27.37) | 8402.03 | (−27.26) | 1017$\underline{1.87}$ | (−1797.10) |

[a] Converged 3D results obtained with the GENIUSH.
[b] 2D results obtained with GENIUSH. $r_1$(HO)= 0.95782 Å was fixed throughout the computations. Nuclear masses, $m_H = 1.0072765$ u and $m_O = 15.990526$ u, and an *xxy* body-fixed frame were used. Underlined digits did not converge upon the increase of the basis size due to the singularity of the Hamiltonian. Deviations from 3D results are given in parentheses, $(\tilde{\nu}(3D) - \tilde{\nu}(2D))$.
[c] The active internal coordinates were the second Jacobi distance, $r_{2j}$ and the Jacobi angle, $\cos\theta_j$ in the Podolsky-form of the vibrational Hamiltonian, given in Eq. (3.9), used here. 30 PO-DVR grid points, optimized on a grid of 80 points and the interval $[0.3, 2.5]$ Å, were used for $r_{2j}$, and 30 primitive Legendre-DVR points were used for the $\cos\theta_j$ coordinate.
[d] The active internal coordinates were $r_2$(HO) and $r_3$(HH). (30,30) primitive grid was used on $r_2 \in [0.3, 2.0]$ Å and $r_3 \in [0.8, 3.2]$ Å intervals.
[e] 2D models constructed with reduction in **g**.
[f] 2D models constructed with reduction in **G**.

coordinate representation, and they also reproduce the benchmark data. However, it is important to point out that the convergence properties of the different sets of coordinates are different. The required number of grid points and the computational effort to achieve an expected accuracy differ significantly. In this case, the convergence is fastest for the Jacobi coordinates.

Table 5.2 contains the most interesting reduced-dimensional test results. Fixing one of the O–H distances and letting the rest of the molecule move freely does not provide a numerically valuable approximation to the 3-dimensional results. Nevertheless, important theoretical relationships are reflected by these numerical results

Table 5.3: Z-matrix representation of the internal coordinates of $NH_3$.

| | | | | | | |
|---|---|---|---|---|---|---|
| N | | | | | | |
| X | N | 1.0 | | | | |
| H1 | N | $r_1$ | X | $\theta$ | | |
| H2 | N | $r_2$ | X | $\theta$ | H1 | $\beta_1$ |
| H3 | N | $r_3$ | X | $\theta$ | H1 | $-\beta_2$ |

– they provide a valuable tool for checking the accuracy and consistency of reduced-dimensional models automatically constructed by GENIUSH for a given choice of coordinates.

Reductions introduced in $\mathbf{g}$ and $\mathbf{G}$ (see Section 5.1.2) were studied in these 2-dimensional numerical examples. Theoretically, the reduction in $\mathbf{g}$ corresponds to fixing the constrained coordinates at given values, while reduction in $\mathbf{G}$ is merely another possible mathematical route to neglect the coupling terms between sets of coordinates. The results presented in Table 5.2 reflect this difference. If the reduction is introduced in $\mathbf{g}$, the converged energy levels are independent of the actual choice of coordinates if the same constraints are introduced. However, if the $\mathbf{G}$ matrix is used to construct a reduced-dimensional model, the results do depend on the choice of the active coordinates even if the same coordinates were fixed at a given value. Thus, these numerical results exemplify the preference of constructing reduced-dimensional models via the $\mathbf{g}$ matrix.

Due to the difference of reduction in $\mathbf{g}$ and $\mathbf{G}$ the results of the two reduction strategies are, in general, different even if the same set of coordinates is used. The case of Jacobi coordinates with constraining the first Jacobi distance to a given value is an exception. This specific coordinate is decoupled from the rest both in the vibrational and in the rovibrational block of the $\mathbf{g}$-($\mathbf{G}$-)matrix. The special behavior of this coordinate is reproduced by the automatically constructed reduced dimensional results of GENIUSH.

### 5.4.2 Testing the flexibility: Full- and reduced-dimensional models of $NH_3$

The inversion-tunneling motion makes ammonia an interesting molecule for spectroscopic and dynamical studies.[73,74,75,76] Reliable computations are straightforward only with properly chosen body-fixed frames and curvilinear internal coordinates. In the present computations the body-fixed frame was the $xy$ (scattering) frame and the primitive internal coordinates are given in Table 5.3. A dummy atom, X, is introduced allowing the definition of a symmetric inversion coordinate, $\theta$.[29] Symmetry-adapted stretching coordinates are introduced in terms of the primitive stretching coordinates as

$$s_1 = \frac{1}{\sqrt{3}}(r_1 + r_2 + r_3), \quad s_2 = \frac{1}{\sqrt{6}}(2r_1 - r_2 - r_3), \quad s_3 = \frac{1}{\sqrt{2}}(r_2 - r_3).$$

It is worth emphasizing that only the number of degrees of freedom and the coordinate definitions were changed to specify the kinetic energy term of the vibrational Hamiltonian for ammonia, which was then automatically generated by the program. In all computations the "refined" PES of Ref. 76 and the corresponding atomic masses were employed.

The effect of couplings of stretching coordinates to the tunneling-inversion motion was monitored through the comparison of inversion splittings, resulting from the low inversion barrier,[77,78] obtained from 1-, 2-, 4-, and (full) 6D vibrational models.

The full, 6D variational results obtained with GENIUSH for $^{14}NH_3$ are presented in Table 5.4. For comparison, approximate variational results are also given there, taken from the reference publication of the actually employed PES.[76] Our converged results (convergence on the order of 0.05 $cm^{-1}$) up to $\sim$6000 $cm^{-1}$ are the first benchmark results with this PES, without introducing any approximation in the variational treatment. They improve the approximate variational results of Ref. 76 only slightly for the first few VBOs; however, for higher-lying vibrational levels substantial improvements can be observed.

In Table 5.5 1-, 2-, and 4D reduced inversion models are compared with our full, 6D benchmark results. Reduced-dimensional models were constructed by reducing

Table 5.4: ZPVE and VBOs of $^{14}NH_3$, in $cm^{-1}$, obtained with GENIUSH using a full, 6D vibrational model and the "refined" PES of ammonia[76] and compared to approximate variational results.[76]

| Label | | $\tilde{\nu}$(6D)[a] | $\delta$[b] | $\Delta$[c] | Label | | $\tilde{\nu}$(6D)[a] | $\delta$[b] | $\Delta$[c] |
|---|---|---|---|---|---|---|---|---|---|
| ZPVE | $A_1'$ | 7436.82 | | −[d] | $2v_2$+$2v_4$ | $A_1'$ | 4753.63 | | (1.35) |
| ZPVE | $A_2''$ | 0.79 | | (0.00) | $2v_2$+$2v_4$ | $E_1'$ | 4772.16 | [0.07] | (1.51) |
| $v_2$ | $A_1'$ | 932.41 | | (0.05) | $3v_4$ | $E_1'$ | 4795.89 | [0.07] | (2.84) |
| $v_2$ | $A_2''$ | 968.15 | | (−0.01) | $3v_4$ | $E_1''$ | 4798.17 | [0.08] | (2.82) |
| $2v_2$ | $A_1'$ | 1597.26 | | (0.12) | $3v_4$ | $A_1'$ | 4838.55 | | (2.22) |
| $v_4$ | $E_1'$ | 1625.62 | [0.00] | (0.60) | $3v_4$ | $A_2'$ | 4838.77 | | (2.92) |
| $v_4$ | $E_1''$ | 1626.73 | [0.00] | (0.60) | $3v_4$ | $A_2''$ | 4840.52 | | (2.21) |
| $2v_2$ | $A_2''$ | 1882.18 | | (−0.09) | $3v_4$ | $A_1''$ | 4840.82 | | (2.88) |
| $3v_2$ | $A_1'$ | 2384.20 | | (−0.14) | $v_3+v_4$ | $E_1'$ | 4954.07 | [0.01] | (1.30) |
| $v_2+v_4$ | $E_1'$ | 2539.60 | [0.00] | (0.67) | $v_3+v_4$ | $E_1''$ | 4955.33 | [0.01] | (1.30) |
| $v_2+v_4$ | $E_1''$ | 2585.38 | [0.00] | (0.56) | $v_1$+$2v_2$ | $A_1'$ | 4999.19 | | (0.17) |
| $3v_2$ | $A_2''$ | 2895.74 | | (−0.24) | $v_1+v_4$ | $A_2'$ | 5049.16 | | (0.77) |
| $2v_2+v_4$ | $E_1'$ | 3189.11 | [0.00] | (0.69) | $v_1+v_4$ | $A_1''$ | 5049.81 | | (0.77) |
| $2v_4$ | $A_1'$ | 3214.45 | | (1.10) | $v_3+v_4$ | $E_1'$ | 5051.77 | [0.00] | (0.54) |
| $2v_4$ | $A_2''$ | 3216.14 | | (1.08) | $v_3+v_4$ | $E_1''$ | 5052.37 | [0.00] | (0.54) |
| $2v_4$ | $E_1'$ | 3238.55 | [0.01] | (1.31) | $v_3+v_4$ | $A_2''$ | 5065.62 | | (0.70) |
| $2v_4$ | $E_1''$ | 3240.05 | [0.01] | (1.30) | $v_3+v_4$ | $A_1'$ | 5065.63 | | (0.70) |
| $v_1$ | $A_1'$ | 3335.77 | | (0.27) | $2v_2$+$2v_4$ | $A_2''$ | 5092.85 | | (0.59) |
| $v_1$ | $A_2''$ | 3336.83 | | (0.27) | $4v_2+v_4$ | $E_1'$ | 5106.19 | [0.03] | (0.20) |
| $v_3$ | $E_1'$ | 3443.91 | [0.00] | (−0.24) | $2v_2$+$2v_4$ | $E_1''$ | 5112.78 | [0.11] | (1.04) |
| $v_3$ | $E_1''$ | 3444.26 | [0.00] | (−0.24) | $v_1$+$2v_2$ | $E_1'$ | 5143.75 | [0.00] | (−0.13) |
| $4v_2$ | $A_1'$ | 3463.00 | | (−0.31) | $v_1$+$2v_2$ | $A_2''$ | 5232.81 | | (0.23) |
| $2v_2+v_4$ | $E_1''$ | 3502.44 | [0.00] | (0.42) | $v_1$+$2v_2$ | $E_1''$ | 5352.85 | [0.00] | (−0.26) |
| $3v_2+v_4$ | $E_1'$ | 4008.04 | [0.01] | (0.35) | $5v_2$ | $A_2''$ | 5362.50 | | (−0.46) |
| $4v_2$ | $A_2''$ | 4062.47 | | (−0.37) | $3v_2$+$2v_4$ | $A_1'$ | 5603.66 | | (0.51) |
| $v_2$+$2v_4$ | $A_1'$ | 4112.38 | | (1.41) | $3v_2$+$2v_4$ | $E_1'$ | 5623.24 | [0.22] | (1.09) |
| $v_2$+$2v_4$ | $E_1'$ | 4133.20 | [0.03] | (1.50) | $v_2$+$3v_4$ | $E_1'$ | 5672.49 | [0.12] | (3.79) |
| $v_2$+$2v_4$ | $A_2''$ | 4171.03 | | (1.00) | $4v_2+v_4$ | $E_1''$ | 5709.29 | [0.12] | (0.50) |
| $v_2$+$2v_4$ | $E_1''$ | 4191.07 | [0.04] | (1.25) | $v_2$+$3v_4$ | $A_1'$ | 5712.07 | | (2.59) |
| $v_1+v_2$ | $A_1'$ | 4294.12 | | (0.14) | $v_2$+$3v_4$ | $A_2'$ | 5713.38 | | (3.73) |
| $v_1+v_2$ | $A_2''$ | 4319.76 | | (0.19) | $3v_2+v_1$ | $A_1'$ | 5736.51 | | (0.29) |
| $v_2+v_3$ | $E_1'$ | 4416.93 | [0.00] | (−0.22) | $v_2$+$3v_4$ | $E_1''$ | 5750.40 | [0.18] | (2.58) |
| $v_2+v_3$ | $E_1''$ | 4435.57 | [0.00] | (−0.24) | $v_2$+$3v_4$ | $A_2''$ | 5784.47 | | (2.16) |
| $3v_2+v_4$ | $E_1''$ | 4531.30 | [0.02] | (0.24) | $v_2$+$3v_4$ | $A_1''$ | 5785.31 | | (3.03) |
| $5v_2$ | $A_1'$ | 4695.91 | | (−0.39) | $3v_2+v_3$ | $E_1'$ | 5855.62 | [0.00] | (−0.23) |

[a] Results obtained with GENIUSH. Number of optimized grid points along the actual internal coordinates $(r_1, r_2, r_3, \theta, \beta_1, \beta_2)$ was (13,13,13,27,13,13). Each set of points was optimized on a primitive grid of 80 points and on $r_1, r_2, r_3 \in [0.35, 2.00]$ Å, $\theta \in [5, 175]^{\circ}$, and $\beta_1, \beta_2 \in [20, 220]^{\circ}$ intervals. Atomic masses, $m_H = 1.007825$ u and $m_N = 14.003074$ u, and an $xy$ body-fixed frame was used.

[b] Deviations between degenerate levels due to the incomplete convergence, are given in brackets, $\delta = [\tilde{\nu}(\text{higher}) - \tilde{\nu}(\text{lower})]$.

[c] Deviations from approximate variational results reported in Ref. 76, $\Delta = (\tilde{\nu}(\text{Ref. 76}) - \tilde{\nu}(\text{6D}))$, are given in parentheses.

[d] ZPVE was not reported in Ref. 76.

Table 5.5: ZPVE and VBOs of $^{14}NH_3$, in $cm^{-1}$, obtained with GENIUSH using full- and reduced-dimensional inversion models (constructed by reduction in the **g**-matrix) and the "refined" PES of ammonia.[76]

| Label | | $\tilde{\nu}$(6D)[a,b] | | $\tilde{\nu}$(1D)[a,c] | | $\tilde{\nu}$(2D)[a,d] | | $\tilde{\nu}$(4D)[a,e] | |
|---|---|---|---|---|---|---|---|---|---|
| ZPVE | $A_1'$ | 7436.8 | | 521.4 | | 2256.7 | | 5828.9 | |
| ZPVE | $A_2''$ | 0.8 | {0.8} | 1.1 | {1.1} | 1.3 | {1.3} | 0.6 | {0.6} |
| $v_2$ | $A_1'$ | 932.4 | | 930.6 | | 900.5 | | 945.7 | |
| $v_2$ | $A_2''$ | 968.2 | {35.7} | 979.8 | {49.2} | 952.8 | {52.3} | 973.9 | {28.2} |
| $2v_2$ | $A_1'$ | 1597.3 | | 1587.0 | | 1537.6 | | 1626.1 | |
| $2v_2$ | $A_2''$ | 1882.2 | {284.9} | 1918.9 | {331.9} | 1868.4 | {330.8} | 1884.4 | {258.3} |
| $3v_2$ | $A_1'$ | 2384.2 | | 2439.7 | | 2375.3 | | 2383.2 | |
| $3v_2$ | $A_2''$ | 2895.7 | {511.6} | 2986.2 | {546.6} | 2906.6 | {531.2} | 2882.3 | {499.1} |
| $v_1$ | $A_1'$ | 3335.8 | | – | | 3442.0 | | 3337.9 | |
| $v_1$ | $A_2''$ | 3336.8 | {1.1} | – | | 3444.0 | {2.0} | 3339.0 | {1.1} |
| $v_3$ | $E_1'$ | 3443.9 | | – | | – | | 3458.5 | |
| $v_3$ | $E_1''$ | 3444.3 | {0.4} | – | | – | | 3458.8 | {0.3} |
| $4v_2$ | $A_1'$ | 3463.0 | | 3586.5 | | 3488.3 | | 3441.4 | |
| $4v_2$ | $A_2''$ | 4062.5 | {599.5} | 4225.9 | {639.4} | 4102.6 | {614.3} | 4033.4 | {592.0} |
| $v_1+v_2$ | $A_1'$ | 4294.1 | | – | | 4376.8 | | 4313.6 | |
| $v_1+v_2$ | $A_2''$ | 4319.8 | {25.6} | – | | 4412.8 | {36.1} | 4332.3 | {18.8} |
| $v_2+v_3$ | $E_1'$ | 4416.9 | | – | | – | | 4442.4 | |
| $v_2+v_3$ | $E_1''$ | 4435.6 | {18.6} | – | | – | | 4456.2 | {13.8} |
| $5v_2$ | $A_1'$ | 4695.9 | | 4901.0 | | 4750.5 | | 4660.1 | |
| $v_1+2v_2$ | $A_1'$ | 4999.2 | | – | | 5041.6 | | 5040.5 | |
| $v_1+2v_2$ | $E_1'$ | 5143.8 | | – | | – | | 5190.6 | |
| $v_1+2v_2$ | $A_2''$ | 5232.8 | {233.6} | – | | 5322.6 | {281.0} | 5241.5 | {201.0} |
| $v_1+2v_2$ | $E_1''$ | 5352.9 | {209.1} | – | | – | | 5372.5 | {181.8} |
| $5v_2$ | $A_2''$ | 5362.5 | {666.6} | 5608.3 | {707.2} | 5429.9 | {679.4} | 5321.0 | {660.9} |

[a] Results obtained with GENIUSH. Inversion splittings are given in curly brackets, $\{\nu_i(\text{upper}) - \nu_i(\text{lower})\}$. Atomic masses, $m_H = 1.007825$ u and $m_N = 14.003074$ u, and an $xxy$ body-fixed frame were used in the calculations.

[b] Results obtained with a 6D vibrational model, see Table 5.4.

[c] Results obtained with a 1D vibrational model. The single active internal coordinate was $\theta$. Converged results were obtained by using 40 grid points optimized on a primitive grid of 100 points and on a $\theta \in [5, 175]^o$ interval. Constrained coordinates were fixed at $r_1 = r_2 = r_3 = 1.01031$ Å, and $\beta_1 = \beta_2 = 120^o$.

[d] Results obtained with a 2D vibrational model. The active internal coordinates were $\theta$, and $s_1$. Converged results were obtained by representing $(\theta, s_1)$ by (25,15) grid points each optimized on a primitive grid of 80 points and on $\theta \in [5, 175]^o$ and $s_1 \in \sqrt{3}[0.35, 2.5]$ Å intervals. The rest of the coordinates were fixed at $s_2 = 0$, $s_3 = 0$, and $\beta_1 = \beta_2 = 120^o$.

[e] Results obtained with a 4D vibrational model. The active internal coordinates were $\theta$, and $r_1, r_2, r_3$. (25,15,15,15) PO-DVR grid points, each optimized on a primitive grid of 80 points and on $\theta \in [5, 175]^o$ and $r_1, r_2, r_3 \in (0.35, 2.5)$ Å intervals, were utilized. The rest of the coordinates were fixed at $\beta_1 = \beta_2 = 120^o$.

Table 5.6: Z-matrix representation of internal coordinates of $CH_4$.

| | | | | | | |
|---|---|---|---|---|---|---|
| C | | | | | | |
| H1 | C | $r_1$ | | | | |
| H2 | C | $r_2$ | H1 | $\theta_1$ | | |
| H3 | C | $r_3$ | H2 | $\theta_2$ | H1 | $\beta_1$ |
| H4 | C | $r_4$ | H3 | $\theta_3$ | H1 | $-\beta_2$ |

the **g** matrix, as this is the preferred route based on both theoretical (Section 5.1.2) and numerical (Section 5.4.1) observations discussed above.

In the 1D model, the only active coordinate was the $\theta$ inversion angle, the rest of the internal coordinates were fixed at their equilibrium values (their values at the minimum of the PES employed). For convenience, a 2D model was also introduced by adding the $s_1$ symmetric stretching coordinate, while restricting $s_2 = s_3 = 0$, which is also equivalent to requiring $r_1 = r_2 = r_3$. A next step to increment this 2D model is to add all the stretching vibrations either by using $(\theta, s_1, s_2, s_3)$ or the $(\theta, r_1, r_2, r_3)$ set of the coordinates. The converged results are independent of the active coordinates as the reduction was introduced in the **g** matrix.

Concerning the splittings resulting from these reduced dimensional models, it can be observed that already the 1D results are reliable in a semi-quantitative sense. Not surprisingly, adding the symmetric stretching, and then all the stretching coordinates improve the inversion splittings and the absolute value of the vibrational band origins (VBOs, referenced to the corresponding zero-point vibrational energies). Interestingly, the inversion splittings of the lower lying levels ($v_2$,$2v_2$,$3v_2$) changes unpredictably, whereas splittings of highly excited levels ($4v_2$,$5v_2$) are clearly improved by turning on the stretching contributions.

### 5.4.3 Testing the efficiency: $CH_4$

$CH_4$ is a typical semi-rigid molecule with a single well-defined and deep minimum on its ground-state PES. Accurate variational computation of the VBOs is still not a straightforward task,[13,64,36] because of the molecule's nine fully coupled vibrational degrees of freedom.

Table 5.7: ZPVE and VBOs of $^{12}CH_4$, in $cm^{-1}$, obtained with GENIUSH using, a full 9D vibrational model and the T8 force field.[79]

| Label | DEWE[a,c] | $\tilde{\nu}$(9D)[b,c] | | |
|---|---|---|---|---|
| (00)(00) $A_1$ | 9691.54 | 9691.39 | | (0.14) |
| (00)(01) $F_2$ | 1311.74 | 1311.74 | [0.03] | (0.01) |
| (00)(10) E | 1533.25 | 1533.23 | [0.00] | (0.01) |
| (00)(02) $A_1$ | 2589.77 | 2589.10 | | (0.67) |
| (00)(02) $F_2$ | 2616.23 | 2616.10 | [0.26] | (0.13) |
| (00)(02) E | 2627.29 | 2626.90 | [0.00] | (0.39) |
| (00)(11) $F_2$ | 2831.52 | 2830.92 | [0.34] | (0.60) |
| (00)(11) $F_1$ | 2846.90 | 2846.84 | [0.15] | (0.07) |
| (10)(00) $A_1$ | 2913.76 | 2912.52 | | (1.24) |
| (01)(00) $F_2$ | 3013.60 | 3012.53 | [0.02] | (1.07) |
| (00)(20) $A_1$ | 3063.48 | 3062.87 | | (0.61) |
| (00)(20) E | 3065.00 | 3064.66 | [0.00] | (0.35) |

[a] Converged results obtained with the DEWE program[25,36] using 8 grid points for the bending-type and 7 grid points for the stretching-type normal coordinates.
[b] Results obtained with GENIUSH. 7 PO-DVR points for the stretching, $r_1, r_2, r_3, r_4$, 7 PO-DVR points for the bending $\theta_1, \theta_2, \theta_3$, and 11 PO-DVR points for the torsion coordinates, $\beta_1, \beta_2$, were used. Each set of points was optimized on a primitive grid of 80 points and on $r_1, r_2, r_3, r_4 \in [0.3, 2.5]$ Å, $\theta_1, \theta_2, \theta_3 \in [1, 179]^o$, and $\beta_1, \beta_2 \in [50, 190]^o$ intervals. An $xxy$ body-fixed frame was employed. Deviations between degenerate levels due to the incomplete convergence, are given in brackets, $[\tilde{\nu}(\text{largest}) - \tilde{\nu}(\text{lowest})]$. Deviations from the converged results obtained with DEWE are given in parentheses, $(\tilde{\nu}(\text{DEWE}) - \tilde{\nu}(9D))$.
[c] Nuclear masses, $m_C = 11.996709$ u and $m_H = 1.0072760$ u were used throughout the computations.

In the previous sections the accuracy and flexibility of the GENIUSH code was demonstrated by computations presented for water and ammonia both in full and reduced vibrational dimensionality and using a variety of internal coordinates. Besides these virtues, a universal code must be numerically efficient not to be constrained to low-dimensional systems. Results of a full, 9D computation are presented in Table 5.7 in order to demonstrate the largest system (the maximally coupled vibrational degrees of freedom) whose study is computationally feasible with the current version of GENIUSH. For convenience, bond lengths, bong angles, and dihedral angles defined in Table 5.6, were employed as internal coordinates. It is worth emphasizing again that only the coordinate definitions are to be specified, the representation of the kinetic energy is automatically generated by the program for the computation of energy levels and wave functions. Table 5.7 shows VBOs of the largest feasible computation for $CH_4$ using the T8 force field,[79] they are converged to about 0.5 $cm^{-1}$on an average.

In order to improve these results one can (a) further increase the size of the direct product grid until convergence; (b) introduce another set of internal coordinates in the hope of an increased convergence rate; (c) make use of the high symmetry of the actual system to split up the whole problem into independent subproblems, thus reducing the size of matrices; and (d) adopt sophisticated contraction techniques in order to make the representation more compact. Along all these four directions work is in progress. It is also worth pointing out that the DEWE code,[25,36] working in normal coordinates, produces converged energy levels using a relatively small direct-product grid. This result shows that normal coordinates and the corresponding basis are very well suited for the vibrational computations on this semi-rigid molecule having a single, well-defined potential energy minimum.

## 5.5 Advantages and limitations of GENIUSH

Using the variational method with a full-dimensional vibrational Hamiltonian the numerically exact vibrational energy levels and wave functions can be obtained, limited only by the accuracy of the actual representation of the potential energy

surface and the Born–Oppenheimer approximation. Due to the exponential scaling of the size of the problem with the number of degrees of freedom, accurate variational treatment in full vibrational dimensionality is still a challenge for systems containing more than four nuclei. Apart from the enormous size, the versatility of the possible choices of body-fixed frames and internal coordinates for systems consisting more than four particles has also been a source of difficulty in dynamical computations. The unfavorable scaling means that the choice of physically meaningful and thus efficient body-fixed frames and internal coordinates is of extreme importance when one is aimed at tackling medium-sized systems.

In this chapter I presented a universal strategy allowing variational vibrational computations using arbitrarily defined embeddings and internal coordinates and full- or reduced-dimensional models, all this in a single code. A highly desirable feature of the GENIUSH protocol is that the vibrational Hamiltonian of arbitrarily chosen body-fixed frame and internal coordinates is constructed automatically during the course of the calculation through fully numerical evaluations. This means that there is no need to know the often complicated form of the kinetic energy operator in internal coordinates *a priori*. The matrices corresponding to this Hamiltonian are constructed using a discrete variable representation on a direct product or truncated (preoptimized) DVR grid. The useful features of DVR allow a straightforward and exact inclusion of an arbitrary representation of the potential energy surface, as well as terms of the kinetic energy operator corresponding to the actual coordinate choice. Eigenvalues and eigenvectors of the huge but sparse Hamiltonian matrix are provided by an iterative eigensolver.

Concerning the technical details of the implementation, I found that the **t**-vector formalism is much better adaptable to our scheme than the **s**-vector one,[33,37] though the two are equivalent from a theoretical point of view. In the **t**-vector formalism the rearranged form of the vibrational Hamiltonian, Eq. (3.11) is often used.[29,31] In order to construct the kinetic energy part of the Hamiltonian matrix of this form, first, second, and third derivatives of the Cartesian coordinates in terms of the internal coordinates must be computed with increased numerical precision if derivatives are evaluated numerically. Otherwise, analytic derivatives are required.

In the current version of GENIUSH numerical derivatives of any kind of coordinate choice can be evaluated using 128-bit reals (quadruple precision in Fortran), and analytic derivatives are available for the $xxy$ (scattering) frame and a Z-matrix-type definition of internal coordinates.

The DVR allows an efficient implementation of the Podolsky-form, Eq. (3.9), of the (ro)vibrational Hamiltonian, which requires only the computation of the first coordinate derivatives on the expense of a slightly higher memory requirement and CPU-usage in the eigensolver part. Evaluation of only the first derivatives of body-fixed Cartesian coordinates in terms of the internal coordinates is not only computationally less expensive, but require a less robust numerical procedure than that for second and especially third derivatives. The usage of the Podolsky-form, given in Eq. (3.9) is thus recommended instead of the rearranged form of the vibrational Hamiltonian, given in Eq. (3.11). It is worth noting that at present the Podolsky-form is implemented only in the GENIUSH program. Besides the Podolsky-form, a carefully tested and numerically stable implementation of the rearranged form of the vibrational Hamiltonian is also available in GENIUSH.

Test vibrational computations for $H_2O$ were carried out in full and reduced vibrational dimensionality. Validation of the results was made by comparing the 3-dimensional results with independent benchmark data, and by checking the fulfillment of fundamental theoretical relationships. If first, second, and third numerical derivatives were computed and only with 64-bit reals (double precision in Fortran) and the rearranged form of the vibrational Hamiltonian, given in Eq. (3.9), was used an error of a couple of wavenumbers appeared in the results compared to the accurate reference data or results obtained with increased precision (128-bit reals) numerical or standard precision (64-bit reals), but exact, analytic derivatives.

Due to the universal ideas lying behind the GENIUSH algorithm, the implementation of reduced-dimensional vibrational models is straightforward. Reduced dimensional models can be constructed either by reducing the $\mathbf{g}$ or the $\mathbf{G}$ matrices. Both routes are implemented in GENIUSH. However, theoretical considerations and their numerical demonstrations through 2-dimensional models of $H_2O$ indicate that reduction in $\mathbf{g}$ should be the preferred route. A simple physical requirement,

the invariance of the converged eigenpairs from the choice of the active coordinates, holds only if the reduced model is constructed by reducing the **g** matrix, but fails, in general, if the **G** matrix is reduced.

Once the main technical difficulties in the implementation of such a universal vibrational algorithm were properly addressed and solved, the inversion tunneling in ammonia was examined through a variety of full- and reduced dimensional models. The freedom of using a range of vibrational models strongly relies on the automatic construction of the actual kinetic energy representation provided by GENIUSH. Our computations show that already the 1D inversion-only model provides a semi-quantitative approximation to the exact inversion splittings (the constrained coordinates are fixed at their equilibrium values). Incrementing this 1D model by stretching coordinates allows the construction of 2- and 4D stretching-inversion models. Improvement in the splittings of lower-lying states is not systematic, while the higher excited states are clearly improved. Furthermore, our 6D results are the first benchmark data, without introducing any approximations, obtained with the actually employed "refined" PES of Ref. 76.

Based on our experience, in molecules most reduced-dimensional vibrational models provide only a semi-quantitative approximation to the full-dimensional results. We expect that the main virtues of reduced-dimensional models can be exploited in at least two ways. First, wave functions of reduced-dimensional Hamiltonians can serve as a kind of "preoptimized basis" to the solution of the full-dimensional problem. This philosophy has already been exploited in the present work via usage of preoptimized DVR points (PO-DVR). In order to carry out such a "preoptimization" in higher dimensions one would likely adopt one of the well-known contraction techniques[80,13] using two- or multiple-stage contractions. Our preliminary results on contraction techniques adopted in GENIUSH indicate that this is a promising way of extending our current limits toward larger systems treatable in full vibrational dimensionality. As for the current computational limitations, a maximum of nine coupled vibrational degrees of freedom can be handled, as was demonstrated for methane. Second, a possible fruitful application of reduced-dimensional models could be the study of intramolecular dynamics of complexes consisting of semirigid

monomer units. For such systems, reliable results can be expected from an approximate model in which the vibrational degrees of freedom of the monomers are fixed (or perhaps relaxed along the active dimensions) and only the intramolecular degrees of freedom are included explicitly.

# Chapter 6

# Sophisticated Lanczos eigensolver techniques

The main goal of my doctoral work was the development of a variational vibrational algorithm universally applicable for either semi-rigid or flexible $N$-atomic molecules with arbitrary bonding arrangement. In Chapters 4 and 5 the construction of the vibrational Hamiltonian matrix was considered in detail, which is indeed a fundamental element of such a procedure. However, in practice, not to be restricted to the computation of a few eigenpairs of small molecules, efficient eigensolver techniques must be employed. The main concepts of the Lanczos eigensolver were introduced in Section 2.4. This chapter is devoted to those sophisticated Lanczos techniques which turned out to be especially useful and those which are expected to be useful for the computation of a large number of (ro)vibrational energy levels and wave functions of medium-sized molecules, more or less independently of the actual Hamiltonian.[36]

The main parts of the original Lanczos algorithm (OL, see Section 2.4) which must be considered to make our approach efficient are a) multiplication of the Hamiltonian matrix with a vector; b) spectral transformation of the Hamiltonian matrix which influences the convergence rate to the required range of the spectrum; c) question of reorthogonalization of Lanczos vectors and handling of Lanczos vectors.

Efficient multiplication of the Hamiltonian matrix with a vector is of fundamental importance, thus efficient algorithms for the matrix-vector multiplication worked out for DEWE and GENIUSH were presented in Sections 4.3 and 5.3, respectively.

Algorithms for the spectral transformation and handling of the Lanczos vectors are considered in what follows specifically adapted for the computation of a large number of energy levels and wave functions of medium-sized molecules. The actual choice of the spectral transformation method and the handling of the spread of round-off errors is a rather delicate problem. Advantages and drawbacks of simple polynomial transformation techniques, exponential filters using a Chebyshev expansion, and shift-invert techniques are addressed in what follows.

## 6.1 Spectral transformation techniques

The conventional Lanczos algorithm converges to the largest eigenvalue of a matrix. The convergence rate of the Lanczos iteration is determined by the relative separation of the eigenvalues, $\eta_i = |E_{i+1} - E_i|/(E_{\max} - E_{\min})$.[81]

In order to compute the lowest or interior eigenvalues instead of the largest ones the original matrix must be transformed so that the required eigenvalues become the largest eigenvalues of the transformed matrix. There are several possibilities to set up such a spectral transformation.[82,83,84] However, the cost of the transformation and the spectral properties of the resultant matrix can be different.

I studied sophisticated polynomial, exponential and shift-invert transformation techniques. In Figure 6.1 a pictorial overview is given about the different transformation techniques, by visualizing the spectral properties of the transformed matrices with respect to the original spectrum. The relative separation, $\eta_i$, of the eigenvalues corresponding to the transformed matrices are given and discussed in detail in the Supplementary Material of Ref. 36. In what follows the most important technical aspects are discussed separately for the different cases considered.

It is worth noting that the converged eigenvectors of the transformed and the original matrices are the same. If necessary, the eigenvalues of the original matrix, $E_i^0$, can be recovered by computing the expectation values of the original matrix using the eigenvectors, *e.g.*, $E_i^0 = \langle \mathbf{v}_i | \mathbf{H} | \mathbf{v}_i \rangle$.

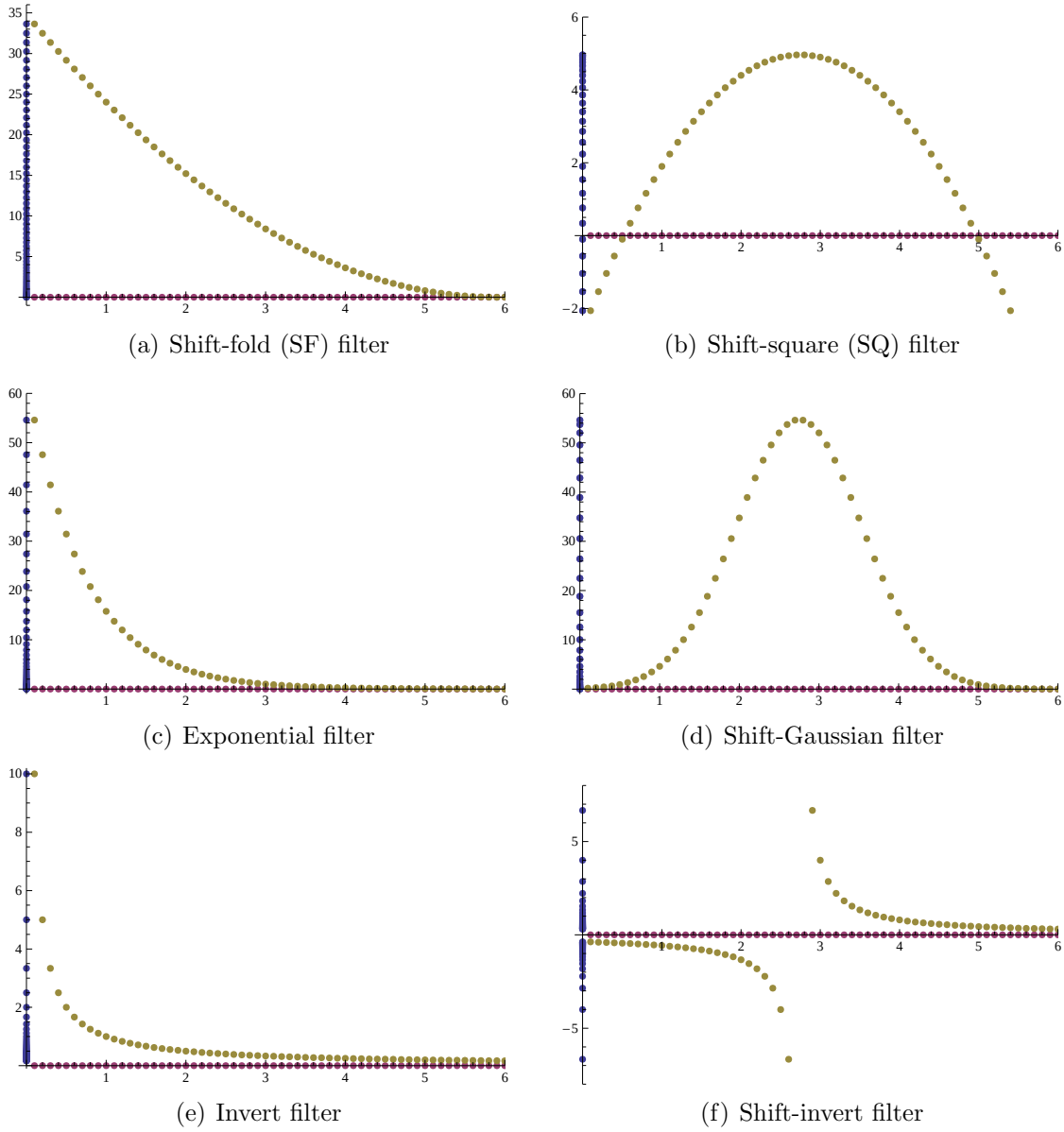

(a) Shift-fold (SF) filter

(b) Shift-square (SQ) filter

(c) Exponential filter

(d) Shift-Gaussian filter

(e) Invert filter

(f) Shift-invert filter

Figure 6.1: Schematic representation of different spectral transformation techniques. Line positions of the original and transformed spectrum are represented on the $x$- and $y$-axes, respectively. The graphs of the transformation functions are also plotted at discrete points on the $x - y$ plane. See the mathematical definition of the filters presented on plots (a)–(f) in the text.

### 6.1.1 Polynomial filtering

The family of polynomial spectral transformation techniques[85,86] can be written in general as

$$\mathcal{P}_n(\mathbf{H}, \alpha, \kappa, \lambda) = \left[\lambda\mathbf{I} - \alpha(\mathbf{H} - \kappa\mathbf{I})^2\right]^{2n+1}, \quad n = 0, 1, 2, \ldots, \tag{6.1}$$

where the parameters $\alpha, \kappa$, and $\lambda$ can be tuned in order to map the required range of the original spectrum to the largest eigenvalues of $\mathcal{P}_n(\mathbf{H}, \alpha, \kappa, \lambda)$. Two special cases of the family of polynomial filters given in Eq. (6.1) were used in the present work, a shift-fold (SF) and a shift-square (SQ) filtering. Polynomial filters can be implemented straightforwardly. The number of matrix-vector multiplications in a single spectral transformation step is $2(2n + 1)$.

The largest eigenvalue of $\mathcal{P}_0(\mathbf{H}, -1, E^0_{\max}, 0) = (\mathbf{H} - E^0_{\max}\mathbf{I})^2$ is the smallest eigenvalue of $\mathbf{H}$. Spectral properties of this so-called shift-fold (SF) transformation are visualized on Figure 6.1(a). In an ideal case, relative separation of the eigenvalues of the SF-transformed matrix can be twice as large as that of the original one, *i.e.,* $\eta^{\mathrm{SF}}_i \leq 2\eta^0_i$.[36] Furthermore, the relative separation of the original spectrum, $\eta^0_i$, can be increased by decreasing the largest eigenvalue of the original matrix, *e.g.,* by means of the truncation of the direct-product grid. Upon the computation of the lowest-lying levels this further increases the relative separation of eigenvalues of the transformed matrix as well, thus increasing the convergence rate of the Lanczos iteration.

The largest eigenvalues of $\mathcal{P}_0(\mathbf{H}, 1, \kappa, \lambda) = \lambda\mathbf{I} - (\mathbf{H} - \kappa\mathbf{I})^2$ are the eigenvalues of $\mathbf{H}$ from the neighborhood of $\kappa$, where $\kappa$ is a point from the required spectral range and $\lambda = \max\left[(\mathbf{H} - \kappa\mathbf{I})^2\right]/2$. Spectral properties of this transformation are visualized on Figure 6.1(b). It is apparent from Figure 6.1(b) that the high end of the transformed spectrum is very dense. Thus, the convergence is expected to be slow. Indeed, one can demonstrate that the relative separation of the transformed eigenvalues is much smaller than that of the original eigenvalues for the interesting spectral range. Furthermore, due to folding (squaring) the original spectrum around

the interior point, $\kappa$, the transformed spectrum becomes nearly doubly degenerate, which worsens the convergence of the Lanczos iteration.

### 6.1.2 Exponential filtering

The usage of an exponential function can provide more advantageous spectral properties to the transformed matrix,[81,87,88] than the polynomial filters. A family of exponential filters can be introduced as

$$\mathcal{T}_n(\mathbf{H}, \alpha, \kappa) = e^{-\alpha\left[(\mathbf{H}-\kappa\mathbf{I})^n - \bar{\lambda}\mathbf{I}\right]/\Delta}, \quad n = 1 \text{ or } 2, \tag{6.2}$$

where $\bar{\lambda} = (\lambda_{\max} + \lambda_{\min})/2$ and $\Delta = (\lambda_{\max} - \lambda_{\min})/2$, where the notations $\lambda_{\max} = \max\left[(\mathbf{H} - \kappa\mathbf{I})^n\right]$ and $\lambda_{\min} = \min\left[(\mathbf{H} - \kappa\mathbf{I})^n\right]$ were used.

Exponential function of matrices can be dealt with efficiently by using a Chebyshev expansion, as suggested originally by Tal-Ezer and Kosloff[89] for the complex case and later adapted, for instance, by Yu and Nyman[81,87,88] for real functions. Let us introduce the notation

$$f(\mathbf{H}) = \mathcal{T}_n(\mathbf{H}, \alpha, \kappa) \quad \text{then} \tag{6.3}$$

$$f(\mathbf{H}) \approx \sum_{l=0}^{L} A_l T_l(\mathbf{H}'), \tag{6.4}$$

where $\mathbf{H}' = (\mathbf{H} - \bar{H})/\Delta H$, $\bar{H} = (E^0_{\max} + E^0_{\min})/2$ and $\Delta H = (E^0_{\max} - E^0_{\min})/2$. $T_l$ stands for the $l$th Chebyshev polynomial of the first kind and the expansion coefficients are

$$A_l = \frac{2 - \delta_{l0}}{\pi} \int_{-1}^{+1} \frac{f(E) T_l(E)}{\sqrt{1 - E^2}} \, \mathrm{d}E, \tag{6.5}$$

which can be computed numerically by Gaussian quadrature. The accuracy of the expansion can be increased by including higher and higher degree Chebyshev polynomials. In each transformation step, the number of multiplications of the original matrix with a vector is $L$, the largest degree of Chebyshev polynomials included in the expansion. Implementation of such an exponential transformation using truncated

Chebyshev expansion is straightforward and its computational cost is proportional to $L$.

The largest eigenvalue of $\mathcal{T}_1(\mathbf{H}, \alpha, 0) = e^{-\alpha\left(\mathbf{H}-\bar{H}\mathbf{I}\right)/\Delta H}$ is the smallest eigenvalue of $\mathbf{H}$, where $\Delta H = (E^0_{\max} - E^0_{\min})/2$, $\bar{H} = (E^0_{\max} + E^0_{\min})/2$, and $E^0_{\max}$ and $E^0_{\min}$ are the largest and the smallest eigenvalues of $\mathbf{H}$. As demonstrated on Figure 6.1(c), the lowest end of the spectrum is mapped to the largest, well-separated eigenvalues of the transformed spectrum. In principle, the relative separation of two close-lying levels can be increased to arbitrarily close to one (note that $0 \leq \eta_i \leq 1$) by choosing an appropriately large $\alpha$. In practice, however, the increasing number of terms in the expansion in Eq. (6.4) and the finite numerical representation can limit this possibility. Apart from the technical difficulties, the transformation $\mathcal{T}_1(\mathbf{H}, \alpha, 0)$, given in Eq. (6.2), allows to speed up the convergence of the Lanczos iteration by increasing $\alpha$ at the expense of an increase in the cost of the transformation. The larger $\alpha$ becomes the higher the order of the terms to be kept in the Chebyshev expansion. This results in more matrix-vector multiplications in a single transformation step.

The largest eigenvalues of $\mathcal{T}_2(\mathbf{H}, \alpha, \kappa) = e^{-\alpha\left[(\mathbf{H}-\kappa\mathbf{I})^2-\bar{\lambda}\mathbf{I}\right]/\Delta}$ correspond to the eigenvalues closest to $\kappa$ in the original spectrum. The spectral properties of the transformed matrix are visualized on Figure 6.1(d). Due to the exponential filter, the relative separation of close-lying eigenvalues could be increased by choosing a sufficiently large $\alpha$. However, similarly to the shift-square case, due to the folding of the original spectrum around an interior point, $\kappa$, the transformed spectrum becomes nearly doubly degenerate, which worsens the convergence rate of the Lanczos iteration.

### 6.1.3 Shift-invert filtering

The required eigenvalues can be mapped into large and well-separated eigenvalues by shifting and inverting the original Hamiltonian matrix,[82]

$$\mathcal{I}_+(\mathbf{H}, \kappa) = (\mathbf{H} - \kappa\mathbf{I})^{-1} \tag{6.6}$$

$$\mathcal{I}_-(\mathbf{H}, \kappa) = (\kappa\mathbf{I} - \mathbf{H})^{-1}. \tag{6.7}$$

The largest eigenvalues of $\mathcal{I}_+(\mathbf{H},\kappa)$ or $\mathcal{I}_-(\mathbf{H},\kappa)$ are the eigenvalues closest to $\kappa$, but respectively larger or smaller than $\kappa$. The advantageous spectral properties of this filtering can be observed on Figures 6.1(e) and 6.1(f).

In practice, the $\mathcal{I}_+(\mathbf{H},\kappa)$ and $\mathcal{I}_-(\mathbf{H},\kappa)$ are introduced in the Lanczos iterations simply by means of matrix-vector multiplications, which can be computed by using iterative linear solvers, *e.g.*, conjugate gradient (CGM), generalized minimal residual (GMRES), or quasi-minimum residual (QMR) methods.[58]

The cost of the transformation, which is determined by the number of multiplications done by the original matrix, $\mathbf{H}$, strongly depends on the spectral properties of $\mathbf{H}$ and the spectral density of $\mathbf{H}$ around $\kappa$. Several applications and improvements of the transformation algorithm have been published;[90,91,92] however, construction of an efficient and in some sense black-box method, for instance a method which is efficient for any spectral range of a rotation-vibration Hamiltonian matrix, still remains a challenging task. The spectral properties of the transformed matrix suggest that once such a shift-invert transformation is set up the Lanczos iteration converges fast.

For the computation of the lowest eigenvalues the simplest choice, $\mathcal{I}_+(\mathbf{H},0) = (\mathbf{H})^{-1}$ can be used. However, the convergence rate of Lanczos can be improved if $\mathcal{I}_+(\mathbf{H},0<\kappa<E^0_{\min}) = (\mathbf{H}-\kappa\mathbf{I})^{-1}$ is employed.

For the computation of interior eigenvalues of $\mathbf{H}$, the $\mathcal{I}_+(\mathbf{H},\kappa)$ and $\mathcal{I}_-(\mathbf{H},\kappa)$ transformations can be used with $E^0_{\min}<\kappa<E^0_{\max}$. In contrast to the polynomial and exponential filters, here the original spectrum is not folded around the interior point, $\kappa$, thus the inconvenient near double degeneracy is not introduced in the transformed spectrum.

This functional form was seemingly suggested for the computation of interior eigenvalues first in 1980.[82] Since then this filter has been recognized as the one which produces the most favorable spectral properties for the computation of a few eigenvalues. However, to carry out such a spectral transformation efficiently for any $\kappa$ remains a challenging task.

To summarize this section, the choice of the spectral transformation is a rather delicate question and the optimal choice seems to depend strongly on the applica-

tion. By choosing an appropriate form of the spectral transformation the required spectral range of the Hamiltonian matrix can be computed in the Lanczos iteration. In each Lanczos step the original matrix is transformed, which requires to carry out a certain number of multiplications of the Hamiltonian matrix with a vector. This matrix-vector multiplication is generally the most CPU intensive part of the computation; thus, the number of matrix-vector multiplications required determines the "cost" of a specific spectral transformation. On the other hand, the spectral properties of matrices produced by different spectral transformation methods can be very different. The relative separation of eigenvalues of the matrix introduced in the Lanczos iteration strongly influences the convergence rate of the iteration.

Although the most efficient spectral transformation technique to compute the few lowest or interior points of a spectrum seems to be the shift-invert filtering, its cost, *i.e.* the number of matrix-vector multiplications required, strongly depends on the spectral properties of the original matrix and it becomes very expensive as the spectrum becomes dense in the required range. A shift-invert transformation is especially efficient for the computation of a few eigenvalues, but this is not necessarily true, for instance, for the lowest few hundred eigenvalues.

Thus, our strategy was to settle for a less efficient spectral transformation method, which is less expensive, *i.e.*, requires less matrix-vector multiplications, and adapt methods which reduces the computational efforts related to the handling of the Lanczos vectors, thus allowing an increased number of Lanczos iteration steps.

## 6.2 Efficient handling of Lanczos vectors

### 6.2.1 Building the Krylov subspace

In exact arithmetics Lanczos vectors are orthogonal by construction.[58,93] However, in the presence of round-off errors this orthogonality is lost. Several approaches have been put forward to remedy this shortcoming of the Lanczos algorithm. The loss of orthogonality manifests itself in the appearance of spurious eigenvalues and copies of correct ones.

Cullum and Willoughby[57] suggested an algorithm, which was later used by Wang and Carrington for rovibrational computations,[94] which removes the extra and spurious eigenvalues *a posteriori* from the computed spectrum. This approach avoids the reorthogonalization of Lanczos vectors and thus their storage. However, the computation of spurious and extra levels wastes considerable CPU time.

In contrast to the approach suggested by Cullum and Willoughby, in DEWE and GENIUSH we prefer to obtain both eigenvalues and eigenvectors. Eigenvectors can be later used for the computation of, for instance, (ro)vibrational intensities, averaged structural parameters, or effective rotational constants.[95] To achieve this we need to store the Lanczos vectors, but in order to avoid redundant storage of information (semi-)orthogonality is maintained among the Lanczos vectors throughout the calculation. Lanczos vectors can be very large and if many eigenpairs are required a large number of such vectors must be stored (typically on the hard disk). Thus, efficient reorthogonalization algorithms and restarting strategies of the Lanczos iteration were sought and implemented.

### 6.2.2 Orthogonality of Lanczos vectors

Reorthogonalization procedures require the knowledge of all previous Lanczos vectors which, in most cases, can be stored only on the hard disk. A careful choice and implementation of the reorthogonalization is important to minimize the number of I/O operations. For quantifying the level of orthogonality two terms are defined in the literature.[93,96] The term full orthogonality means that the dot product of different Lanczos vectors is not larger than a round-off error, $\varepsilon_u$, whereas the term semi-orthogonality is used if the dot product of different Lanczos vectors is not larger than $\sqrt{\varepsilon_u}$.

Full orthogonality among Lanczos vectors can be maintained by reorthogonalizing the new Lanczos vector against all previous ones in each Lanczos step. This brute-force procedure will be referred to as full-reorthogonalization (FRO). Reorthogonalization is carried out by using a numerically stable version of the Gram–Schmidt procedure (modified Gram–Schmidt procedure, MGS).[97]

It was demonstrated in Ref. 93 that the requirement of full orthogonality can be alleviated and semi-orthogonality of Lanczos vectors[93,96] is sufficient to compute accurate eigenpairs without extra or spurious levels entering the spectrum. The partial reorthogonalization (PRO) algorithm[93,96] estimates the spread of the round-off error during the Lanczos iteration using a recurrence formula, without the explicit computation of the dot products of Lanczos vectors. PRO was implemented in DEWE and GENIUSH.[36] Our limited experience shows that for (ro)vibrational Hamiltonian matrices in DVR of size on the order of millions by millions PRO is typically 55–60 % cheaper than FRO if 10–500 eigenpairs are to be computed.

This gain is close to the gain 55 % achievable with a so-called periodic reorthogonalization (PerRO) originally suggested by Grcar.[98] PerRO, which is based on a much simpler algorithm than PRO, reorthogonalizes every second Lanczos vector against all the previous ones. According to our extensive computations of 100–500 eigenpairs of matrices up to the size of 400 millions by 400 millions, PerRO is a stable method providing accurate eigenvalues and eigenvectors without the introduction of spurious levels. The main advantage of PerRO over PRO is that it is based on a very simple algorithm, while the recurrence scheme of PRO contains parameters to be optimized. Furthermore, in contrast to PRO, PerRO showed robustness against round-off errors introduced by certain spectral transformation methods (*e.g.,* CGM) tested, thus it can be used in a black-box way also with restarted Lanczos iterations (see Section 6.2.3).

### 6.2.3 Restarted Lanczos algorithms

In general, it is not possible to predict the number of Lanczos iterations required to achieve convergence. Therefore, it is impossible to predict the storage requirements of the original procedure, OL. Thus, to keep storage requirements under control the Lanczos algorithm must be occasionally restarted.

The thick-restart Lanczos method (TRLM)[96,99] was implemented in DEWE and GENIUSH in order to compact the ever-growing Krylov subspace periodically. With an optimal choice of related parameters, the convergence rate of the Lanczos iteration

is not worsened significantly. This algorithm was implemented and can be used in a nearly black-box way with the FRO and PerRO techniques.

An upper limit of the hard disk requirements can be defined for the restarted Lanczos procedures. This upper limit cannot be arbitrarily small. In principle, the number of Lanczos vectors stored must be at least as large as the number of eigenpairs to be computed. At the end of the computation, the Lanczos vectors can be replaced by the eigenvectors. In practice, in DEWE and GENIUSH the minimal storage requirement (on the hard disk) for the computation of $n_{\mathrm{eig}}$ eigenvectors corresponds to the storage of $n_{\mathrm{eig}} + 25$ Lanczos vectors, which is close to the optimal choice suggested also by other applications.[96,99,100]

TRLM is specifically adapted for a symmetric eigenvalue problem, and it is relatively tolerant to the loss of orthogonality of the vectors spanning the Krylov subspace. The main advantages of TRLM are that it can be restarted with any number of starting vector and it retains a large part of the basis.

In order to use TRLM, the OL algorithm must be modified. Before any restarts, the Lanczos iteration runs according to the OL algorithm given in Section 2.4. After step $m$ the Lanczos iteration is restarted, which assumes the following manipulations.[100]

**(R1)** Find all eigenvalues and eigenvectors of $\mathbf{T}_m$. The eigenvalues are the Ritz values.

**(R2)** Choose $k$ Ritz values, $\lambda_1, \ldots, \lambda_k$, and the corresponding eigenvectors of $\mathbf{T}_m$, $\mathbf{y}_1, \ldots, \mathbf{y}_k$, to be saved in the restart procedure.

**(R3)** Let $\mathbf{Y}_k := [\mathbf{y}_1, \ldots, \mathbf{y}_k]$ and replace the first $k$ columns of $\mathbf{Q}_m$ with $\mathbf{Q}_k\mathbf{Y}_k$, *i.e.*, $\mathbf{Q}_k = \mathbf{Q}_k\mathbf{Y}_k$. The corresponding $\alpha_i$ and $\beta_i$ values are replaced by $\alpha_i = \lambda_i$ and $\beta_i = \beta_m y_{mi}$, $i = 1, 2, \ldots, k$.

**(R4)** Set $\mathbf{q}_{k+1} = \mathbf{q}_{m+1}$.

**(R5)** Full reorthogonalization of $\mathbf{q}_{k+1}$ against $\mathbf{q}_i$, $i = 1, 2, \ldots, k$.

**(R6)** $\alpha_k = \mathbf{q}_k^{\mathrm{T}}\mathbf{q}_{k+1}$

**(R7)** $\mathbf{q}_{k+1} = \mathbf{q}_{k+1} - \alpha_k \mathbf{q}_k - \sum_{i=1}^{k} \beta_i \mathbf{q}_i$

**(R8)** Continue the Lanczos iteration according to the original algorithm until the next restart, which repeats the steps (R1)–(R8), or until convergence of the Lanczos iteration.

Note that $\mathbf{Q}_k \mathbf{Y}_k$ are the Ritz vectors. The Ritz values and Ritz vectors are approximations to eigenvalues and eigenvectors of the matrix entering the Lanczos iteration. Due to step (R3) the projected matrix $\mathbf{T}_m$ is not tridiagonal in TRLM but has a special block structure.

$$\mathbf{T}_m = \begin{pmatrix} \alpha_1 & & & \beta_1 & & & \\ & \ddots & & \vdots & & & \\ & & \alpha_k & \beta_k & & & \\ \beta_1 & \dots & \beta_k & \alpha_{k+1} & \beta_{k+1} & & \\ & & & \beta_{k+1} & \alpha_{k+2} & \ddots & \\ & & & & \ddots & \ddots & \beta_{m-1} \\ & & & & & \beta_{m-1} & \alpha_m \end{pmatrix} \tag{6.8}$$

In this algorithm the Ritz vector production in step (R3) and the step (R7) are strongly I/O dependent. In these steps vectors of the size of the Lanczos vectors are read from and written to the hard disk. The I/O operations can be minimized throughout these manipulations if the Lanczos vectors are stored on the hard disk in smaller blocks in direct access files. During the restart procedure the Ritz vectors are produced not one by one, but small blocks of all Ritz vectors are computed at once. In this way the Lanczos vectors are read from the disk and the Ritz vectors are written to the disk only once during each restart. Furthermore, during the computation of Ritz vectors the sum in (R7) is also evaluated, thus saving further I/O operations. The maximum size of the Krylov subspace is dynamically increased to the limiting value during the iteration, which also reduces the number of I/O operations.

Due to the restarts, the Krylov subspace grows slower and thus the cost the reorthogonalization is also reduced compared to the non-restarted version.

### 6.2.4 Efficiency considerations

In the algorithms presented above the storage requirements are as follows. The Lanczos iteration requires two vectors of the size of the direct product grid, $\mathcal{N}$, the spectral transformation step needs an extra one to three vectors (depending on the actual spectral transformation techniques) of size $\mathcal{N}$. Memory requirement of the matrix-vector multiplication algorithms were given in Sections 4.3 and 5.3. Lanczos vectors, each of size $\mathcal{N}$, are stored on the hard disk.

In each reorthogonalization step the required Lanczos vectors are read from the hard disk. If a large number of eigenpairs is to be computed the usage of an efficient reorthogonalization together with a restarted Lanczos method is essential. Figure 6.2 presents the timing (real time, including also the spectral transformation part) of the DEWE program using the thick-restart Lanczos algorithm (TRLM) with periodic reorthogonalization (PerRO) and the original Lanczos algorithm (OL), without restart, and with full reorthogonalization (FRO). As a reference the time required for a single spectral transformation step is also shown. Figure 6.2 shows the Lanczos steps until the convergence of the lowest 100 eigenpairs for the $^{12}CH_4$ molecule computed with DEWE. CGM was used to carry out the spectral transformation to compute the lowest eigenvalues. Convergence is achieved after 654 and 662 steps using OL-FRO and TRLM-PerRO, respectively. Apparently, the number of Lanczos iterations required is only slightly increased in the case of thick-restart Lanczos with periodic reorthogonalization; however, the gain in real timing is enormous compared to the original Lanczos technique with FRO.

The spectral transformation part, curve (a) of Figure 6.2, consists of matrix-vector multiplications that are CPU-intensive, and are parallelized with OpenMP as it was presented in Sections 4.3 and 5.3. The differences between curves (b) and (a) or (c) and (a) of Figure 6.2 basically originate from reorthogonalization and restarting parts. In these parts the dot product of the Lanczos vectors are computed. Computation of dot products corresponds to CPU usage, but most importantly to the time of reading the Lanczos vectors from the hard disk (I/O intensive part).

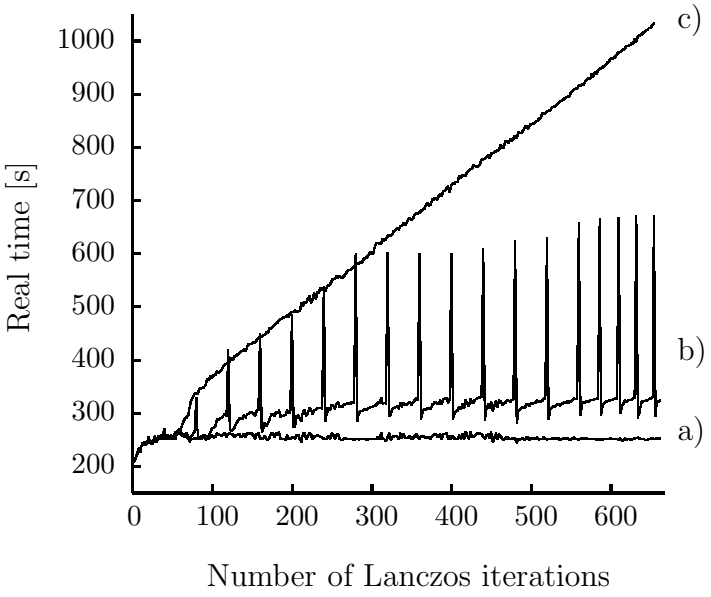


Figure 6.2: Comparison of real timing of different Lanczos techniques using reorthogonalization, curves (b) and (c), during the course of the Lanczos iteration steps. For reference, the time required for preconditioning (CGM), curve (a), is presented. Results are obtained for $CH_4$ using 6 grid points on each vibrational degree of freedom, which corresponds to a Hamiltonian matrix of size $10^7 \times 10^7$. Wall time in seconds of
(a) the CGM preconditioning part of a single Lanczos iteration step;
(b) the average of two subsequent Lanczos steps using the thick-restart Lanczos method with periodic reorthogonalization (TRLM-PerRO). The Lanczos iteration was restarted after each 40 steps, and maximally 155 eigenvectors were saved on the hard disk. The lowest 100 eigenvalues were converged after 662 Lanczos iteration steps.
(c) a single Lanczos step of the original Lanczos algorithm (without restart) with full reorthogonalization (OL-FRO). The lowest 100 eigenvalues were converged after 654 Lanczos iteration steps.

Indeed, an enormous difference is experienced depending on the way of handling of Lanczos vectors, compare curves (b) and (c) of Figure 6.2.

If the Lanczos iteration is not restarted and full orthogonality is maintained among the Lanczos vectors, the real timing increases linearly with the number of Lanczos iteration steps. After 100 Lanczos iterations, the timing (mainly I/O operations) exceeds the time of the CGM spectral transformation step (parallelized, using eight cores in this example).

If the Lanczos iteration is restarted periodically, which corresponds to the peaks on curve (b), the Krylov subspace remains manageable throughout the Lanczos

iteration. Note that between restarts the real timing increases approximately linearly, which corresponds to the increasing time required to maintain (semi-)orthogonality among the increasing number of Lanczos vectors. The slope of the linear segments of curve (b) is approximately half of the slope of curve (c), corresponding to the relative timing of a periodic compared to a full reorthogonalization.

Finally, it is worth noting that by using CGM the Lanczos scheme converges within less iteration steps than than, for instance, by using a shift-fold filter. Thus, without the sophisticated reorthogonalization and restarting techniques used here, it would be hopeless to try and adapt less efficient, but cheaper spectral transformation techniques, such as the shift-fold filter. According to our experience the overall number of matrix-vector multiplications using, for instance, the shift-fold filter can be much lower than that of using CGM to converge the lowest few hundred eigenvalues of a vibrational Hamiltonian matrix. The shift-fold filter requires two matrix-vector multiplications, whereas CGM needs $30 - 50$ in each Lanczos steps. At the same time the shift-fold filter produces a matrix with less optimal spectral properties than CGM, so it typically requires $3 - 5$ times as many Lanczos iterations than CGM. Finally, during the course of the whole Lanczos procedure the shift-fold filter requires $5 - 10$ times less matrix-vector multiplications than CGM. This gain in the CPU usage can be exploited only if the presented reorthogonalization and restarting techniques are employed to handle efficiently the increased number of Lanczos iteration steps.

## 6.3 Lanczos eigensolver for (ro)vibrational computations

In order to compute a large number of (ro)vibrational energy levels and wave functions of medium-sized molecules, one has to use sophisticated eigensolver techniques. There are three main constituents of a rovibrational algorithm coupled to a Lanczos eigensolver. Efficient CPU-intensive matrix vector multiplications were presented in Sections 4.3 and 5.3, and this chapter was devoted to the delicate problem of

the choice of a spectral transformation technique, as well as to an efficient way of handling Lanczos vectors if the computation of eigenvectors is also required.

The combination of the shift-folder spectral transformation technique, periodic reorthogonalization, and the thick-restart Lanczos method (SF-PerRO-TRLM) turned out as a simple but effective choice (see Chapter 7). This method can be further improved by replacing the shift-fold filter by a carefully optimized exponential filter using Chebyshev expansion (see Section 6.1).

If not the lowest eigenvalues but an interior part of the spectrum is to be computed, the shift-invert technique seems to be an appealing choice. However, an efficient black-box method to carry out the spectral transformation is a challenging task. Finally, a safe and practical technique might be the usage of a shifted version of the exponential transformation, shift-Gaussian filter, optimized carefully. The computation of interior eigenvalues opens a promising route toward the computation of a very large number of eigenvalues and eigenvectors, *i.e.*, toward the determination of the complete spectrum. This task could be distributed to practically independent computing nodes by distributing smaller ranges of the spectrum to different machines. Eigenpairs from different ranges of the spectrum can be converged independently, *i.e.* the lower end of the spectrum could be computed using a smaller grid. If only very few interior eigenvalues, *e.g.* 10 eigenvalues, are required in each run the total storage requirement, Lanczos and a few auxiliary vectors, of the computation fits into the main memory of nowadays standard machines, which eliminates the time-consuming I/O operations on the hard disk.

The algorithm can be further improved if symmetry properties are exploited for the computation of eigenpairs of symmetric species. The symmetry-adapted Lanczos (SAL) algorithm suggested by Carrington *et al.*[101] seems to be a good choice for DEWE and maybe for GENIUSH too. The original version of the SAL has been recently implemented in DEWE for Abelian groups,[70] which might be further improved in the near future to reduce the storage requirements.

If only (ro)vibrational energy levels were required without the computation of wave functions, the method originally suggested by Cullum and Willoughby,[57] and used later by Wang and Carrington,[94] might be a good choice.

# Chapter 7

# Vibrational energy levels of $CH_4$ and $CH_2D_2$

An optimal combination of the Eckart–Watson Hamiltonian, the Hermite-DVR, and the sophisticated eigensolver techniques presented in Chapters 4 and 6 allow the computation of hundreds of numerically exact eigenpairs of arbitrary semi-rigid, up to five-atomic molecules on a nowadays standard server machine. Until now such a goal was only achievable by using tailor-made Hamiltonians with contracted basis sets and by exploiting symmetry of the molecules investigated.[64,102,103] As presented, our approach is computationally feasible for five-atomic systems even if the molecule studied has no symmetry or if it is not exploited. For symmetrical molecules the computational requirements can be further reduced, but this was not done during these preliminary applications.

The efficiency of the presented approaches is demonstrated for the five-atomic methane molecule. The knowledge of a complete rovibrational spectrum (linelist) of methane is of extreme significance in the improvement of atmospheric models of, for instance, the Earth and Titan. Our work is a step toward such a complete linelist of this important molecule, which cannot certainly be acquired by means of purely experimental methods, due to the enormous number of possible transitions. In this chapter I present well-converged energy levels of $^{12}CH_4$ and those of its $^{12}CH_2D_2$ isotopologue. Besides energy levels, wave functions were computed too. It is also worth emphasizing already at this point, that the usage of the DEWE program

is not limited to methane-like molecules, but vibrational energy levels and wave functions of any semi-rigid molecule can be computed similarly.

Due to the impossibility to produce a detailed experimental linelist for isotopologues of methane, there have been several attempts to develop algorithms allowing the computation of a large number of accurate eigenpairs. These studies include non-variational attempts, like that of Wang and Sibert,[104] Duncan and Law,[105] and Halonen *et al.*[106,107] As to variational ones, Xie and Tennyson[61,60] solved the stretching and bending subproblems of a molecule of $XY_4$ composition. Carter *et al.*[108,109] computed variationally the rovibrational energy levels of $CH_4$, $CH_3D$, $CH_2D_2$, $CHD_3$, and $CD_4$ using the MULTIMODE program via using an approximate kinetic energy operator and the original and an adjusted form of the quartic force field of Lee *et al.*[110] Chakraborty *et al.*[111] computed the rovibrational energy levels of $CH_4$ for $J = 0 - 50$ using MULTIMODE and certain approximations in the kinetic energy operator.

As to sophisticated PESs of methane, Marquardt *et al.* constructed a global analytic potential energy surface of the electronic ground state of methane by fitting a flexible and robust model potential to lower-level *ab initio* energies and adjusting this fit empirically to experimental observables.[112,113]

Schwenke *et al.* computed an eighth-order force field, called T8 of methane and computed vibrational energy levels using a tailor-made variational program developed for this molecule. The published variational vibrational energy levels were converged to about 15 $cm^{-1}$.[79,114] Carrington *et al.*[102,103] used the T8 PES and developed a variational computer code for the computation of rovibrational energy levels of methane employing an internal-coordinate Hamiltonian, a two-stage contraction technique, and iterative eigensolver methods. At about the same time, Yu has also developed a similar tailor-made variational code for methane.[64]

Oyanagi *et al.*, Ref. 115, developed full-dimensional *ab initio* potential energy and dipole moment surfaces using the modified Shepard interpolation method based on a fourth order Taylor expansion. The generated surface was used with MULTIMODE and approximate kinetic energy operators, and vibrational band origins and vibrational intensities of methane were determined.

In this work, the T8 force field[79] was employed in order to demonstrate the accuracy, efficiency, and robustness of the DEWE protocol and code. The accuracy of our results can be demonstrated by comparing the computed vibrational levels for $^{12}CH_4$ with reference data computed previously with tailor-made variational programs.[64,102,103] Completely new vibrational band origins (VBOs) are given here, employing the same PES, for the isotopologue $^{12}CH_2D_2$.

To obtain the results described below, the reference structure, **c**, was chosen as the minimum of the actual T8 PES. The elements of the **l** matrix [Eq. 2.6] were constructed by carrying out a harmonic analysis with the diagonal-only force-constants of Ref. 110. The actual values of **c** and **l** used are provided in the Supplementary Material of Ref. 36. As the DEWE approach is numerically exact, the actual values of **c** and **l**, satisfying the conditions given in Eqs. (2.6), affects only the convergence rate but does not influence the values of the converged eigenpairs. This observation is in line with the simple physical fact that the choice of **c** and **l** is merely a possible choice of coordinates. It is worth noting that degenerate levels converge fast enough only if the corresponding symmetry of the molecule is accurately reflected by the numerical values of **c** and **l**.

## 7.1 $CH_4$

The $^{12}CH_4$ molecule was chosen to be one of the numerical examples of the present work in order to demonstrate the utility of the DEWE code, which is universally applicable also for other, even larger semi-rigid molecules. $^{12}CH_4$ is an ideal choice for such purposes as variational results are available in the literature obtained with codes specifically developed for this system[102,103,64] and using the same T8[79] force field. The nuclear masses, $m_C = 11.996709$ u and $m_H = 1.007276$ u, corresponding to the T8 PES were employed throughout the computations.

### Fundamentals

In Table 7.1 the favorable convergence properties of the DEWE approach are demonstrated by comparing the fundamentals of $^{12}CH_4$ obtained with small direct-product

Table 7.1: Convergence properties of the DEWE approach: ZPVE and vibrational fundamentals of $^{12}CH_4$, in $cm^{-1}$, obtained with the T8 force field.[79]

| Label | Conv [a,b] | (3,3) [a,c] | | (4,4) [a,c] | | (5,5) [a,c] | |
|---|---|---|---|---|---|---|---|
| (00)(00) $A_1$ | 9691.5 | 9684.2 | [7.4] | 9690.9 | [0.6] | 9691.5 | [0.1] |
| (00)(01) $F_2$ | 1311.7 | 1307.6 {2.4} | [4.1] | 1310.6 {0.3} | [1.1] | 1311.7 {0.0} | [0.0] |
| (00)(10) E | 1533.2 | 1533.0 {0.9} | [0.3] | 1532.6 {0.1} | [0.7] | 1533.2 {0.0} | [0.0] |
| (10)(00) $A_1$ | 2913.8 | – | – | 2922.9 | [−9.2] | 2910.5 | [3.3] |
| (01)(00) $F_2$ | 3013.6 | 3010.8 {4.0} | [2.8] | 2999.3 {0.0} | [14.3] | 3013.5 {0.1} | [0.1] |

[a] Results obtained with DEWE using a $(n_b, n_s)$ direct product grid. $n_b$ and $n_s$, referred to as $(n_b, n_s)$, grid points were used for the bending- and stretching-type vibrational degrees of freedom, resulting in a direct product grid of size $n_b^5 n_s^4$. Nuclear masses, $m_C = 11.996709$ u and $m_H = 1.007276$ u were employed. The reference structure was a tetrahedron with the carbon in the center and hydrogens on the apices with $r(CH) = 1.0890$ Å. The actual values of **c** and **l** matrices employed are given in the Supplementary Material of Ref. 36.
[b] Converged results obtained with DEWE using (8,7) grid.
[c] Maximum splittings of degenerate levels due to the incomplete convergence are given in braces as $\{\nu(\text{highest}) - \nu(\text{lowest})\}$. Deviation of energy levels from converged results is given in brackets, $[\nu(\text{Conv}) - \nu(n_b, n_s)]$.

grids to the converged results. In the notation $(n_b, n_s)$ used henceforth, $n_b$ and $n_s$ correspond to the number of grid points used for each bending- and stretching-type vibrational degree of freedom, respectively, and to a direct product grid of size $n_b^5 n_s^4$. The accuracy of the ZPVE is remarkable already with a (3,3) grid (total size of 19 683) and it is converged to better than 1 $cm^{-1}$ using a (4,4) grid (total size of 262 144). Using a (5,5) grid (total size of 1 953 125) the ZPVE and the fundamentals, except (10)(00) $A_1$, are converged to better than 0.1 $cm^{-1}$. This behavior contradicts somewhat the traditional view that DVR requires the usage of a relatively large number of quadrature points.

The timing and storage requirements of the computation of 20 eigenvalues and eigenvectors on a (5,5) grid are as follows. The size of a single Lanczos vector is 15 MB, thus 194 MB and 745 MB were the total memory and hard disk requirements, respectively. On a nowadays standard server machine such a computation lasts 20–30 minutes using eight computing cores.

**Vibrational energy levels and wave functions up to ∼5500 cm$^{-1}$**

Well-converged energy levels of $^{12}CH_4$ up to 5500 cm$^{-1}$ are presented in Table 7.2. By comparing the two largest computations using (9,8) and (8,7) grids, one can observe that the results presented in the table and corresponding to the (9,8) grid are certainly converged better than 0.05 cm$^{-1}$ with the exception of the (00)(04)$A_1$ level, whose convergence might be better than 0.1 cm$^{-1}$.

Additionally, we note that based on results obtained with DEWE and an (8,7) grid, the symmetry labels corresponding to the VBOs at 5619.44 cm$^{-1}$ and 5624.75 cm$^{-1}$ were given incorrectly in all previously published tables.[64,102,103] The correct assignment, is (00)(22)E and (01)(02)$F_1$, for the lower and upper levels, respectively. These energy levels are not tabulated in Table 7.2 but they can be found in the Supplementary Material in Ref. 36.

The timing and storage requirements corresponding to the results presented in Table 7.2, corresponding to a (9,8) grid [(8,7) grid], a total size of 241 864 704 [a total size of 78 675 968] and 200 eigenvalues are as follows. The size of a single Lanczos vector is 1.80 GB [0.59 GB], thus 23.4 GB [7.6 GB] memory is used by DEWE, and 464 GB [152 GB] data is stored on the hard disk. On a nowadays standard server machine using eight computing cores the computation takes ∼4 months [∼1 months], depending on the processor and the disk capacities.

## 7.2 $CH_2D_2$

The first 40 well-converged vibrational energy levels of $^{12}CH_2D_2$ are presented in Table 7.3. For this isotopologue of methane these are the first numerically exact results, i.e., without introducing any approximations in the variational vibrational computation. The Radau coordinates employed in the T8 PES were computed using the nuclear masses of the parent molecule. In the kinetic energy part the nuclear masses corresponding to $^{12}CH_2D_2$, $m_C = 11.996709$ u, $m_D = 2.013553$ u, and $m_H = 1.007276$ u were employed.

In Table 7.3 the ZPVE and the first 39 VBOs referenced to the ZPVE are presented for $^{12}CH_2D_2$ up to ∼3500 cm$^{-1}$. Most of the energy levels obtained from the

largest computation using a (10,8) grid are most likely converged within 0.01 $cm^{-1}$. In Table 7.3 deviation of the results obtained with the (10,8) and (9,7) grids is given, which is typically less than 0.05 $cm^{-1}$. There is a single level which does not fit in this threshold, located at 2970.98 $cm^{-1}$. It changed by $-0.21$ $cm^{-1}$ upon the increase of the basis to (10,8) from (9,7). Based on the available experimental results this level was assigned to $\nu_1 A_1$.

The timing and storage requirements corresponding to the results presented in Table 7.2, corresponding to an (10,8) grid of total size of 409 600 000, and 40 eigenvalues are as follows. The size of a single Lanczos vector is 3.1 GB, thus 40 GB memory is used by DEWE, and 214 GB data is stored on the hard disk. On a nowadays standard server machine using eight computing cores the computation lasts 6–8 weeks, depending on the processor and the disk capacities.

Table 7.2: ZPVE and VBOs of $^{12}CH_4$, in $cm^{-1}$, obtained with DEWE and the T8 force field.[79]

| Label[a] | DEWE[b] | $\delta$[c] | $\Delta_C$[d] | $\Delta_E$[e] | Label[a] | DEWE[b] | $\delta$[c] | $\Delta_C$[d] | $\Delta_E$[e] |
|---|---|---|---|---|---|---|---|---|---|
| (00)(00)$A_1$ | 9691.54 | 0.00 | 0.00 | – | (01)(01)$F_1$ | 4317.82 | 0.00 | 0.01 | 4.76 |
| (00)(01)$F_2$ | 1311.74 | 0.00 | 0.00 | −0.98 | (01)(01)$A_1$ | 4318.41 | 0.01 | 0.01 | 4.28 |
| (00)(10)E | 1533.25 | 0.00 | 0.00 | 0.08 | (00)(21)$F_2$ | 4350.02 | 0.00 | 0.04 | −1.31 |
| (00)(02)$A_1$ | 2589.77 | 0.00 | 0.00 | −2.73 | (00)(21)$F_1$ | 4364.68 | 0.00 | 0.03 | −1.09 |
| (00)(02)$F_2$ | 2616.23 | 0.00 | 0.00 | −1.97 | (00)(21)$F_2$ | 4379.71 | 0.00 | 0.02 | −0.73 |
| (00)(02)E | 2627.29 | 0.00 | 0.00 | −2.67 | (10)(10)E | 4432.22 | −0.05 | 0.00 | 2.90 |
| (00)(11)$F_2$ | 2831.52 | 0.00 | 0.00 | −1.20 | (01)(10)$F_1$ | 4531.36 | 0.00 | 0.01 | 6.19 |
| (00)(11)$F_1$ | 2846.90 | 0.00 | 0.00 | −0.82 | (01)(10)$F_2$ | 4537.81 | 0.00 | 0.01 | 5.95 |
| (10)(00)$A_1$ | 2913.71 | −0.05 | 0.00 | 2.77 | (00)(30)E | 4591.88 | 0.01 | 0.04 | 0.13 |
| (01)(00)$F_2$ | 3013.60 | 0.00 | 0.00 | 5.89 | (00)(30)$A_2$ | 4595.13 | 0.00 | 0.03 | 0.15 |
| (00)(20)$A_1$ | 3063.48 | 0.00 | 0.00 | 0.17 | (00)(30)$A_1$ | 4595.40 | 0.00 | 0.03 | 0.06 |
| (00)(20)E | 3065.00 | 0.00 | 0.00 | 0.14 | (00)(04)$A_1$ | 5128.02 | 0.11 | 0.27 | −6.68 |
| (00)(03)$F_2$ | 3874.69 | 0.00 | 0.05 | −4.20 | (00)(04)$F_2$ | 5148.96 | 0.04 | 0.23 | −5.72 |
| (00)(03)$A_1$ | 3912.22 | 0.00 | 0.03 | −3.03 | (00)(04)E | 5173.81 | 0.05 | 0.19 | −6.65 |
| (00)(03)$F_1$ | 3924.04 | 0.00 | 0.03 | −3.52 | (00)(04)$F_2$ | 5215.52 | 0.03 | 0.16 | −4.23 |
| (00)(03)$F_2$ | 3935.30 | 0.00 | 0.02 | −4.38 | (00)(04)E | 5234.63 | 0.03 | 0.14 | −5.72 |
| (00)(12)E | 4104.38 | 0.00 | 0.06 | 0.24 | (00)(04)$F_1$ | 5236.32 | 0.03 | 0.14 | −5.54 |
| (00)(12)$F_1$ | 4131.22 | 0.00 | 0.04 | −2.49 | (00)(04)$A_1$ | 5247.02 | 0.04 | 0.12 | −7.04 |
| (00)(12)$A_1$ | 4135.72 | 0.00 | 0.03 | −2.70 | (00)(13)$F_2$ | 5375.41 | 0.01 | 0.25 | 1.54 |
| (00)(12)$F_2$ | 4144.81 | 0.00 | 0.02 | −1.95 | (00)(13)$F_1$ | 5393.98 | 0.00 | 0.23 | −0.29 |
| (00)(12)E | 4153.70 | 0.00 | 0.02 | −2.70 | (00)(13)E | 5428.38 | 0.00 | 0.17 | −3.72 |
| (00)(12)$A_2$ | 4164.30 | 0.00 | 0.03 | −2.39 | (00)(13)$F_2$ | 5434.05 | 0.01 | 0.17 | −4.47 |
| (10)(01)$F_2$ | 4221.84 | −0.05 | 0.00 | 1.62 | (00)(13)$F_1$ | 5441.27 | 0.00 | 0.15 | −4.48 |
| (01)(01)$F_2$ | 4314.22 | 0.00 | 0.01 | 4.99 | (00)(13)$F_2$ | 5448.36 | 0.00 | 0.12 | −3.24 |
| (01)(01)E | 4317.58 | 0.00 | 0.01 | 4.62 | (00)(13)$F_1$ | 5467.01 | 0.00 | 0.11 | −4.09 |

[a] Energy levels are labeled as $(v_1v_3)(v_2v_4)$, following the polyad notation of Carrington *et al.*[102,103]

[b] Results obtained with the DEWE program. Nuclear masses, $m_C$ = 11.996709 u and $m_H$ = 1.007276 u were used. The reference structure was a tetrahedron with the carbon in the center and hydrogens on the apices with $r$(CH) = 1.0890 Å. The actual values of **c** and **l** matrices employed are given in the Supplementary Material of Ref. 36. 9 and 7, referred to as (9,8), grid points were used for the bending- and stretching-type vibrational degrees of freedom, resulting in a direct-product grid of a total size of 241 864 704.

[c] Deviations of vibrational energy levels obtained with (9,8) and (8,7) grid points, $\delta = \tilde{\nu}(\text{DEWE}(9,8)) - \tilde{\nu}(\text{DEWE}(8,7))$.

[c] Deviations of vibrational energy levels obtained with DEWE(9,8) from results of Carrington *et al.*,[102,103] $\Delta_C = \tilde{\nu}(\text{Ref. 103}) - \tilde{\nu}(\text{DEWE}(9,8))$.

[d] Deviations of vibrational energy levels obtained with DEWE(9,8) and vibrational band origins extracted from experimental data,[116,117,118] $\Delta_E = \tilde{\nu}(\text{Exp}) - \tilde{\nu}(\text{DEWE}(9,8))$.

Table 7.3: ZPVE and VBOs of $^{12}CH_2D_2$, in $cm^{-1}$, obtained with DEWE and the T8 force field.[79]

| Label[a] | | DEWE[b] | $\delta$[c] | $\Delta_E$[d] | Label[a] | | DEWE[b] | $\delta$[c] | $\Delta_E$[d] |
|---|---|---|---|---|---|---|---|---|---|
| ZPVE | $A_1$ | 8432.21 | 0.01 | – | $\nu_3+\nu_9$ | $B_2$ | 2672.46 | 0.00 | −0.77 |
| $\nu_4$ | $A_1$ | 1033.11 | 0.00 | −0.06 | $\nu_3+\nu_5$ | $A_2$ | 2765.98 | 0.00 | |
| $\nu_7$ | $B_1$ | 1091.54 | 0.00 | −0.35 | $2\nu_3$ | $A_1$ | 2856.07 | −0.02 | −0.40 |
| $\nu_9$ | $B_2$ | 1236.90 | 0.00 | −0.62 | $\nu_1$ | $A_1$ | 2970.98 | −0.21 | 5.50 |
| $\nu_5$ | $A_2$ | 1331.23 | 0.00 | 0.18 | $\nu_6$ | $B_1$ | 3006.09 | −0.04 | 6.17 |
| $\nu_3$ | $A_1$ | 1435.27 | 0.00 | −0.14 | $3\nu_4$ | $A_1$ | 3066.96 | −0.02 | |
| $2\nu_4$ | $A_1$ | 2054.51 | −0.01 | −0.35 | $2\nu_4+\nu_7$ | $B_1$ | 3142.32 | −0.01 | |
| $\nu_4+\nu_7$ | $B_1$ | 2125.13 | 0.00 | −0.45 | $\nu_2+\nu_4$ | $A_1$ | 3182.58 | −0.03 | |
| $\nu_2$ | $A_1$ | 2144.29 | −0.05 | 1.40 | $\nu_4+2\nu_7$ | $A_1$ | 3209.95 | −0.03 | |
| $2\nu_7$ | $A_1$ | 2202.31 | −0.04 | 0.91 | $\nu_2+\nu_7$ | $B_1$ | 3233.07 | −0.03 | |
| $\nu_8$ | $B_2$ | 2231.83 | −0.01 | 2.86 | $\nu_4+\nu_8$ | $B_2$ | 3241.24 | −0.01 | |
| $\nu_4+\nu_9$ | $B_2$ | 2284.55 | 0.00 | 1.43 | $3\nu_7$ | $B_1$ | 3306.23 | −0.04 | |
| $\nu_7+\nu_9$ | $A_2$ | 2331.28 | 0.00 | −1.58 | $2\nu_4+\nu_9$ | $B_2$ | 3312.08 | −0.01 | |
| $\nu_4+\nu_5$ | $A_2$ | 2364.85 | 0.00 | | $\nu_7+\nu_8$ | $A_2$ | 3319.38 | −0.01 | |
| $\nu_5+\nu_7$ | $B_2$ | 2422.44 | 0.00 | −0.41 | $\nu_4+\nu_7+\nu_9$ | $A_2$ | 3375.92 | 0.00 | |
| $2\nu_9$ | $A_1$ | 2460.04 | −0.01 | −1.24 | $\nu_2+\nu_9$ | $B_2$ | 3380.77 | −0.05 | |
| $\nu_3+\nu_4$ | $A_1$ | 2470.07 | 0.00 | −0.87 | $2\nu_4+\nu_5$ | $A_2$ | 3386.52 | −0.01 | |
| $\nu_3+\nu_7$ | $B_1$ | 2516.53 | 0.00 | −1.08 | $2\nu_7+\nu_9$ | $B_2$ | 3440.30 | −0.03 | |
| $\nu_5+\nu_9$ | $B_1$ | 2561.19 | 0.00 | −0.64 | $\nu_4+\nu_5+\nu_7$ | $B_2$ | 3447.78 | 0.00 | |
| $2\nu_5$ | $A_1$ | 2658.05 | 0.00 | 0.29 | $\nu_8+\nu_9$ | $A_1$ | 3456.42 | 0.00 | |

[a] Assignment of vibrational energy levels according to Ref. 119.

[b] Results obtained with the DEWE program. Nuclear masses, $m_C = 11.996709$ u, $m_D = 2.013553$ u, and $m_H = 1.007276$ u were used. The reference structure was a tetrahedron with the carbon in the center and hydrogens on the apices with $r(CH) = r(CD) = 1.0890$ Å were used. The actual values of **c** and **l** matrices employed are given in the Supplementary Material of Ref. 36. 10 and 8, referred to as (10,8), grid points were used for the bending- and stretching-type vibrational degrees of freedom, resulting in a direct-product grid of a total size of 409 600 000.

[c] Deviation of vibrational energy levels obtained by using the DEWE program and (10,8) and (9,7) grids, $\delta = \tilde{\nu}(\text{DEWE(10,8)}) - \tilde{\nu}(\text{DEWE(9,7)})$.

[d] Deviations of computed levels from experimental data, $\Delta_E = \tilde{\nu}(\text{Ref. 119}) - \tilde{\nu}(\text{DEWE(10,8)})$. $\Delta_E$ is given where experimental data was available.

# Chapter 8

# Vibrational assignments: Normal mode decomposition

The vibrational part of the Eckart–Watson Hamiltonian, introduced in Eq. (4.6), can be written as

$$\hat{H}^{\mathrm{vib}} = \frac{1}{2}\sum_{k=1}^{3N-6}\left(\hat{P}_k^2 + \lambda_k Q_k^2\right) + \frac{1}{2}\sum_{\alpha\beta}\hat{\pi}_\alpha \mu_{\alpha\beta}\hat{\pi}_\beta - \frac{\hbar^2}{8}\sum_{\alpha}\mu_{\alpha\alpha} + V^{\mathrm{anh}}, \tag{8.1}$$

where $V^{\mathrm{anh}}$ is the anharmonic potential energy function, which is the total potential energy minus the harmonic potential energy. Using the DEWE program described in Chapter 4, numerically exact eigenvalues, $E_n$, and eigenvectors, $\psi_n$ corresponding to this exact operator can be computed. A particularly simple approximation to this operator is

$$\hat{H}^{\mathrm{HO}} = \frac{1}{2}\sum_{k=1}^{3N-6}\left(\hat{P}_k^2 + \lambda_k Q_k^2\right), \tag{8.2}$$

which is the quantum Hamiltonian of $3N-6$ uncoupled harmonic oscillators (HO) of $\omega_k = \hbar\lambda_k^{1/2}$ frequency. Eigenvalues and eigenvectors of this operator can be given in a closed analytic form,[42,120] and they are going to be referred to as the harmonic oscillator energy levels and wave functions. They have the form $E_v^{\mathrm{HO}} = \frac{1}{2}\sum_{k=1}^{3N-6} v_k\omega_k$ and $\psi_v^{\mathrm{HO}} = \prod_{k=1}^{3N-6}\phi_{v_k}(Q_k)$, respectively, where $v = (v_1, v_2, \ldots, v_k)$ and $\phi_{v_k}(Q_k) =$

$N_{v_k} H_{v_k}(\lambda_k^{1/2} Q_k) e^{-\lambda_k Q_k^2/2}$, where $N_{v_k} = \lambda^{1/4} / \left(\pi^{1/2} 2^{v_k} v_k!\right)^{1/2}$. In what follows let us use the notation $|\psi_v\rangle = |v_1, v_2, \ldots, v_{3N-6}\rangle$

In order to qualitatively and semi-quantitatively characterize an exact vibrational level, let us expand $\psi_n$ on the set of the harmonic oscillator eigenfunctions as

$$|\psi_n\rangle = \sum_v c_{nv} |\psi_v^{\mathrm{HO}}\rangle = \sum_v c_{nv} |v_1, v_2, \ldots, v_{3N-6}\rangle. \tag{8.3}$$

Due to the normalization of the wave function,

$$\sum_v |c_{nv}|^2 = 1, \tag{8.4}$$

thus the $|c_{nv}|^2$ values can be considered as the weights of the $v = (v_1, v_2, \ldots, v_{3N-6})$ normal mode to the $n$th exact level. The $|c_{nv}|^2$ coefficients (*e.g.,* tabulated in a matrix form and expressed in %) are, from now on, referred to as a normal mode decomposition (NMD).[66,68,69,121] The labeling of the exact levels by the usual but approximate normal mode labels can be carried out based on the most dominant harmonic oscillator eigenfunction(s) to a given exact vibrational level, which can be directly read from an NMD table.

Computation of NMD coefficients is straightforward by using wave functions provided by DEWE, if normal coordinates corresponding to the actual PES are chosen as the rectilinear internal coordinates.

## 8.1 NMD of $H_2{}^{16}O$

A part of the NMD table of $H_2{}^{16}O$ is given in Table 8.1. Wave functions, $\psi_n$ ($n = 0, 1, \ldots,$) were computed with DEWE using the CVRQD PES,[9,35] the corresponding nuclear masses, and normal coordinates. For the reference structure the minimum point of the CVRQD PES was chosen. Normal coordinates were generated with the INTDER2000 program using the force constants corresponding to the CVRQD PES. For the first ten vibrational energy levels, which include the fundamentals, a single harmonic oscillator wave function dominates in the anhar-

Table 8.1: NMD of $H_2{}^{16}O$ obtained with DEWE (20 basis functions were applied for each vibrational degree of freedom, and 80 eigenpairs were involved in the NMD summation.)

| % | | 4715.52 (0 0 0) | 1649.78 (0 1 0) | 3299.56 (0 2 0) | 3835.07 (1 0 0) | 3946.19 (0 0 1) | 4949.35 (0 3 0) | 5484.85 (1 1 0) | 5595.98 (0 1 1) | 6599.13 (0 4 0) | 7134.63 (1 2 0) | 7245.76 (0 2 1) | 7670.14 (2 0 0) | 7781.26 (1 0 1) | 7892.39 (0 0 2) | | $\sum$ |
|---|---|---|---|---|---|---|---|---|---|---|---|---|---|---|---|---|---|
| 4638.31 | $\psi_0$ | 97 | 0 | 0 | 2 | 0 | 0 | 0 | 0 | 0 | 0 | 0 | 0 | 0 | 0 | ... | 100 |
| 1595.08 | $\psi_1$ | 0 | 98 | 0 | 0 | 0 | 0 | 1 | 0 | 0 | 0 | 0 | 0 | 0 | 0 | ... | 100 |
| 3152.20 | $\psi_2$ | 0 | 0 | 95 | 2 | 0 | 1 | 0 | 0 | 0 | 1 | 0 | 0 | 0 | 0 | ... | 100 |
| 3657.05 | $\psi_3$ | 2 | 0 | 2 | 83 | 0 | 0 | 0 | 0 | 0 | 0 | 0 | 10 | 0 | 1 | ... | 100 |
| 3755.73 | $\psi_4$ | 0 | 0 | 0 | 0 | 89 | 0 | 0 | 0 | 0 | 0 | 0 | 0 | 9 | 0 | ... | 100 |
| 4667.57 | $\psi_5$ | 0 | 0 | 1 | 0 | 0 | 88 | 5 | 0 | 3 | 1 | 0 | 0 | 0 | 0 | ... | 100 |
| 5235.49 | $\psi_6$ | 0 | 2 | 0 | 0 | 0 | 5 | 83 | 0 | 0 | 0 | 0 | 0 | 0 | 0 | ... | 100 |
| 5331.51 | $\psi_7$ | 0 | 0 | 0 | 0 | 0 | 0 | 0 | 90 | 0 | 0 | 0 | 0 | 0 | 0 | ... | 100 |
| 6135.11 | $\psi_8$ | 0 | 0 | 0 | 0 | 0 | 4 | 0 | 0 | 75 | 8 | 0 | 0 | 0 | 0 | ... | 100 |
| 6775.96 | $\psi_9$ | 0 | 0 | 1 | 0 | 0 | 0 | 0 | 0 | 8 | 78 | 0 | 3 | 0 | 0 | ... | 99 |
| 6872.15 | $\psi_{10}$ | 0 | 0 | 0 | 0 | 0 | 0 | 0 | 0 | 0 | 0 | 89 | 0 | 2 | 0 | ... | 99 |
| 7201.19 | $\psi_{11}$ | 0 | 0 | 0 | 11 | 0 | 0 | 0 | 0 | 0 | 3 | 0 | 48 | 0 | 6 | ... | 97 |
| 7249.22 | $\psi_{12}$ | 0 | 0 | 0 | 0 | 9 | 0 | 0 | 0 | 0 | 0 | 2 | 0 | 57 | 0 | ... | 97 |
| 7444.88 | $\psi_{13}$ | 0 | 0 | 0 | 0 | 0 | 0 | 0 | 0 | 0 | 0 | 0 | 10 | 0 | 69 | ... | 98 |
| | | ⋮ | ⋮ | ⋮ | ⋮ | ⋮ | ⋮ | ⋮ | ⋮ | ⋮ | ⋮ | ⋮ | ⋮ | ⋮ | ⋮ | | |
| | $\sum$ | 100 | 100 | 100 | 99 | 100 | 100 | 100 | 100 | 100 | 100 | 100 | 98 | 97 | 98 | | |

monic wave function. Thus, the assignment and the description of the anharmonic levels is straightforward and simple.

## 8.2 NMD of *t*-HCOD

In contrast to the simple case of water, the mixing pattern of harmonic oscillator wave functions in the exact wave function was found to be considerably more complex in several four-atomic species studied. During my doctoral research I studied the NMD table of *t*-HCOH, *t*-HCOD,[66] six isotopologues of NCCO,[68] and the HNCO and DNCO[69] four-atomic species. I observed in each cases a rather strong mixing of fundamentals with other combination levels, making the assignment of already the fundamentals difficult. Table 8.2 presents part of the NMD table of

Table 8.2: NMD of *t*-HCOD obtained with DEWE (9 basis functions were applied for each vibrational degrees of freedom, and 40 eigenpairs were involved in the NMD summation.)

| % | | ZPVE | $v_6$ | $v_5$ | $v_4$ | $v_3$ | $2v_6$ | $v_5+v_6$ | $2v_5$ | $v_4+v_6$ | $v_4+v_5$ | $v_3+v_6$ | $v_3+v_5$ | $2v_4$ | $v_2$ | $v_3+v_4$ | $3v_6$ | $v_5+2v_6$ | $2v_5+v_6$ | $3v_5$ | $v_1$ | | $\sum$ |
|---|---|---|---|---|---|---|---|---|---|---|---|---|---|---|---|---|---|---|---|---|---|---|---|
| | | 5902.1 | 1094.3 | 1220.0 | 1334.1 | 1513.7 | 2188.6 | 2314.3 | 2428.4 | 2440.0 | 2554.1 | 2608.0 | 2668.2 | 2733.7 | 2847.8 | 2876.6 | 3027.4 | 3282.9 | 3408.6 | 3522.7 | 3534.3 | | |
| 5067.4 | $\psi_0$ | 98 | 0 | 0 | 1 | 0 | 0 | 0 | 0 | 0 | 0 | 0 | 0 | 0 | 0 | 0 | 0 | 0 | 0 | 0 | 1 | … | 100 |
| 907.1 | $\psi_1$ | 0 | 98 | 0 | 0 | 0 | 0 | 0 | 0 | 1 | 0 | 0 | 0 | 0 | 0 | 0 | 0 | 0 | 0 | 0 | 0 | … | 99 |
| 928.7 | $\psi_2$ | 0 | 0 | 98 | 0 | 0 | 0 | 0 | 0 | 0 | 1 | 0 | 0 | 0 | 0 | 0 | 0 | 0 | 0 | 0 | 0 | … | 99 |
| 1294.1 | $\psi_3$ | 1 | 0 | 0 | 92 | 0 | 0 | 0 | 0 | 0 | 0 | 0 | 0 | 5 | 0 | 0 | 0 | 0 | 0 | 0 | 0 | … | 98 |
| 1420.8 | $\psi_4$ | 0 | 0 | 0 | 0 | 97 | 0 | 0 | 0 | 0 | 0 | 0 | 0 | 0 | 0 | 1 | 0 | 1 | 0 | 0 | 0 | … | 99 |
| 1798.0 | $\psi_5$ | 0 | 0 | 0 | 0 | 0 | 90 | 0 | 5 | 0 | 0 | 0 | 0 | 0 | 1 | 0 | 0 | 0 | 0 | 0 | 1 | … | 99 |
| 1833.6 | $\psi_6$ | 0 | 0 | 0 | 0 | 0 | 0 | 97 | 0 | 0 | 0 | 0 | 0 | 0 | 0 | 0 | 0 | 0 | 0 | 0 | 0 | … | 99 |
| 1847.1 | $\psi_7$ | 0 | 0 | 0 | 0 | 0 | 5 | 0 | 90 | 0 | 0 | 0 | 0 | 0 | 1 | 0 | 0 | 0 | 0 | 0 | 0 | … | 98 |
| 2192.5 | $\psi_8$ | 0 | 1 | 0 | 0 | 0 | 0 | 0 | 0 | 91 | 0 | 0 | 0 | 0 | 0 | 0 | 0 | 0 | 0 | 0 | 0 | … | 99 |
| 2215.3 | $\psi_9$ | 0 | 0 | 1 | 0 | 0 | 0 | 0 | 0 | 0 | 91 | 0 | 0 | 0 | 0 | 0 | 0 | 0 | 0 | 0 | 0 | … | 98 |
| 2328.5 | $\psi_{10}$ | 0 | 0 | 0 | 0 | 0 | 0 | 0 | 0 | 0 | 0 | 97 | 0 | 0 | 0 | 0 | 0 | 0 | 0 | 0 | 0 | … | 97 |
| 2344.1 | $\psi_{11}$ | 0 | 0 | 0 | 0 | 0 | 0 | 0 | 0 | 0 | 0 | 0 | 95 | 0 | 0 | 0 | 0 | 0 | 0 | 0 | 1 | … | 97 |
| 2566.4 | $\psi_{12}$ | 0 | 0 | 0 | 5 | 0 | 0 | 0 | 0 | 0 | 0 | 0 | 0 | 78 | 0 | 0 | 0 | 0 | 0 | 0 | 0 | … | 83 |
| 2626.8 | $\psi_{13}$ | 1 | 0 | 0 | 0 | 0 | 1 | 0 | 2 | 0 | 0 | 0 | 0 | 0 | 83 | 2 | 0 | 2 | 0 | 0 | 2 | … | 92 |
| 2675.5 | $\psi_{14}$ | 0 | 0 | 0 | 0 | 0 | 0 | 0 | 0 | 1 | 0 | 0 | 0 | 0 | 0 | 0 | 85 | 0 | 6 | 0 | 0 | … | 94 |
| 2682.8 | $\psi_{15}$ | 0 | 0 | 0 | 0 | 0 | 0 | 0 | 0 | 0 | 0 | 0 | 1 | 0 | 5 | 37 | 0 | 37 | 0 | 0 | 45 | … | 92 |
| 2713.4 | $\psi_{16}$ | 0 | 0 | 0 | 0 | 0 | 0 | 0 | 0 | 0 | 0 | 0 | 0 | 0 | 0 | 0 | 0 | 0 | 0 | 21 | 0 | … | 92 |
| 2729.5 | $\psi_{17}$ | 0 | 0 | 0 | 0 | 1 | 0 | 0 | 0 | 0 | 0 | 0 | 1 | 0 | 0 | 51 | 0 | 0 | 0 | 0 | 33 | … | 91 |
| 2752.1 | $\psi_{18}$ | 0 | 0 | 0 | 0 | 0 | 0 | 0 | 0 | 0 | 0 | 0 | 0 | 0 | 0 | 0 | 7 | 0 | 88 | 0 | 0 | … | 96 |
| 2757.9 | $\psi_{19}$ | 0 | 0 | 0 | 0 | 0 | 0 | 0 | 0 | 0 | 0 | 0 | 0 | 0 | 0 | 0 | 0 | 0 | 0 | 68 | 0 | … | 93 |
| | | ⋮ | ⋮ | ⋮ | ⋮ | ⋮ | ⋮ | ⋮ | ⋮ | ⋮ | ⋮ | ⋮ | ⋮ | ⋮ | ⋮ | ⋮ | ⋮ | ⋮ | ⋮ | ⋮ | ⋮ | | |
| | $\sum$ | 100 | 99 | 99 | 98 | 99 | 99 | 99 | 98 | 93 | 98 | 97 | 97 | 83 | 92 | 92 | 92 | 92 | 94 | 94 | 90 | | |

*t*-HCOD obtained with DEWE and using a quartic force field computed at the AE-CCSD(T)/cc-pCVQZ level of theory,[66] which is a typical example for the four-atomic species studied. In this case the NMD table is diagonally dominant up to 2626.8 $cm^{-1}(\psi_{13})$ and the assignment is unambiguous. As to the assignment of the $\nu_1$ fundamental, one can observe that the $\phi^{HO}_{\nu_1}$ has significant contributions to two exact levels, namely to $\psi_{15}$ at 2682.8 $cm^{-1}$ and to $\psi_{17}$ at 2729.5 $cm^{-1}$. Based on its larger contribution, 45 %, to the 2628.8 $cm^{-1}$ ($\psi_{15}$) exact energy level, this is assigned to be the $\nu_1$ fundamental of this molecule. However, one has to note that the $\phi^{HO}_{\nu_1}$ harmonic oscillator wave function is strongly mixing with other harmonic oscillator wave functions, in particular with $\phi^{HO}_{\nu_3+\nu_4}$ and $\phi^{HO}_{\nu_5+2\nu_6}$.

# Chapter 9

# Outlook and further applications

## 9.1 Zero-point vibrational energies for thermochemistry

To compute high-quality thermochemical data,[67,122] such as enthalpies of formation of small molecules, one needs to know the anharmonic zero-point vibrational energies (ZPVE). Supposing that an appropriate anharmonic (quartic) force field is available, anharmonic ZPVEs can be computed by means of vibrational perturbation theory (VPT),[123] diffusion Monte-Carlo (DMC) methods,[124,125] or by using a variational approach. Undoubtedly, the cost of evaluating approximate VPT formulae, especially at second order, is by far the lowest. The computation of ZPVEs for medium-sized and large molecules, with more than 8–10 nuclei, is straightforward only by using second-order vibrational perturbation theory (VPT2) formulae. It is thus of considerable interest to check the accuracy of VPT2 ZPVEs of small molecules also manageable by the variational approaches presented in the previous chapters, as the latter provide the numerically exact results corresponding to a given representation of the PES.

The complete VPT2 expression for the zero-point vibrational energy is[126]

$$\mathrm{ZPVE} = G_0 + \frac{1}{2}\sum_i d_i\omega_i + \frac{1}{4}\sum_{i\geq j} d_i d_j \chi_{ij} \tag{9.1}$$

where $d_i$ is the degeneracy of vibrational mode $i$. This expression can be further simplified to obtain

$$\mathrm{ZPVE} = \frac{1}{2}\sum_i \omega_i - \frac{1}{32}\sum ijk\frac{\phi_{iik}\phi_{kjj}}{\omega_k} - \frac{1}{48}\sum_{ijk}\frac{\phi_{ijk}^2}{\omega_i+\omega_j+\omega_k} + \frac{1}{32}\sum_{ij}\phi_{iijj} + Z_{\mathrm{kin}}, \tag{9.2}$$

where the $Z_{\mathrm{kin}}$ term is given in Ref. 126 for asymmetric top, symmetric top and linear molecules. The remarkable feature of these complete VPT2 expressions for the anharmonic ZPVE is that they are free of resonant denominators, which are responsible for most of the technical difficulties in using perturbational techniques. These formulae are implemented, for instance, in the program ANHARM.[127,128] It is worth noting that the most popular quantum chemistry packages use an incomplete VPT2 expression, which suffers from the problem of resonant denominators and mostly the $G_0$ term is not considered.

Table 9.1 presents the ZPVE of 3–4-atomic molecules with linear and nonlinear equilibrium structures. The presented VPT2 results include the $G_0$ term, as given in Eq. (9.2), and were obtained by using the ANHARM program. The variational ZPVEs were computed by the DEWE program. The VPT2 results agree within 1 $\mathrm{cm}^{-1}$ with the variational results obtained with the DEWE program, which is better than one could have expected. It is worth noting that in variational DEWE computations the quartic force field was expressed in terms of internal coordinates, whereas the perturbational expressions use the corresponding quartic force field expressed in normal coordinates. This latter provides, in general, a less accurate representation of the PES. Thus, the excellent VPT2 results originate from a fortunate cancelation of errors corresponding to the truncation of the perturbational treatment and that of the force field representation.

In any case, the ease of use of VPT2[$G_0$] expressions for the ZPVE due to the lack of resonant denominators, the low (practically zero) computational cost, and the promising accuracy compared to numerically exact variational results, support the usage of the expression given in Eq. (9.2) for anharmonic ZPVEs required. Nev-

Table 9.1: Zero-point vibrational energies computed by vibrational perturbational theory carried out to second order (VPT2) and the variational DEWE program.

| Molecule | Ref.* | Harmonic $\hat{W}_{00}(\mathrm{II})^{c}$ | VPT2[$G_0$][a] $\hat{W}_{11}(\mathrm{IV})^{c}$ | DEWE $\hat{W}_{11}(4)^{c}$ | $\Delta^{b}$ |
|---|---|---|---|---|---|
| $H_2O$ | A | 4709.4 | 4633.7 | 4634.0 | 0.3 |
| $H_2S$ | B | 3327.3 | 3285.2 | 3285.3 | 0.1 |
| $CH_2$ $^1A_1$ | C | 3667.0 | 3609.7 | 3610.0 | 0.2 |
| $CO_2$ | D | 2531.7 | 2519.8 | 2519.7 | 0.0 |
| $N_2O$ | D | 2391.1 | 2374.0 | 2374.0 | 0.0 |
| $H_2CO$ | E | 5858.0 | 5783.4 | 5783.8 | 0.5 |
| $D_2CO$ | E | 4594.7 | 4551.4 | 4551.5 | 0.1 |
| HNCO | F | 4678.2 | 4628.3 | 4628.2 | −0.1 |
| DNCO | F | 4073.3 | 4040.7 | 4040.5 | −0.1 |
| *t*-HCOH | G | 5902.1 | 5803.2 | 5803.7 | 0.5 |
| *t*-HCOD | G | 5141.6 | 5067.1 | 5067.4 | 0.3 |
| $^{14}N^{12}C^{12}C^{16}O$ | H | 3014.6 | 2992.0 | 2991.6 | −0.4 |
| $^{14}N^{12}C^{13}C^{16}O$ | H | 2980.5 | 2958.5 | 2958.2 | −0.3 |
| $^{14}N^{13}C^{12}C^{16}O$ | H | 2976.1 | 2954.0 | 2953.7 | −0.3 |
| $^{14}N^{13}C^{13}C^{16}O$ | H | 2941.8 | 2920.4 | 2920.1 | −0.3 |
| $^{15}N^{12}C^{12}C^{16}O$ | H | 2993.4 | 2971.0 | 2970.7 | −0.4 |
| $^{15}N^{12}C^{13}C^{16}O$ | H | 2959.3 | 2937.5 | 2937.2 | −0.3 |
| $NH_3$ | I | 7581.2 | 7453.6 | 7453.7 | 0.1 |
| $BH_3$ | J | 5798.3 | 5723.2 | 5723.4 | 0.3 |
| $BD_3$ | J | 4291.1 | 4249.5 | 4249.6 | 0.1 |
| $C_2H_2$ | K | 5816.3 | 5743.1 | 5742.4 | −0.6 |
| $C_2DH$ | K | 5206.6 | 5147.5 | 5146.7 | −0.8 |
| $C_2D_2$ | K | 4593.5 | 4548.8 | 4548.5 | −0.3 |

[a] VPT2 expression including the $G_0$ term, given in Eq. (9.2), as implemented in ANHARM.[127,128]

[b] $\Delta = \mathrm{ZPVE(DEWE)} - \mathrm{ZPVE(VPT2[G_0])}$.

[c] $\hat{W}_{nm}(\mathfrak{N}) = \hat{W}_{nm} = n \cdot \frac{1}{2}\sum_{\alpha\beta}\mu_{\alpha\beta}\hat{\pi}_\alpha\hat{\pi}_\beta - m \cdot \frac{\hbar^2}{8}\sum_\alpha \mu_{\alpha\alpha} + \frac{1}{2}\sum_{k=1}^{3N-6}\hat{P}_k^2 + V(\mathfrak{N})$. $V(II)$: second-order force field expressed in terms of normal coordinates; $V(IV)$: quartic force field expressed in terms of normal coordinates; $V(4)$: quartic force field expressed in terms of curvilinear internal coordinates, SPF[44] coordinates were used to describe the bond stretching efficiently.[6]

* Details of the electronic structure methods used to generate the force field, taken from the specified reference. A: CCSD(T)/aug-cc-pVQZ, Ref: 129; B: CCSD(T)/cc-pVQZ for harmonic force constants, and CCSD(T)/cc-pVTZ for anharmonic force constants, Ref: 130; C: AE-CCSD(T)/aug-cc-pCVQZ, Ref: 131; D: CCSD(T)/cc-pVQZ, Ref: 132; E: CCSD(T)/cc-pVQZ, Ref: 133; F: AE-CCSD(T)/cc-pCV5Z, Ref. 69; G: AE-CCSD(T)/cc-pCVQZ, Ref. 66; H: AE-ROCCSD(T)/cc-pCVQZ, Ref. 68; I: AE-CCSD(T)/cc-pCVQZ, Ref. 67; J: CCSD(T)/cc-pCVQZ, Ref. 134; K: CCSD(T)/cc-pVQZ, Ref. 135.

ertheless, the accuracy and reliability of Eq. (9.2) must be further studied, especially for larger (5–7-atomic) systems.

## 9.2 Computation of cumulative reaction probabilities

Besides the computation of (ro)vibrational energy levels and wave functions, nuclear motion theory based on quantum mechanics is also concerned with the quantum mechanical rate of chemical reactions. Computation of very accurate rate coefficients can have an important role, for example, in the improvement of the modeling of atmospheric chemical processes or in reactions where tunneling effects might have an overly important role.[66]

The quantum mechanical rate coefficients of a bimolecular reaction is[136,137]

$$k(T) = \frac{1}{2\pi\hbar Q_{\mathrm{r}}(T)} \int_{-\infty}^{\infty} \mathrm{d}E \; \mathrm{e}^{-\beta E} N(E), \tag{9.3}$$

where $E$ is the total energy of the reactant system, $Q_{\mathrm{r}}(T)$ is the partition function of the reactants, and $N(E)$ is the quantum cumulative reaction probability (CRP). Seideman and Miller have demonstrated that the quantum CRP can be written in a compact form as[138,139,140]

$$N(E) = \mathrm{Tr}\hat{P}(E), \quad \text{where} \tag{9.4}$$

$$\hat{P}(E) = \left[\epsilon_{\mathrm{r}} \hat{G}(E + i\varepsilon) \epsilon_{\mathrm{p}} \hat{G}(E - i\varepsilon)\right] \tag{9.5}$$

$$\hat{G}(E \pm i\varepsilon) = (E \pm i\varepsilon - \hat{H})^{-1}, \tag{9.6}$$

where $i\varepsilon = (i\varepsilon_{\mathrm{r}} + i\varepsilon_{\mathrm{p}})/2$ is a complex absorbing potential (CAP) and $\varepsilon \to 0$. $\hat{P}(E)$ is often referred to as the reaction probability operator.

The reactants and the products are distinguished mathematically by defining a dividing surface. $\varepsilon_{\mathrm{r}} > 0$ holds on the reactant side, otherwise it is zero, whereas $\varepsilon_{\mathrm{p}} > 0$ holds on the product side, otherwise it is zero. The value of $N(E)$ is independent of the choice of the dividing surface,[137] which is used only for technical reasons. $\varepsilon$ can

Table 9.2: Comparison of algorithms used for the computation of (ro)vibrational energy levels and quantum cumulative reaction probabilities.

| | (Ro)vibrational levels | Cumulative reaction probability |
|---|---|---|
| PES | Bound system | Reactive system |
| DVR | Hermite or Legendre DVR | Sine DVR |
| CAP | – | Woods–Saxon,[136,137] GLM[139] |
| Hamiltonian | Matrix-vector multiplication | Matrix-vector multiplication |
| Other | Spectral transformation (real): → SF,Exponential,CGM,QMR | Green function (complex): → GMRES, QMR |
| Eigensolver | Lanczos (real arithmetics) | Arnoldi (complex arithmetics) |
| Eigenvalues | Lowest, many | Largest, few |

also be considered as a convergence parameter, and $N(E)$ tends to its exact value as $\varepsilon \to 0$. Technically, $\varepsilon$ is chosen so that it vanishes in the physically interesting region, but is different from zero at the edges of the grid used in a computation.

The expressions given in Eqs. (9.4)–(9.6) provide a direct route for the computation of quantum CRPs without having to solve the complete reactive scattering problem. After careful examination of the terms of these expressions, one should notice that their implementation in a (ro)vibrational (nuclear motion) variational code, such as GENIUSH, requires only minor modifications. The expressions given in Eqs. (9.4)–(9.6) were implemented by Seideman and Manthe using the Eckart–Watson Hamiltonian. Due to the inefficiency of the Eckart–Watson Hamiltonian for the description of large-amplitude motions over several minima, the computed quantum CRPs had to be corrected *a posteriori*.[141]

In the GENIUSH program, presented in Chapter 5, one can define an appropriate body-fixed frame and internal coordinates which describe efficiently large-amplitude motions of a system. Although the GENIUSH program was originally written for the computation of (ro)vibrational energy levels and wave functions, the quantum CRP expression, given in Eq. (9.4) can be straightforwardly implemented in it. The main differences of the computation of quantum CRP compared to (ro)vibrational energy levels are collected in Table 9.2. The matrix of the Hamiltonian enters both algorithms through multiplication of the Hamiltonian matrix and a vector. For com-

putation of CRPs an iterative Arnoldi eigensolver available in ARPACK[142] and other library routines such as GMRES are used.[143]

# Chapter 10

# Summary and conclusions

During my doctoral research I have developed algorithms and implemented computer codes universally applicable for the variational computation of vibrational energy levels and wave functions of small to medium-sized molecular species. One of the main difficulty in developing such black-box programs for theoretical rovibrational spectroscopy is the so-called "coordinate problem".

In order to compute vibrational energy levels and wave functions efficiently one has to replace the $3N$ Cartesian coordinates of the nuclei by coordinates adapted to the different kinds of nuclear motions. This means that after separating the translational degrees of freedom, it is useful to introduce Euler angles, which describe the relative orientation of the body-fixed frame with respect to the laboratory-fixed frame, and internal coordinates more or less adapted to the different types of internal motions of the system. Until very recently, for different body-fixed frames and internal coordinates, different kinetic energy operators had to be derived in an analytic form[5,144] and different algorithms and computer codes had to be implemented. Although there are several successful applications of such tailor-made procedures developed for specific systems,[6,7,8,9,10,11,12,13] it appears preferable to develop algorithms and computer codes for variational computation of vibrational energy levels and wave functions universally applicable for molecules of different size and bonding arrangements.

As a first step toward the stated goal of a universally applicable nuclear motion code, I have chosen Eckart's frame[41] as a body-fixed frame and Watson's rectilinear

internal coordinates[14] defined for molecules of arbitrary bonding arrangements. The simplest form of the (ro)vibrational Hamiltonian of these universally defined coordinates is often referred to as the Watson Hamiltonian.[14] I have developed a variational algorithm using this form of the vibrational Hamiltonian and implemented it in a computer code called DEWE (Chapter 4).[25,36] The name DEWE refers to the main constituents of the algorithm. I constructed the Discrete variable representation of the Eckart–Watson Hamiltonian with the numerically Exact inclusion of the PES, however complicated its actual form is. The required vibrational energy levels and wave functions are computed by using sophisticated Lanczos eigensolver techniques (Chapter 6).

A special case of the coordinates used within the DEWE approach are the normal coordinates. The Hamiltonian can be approximated by the Hamiltonian of $3N-6$ uncoupled harmonic oscillators, whose wave functions contain the Hermite polynomials. Thus a DVR based on normalized Hermite polynomials is used in DEWE, resulting in a numerically very efficient approach. Meaningful results can be obtained already by using a very small number of quadrature points on the vibrational degrees of freedom (see Table 7.1 of Chapter 7). This behavior contradicts somewhat the traditional view that DVR requires the use of a large number of quadrature points (basis functions).

The Watson Hamiltonian has a universal form for $N$-atomic molecules. In line with this property, the DEWE algorithm and computer code do not contain any inherent limitations for the number of nuclei or the actual bonding arrangement. Furthermore, DEWE is able to provide the numerically exact vibrational energy levels and wave functions of an $N$-atomic molecule without introducing any approximations in the kinetic or potential energy terms.

In principle, the single restriction on the coordinates is that the reference structure must be nonlinear.[14] The Watson Hamiltonian has a version for linear reference structures as well,[15] which is implemented in Lin-DEWE,[25,65] to cover a wider range of molecules. Note that the implementation of this Hamiltonian with a linear reference structure is very similar to that of using a nonlinear reference structure; thus, it was not discussed in the present thesis, and details can be found in Ref. 25.

DEWE has been validated against results of independent tailor-made variational programs,[6,102,7,103] and it has had several applications during the last two years.[25,67,66,68,69] Some of these applications are discussed in Chapters 7, 8, and Section 9.1, and are summarized below. The main code is supplemented by auxiliary programs, which compute the normal mode decomposition (Chapter 8)[121] of the variational wave functions and which extract the fundamentals and combination or overtone levels strongly mixing with fundamentals from a possibly large NMD table.

Besides the assignment of energy levels, vibrational intensities can be computed if a representation of the electric dipole moment vector surface (DMS) is available. This work was not discussed in the present thesis, but a working computer code has been developed and the details are described in Ref. 68.

Although the DEWE program has very favorable properties, it suffers from some serious limitations. First, due to the properties of the Eckart frame and Watson's rectilinear internal coordinates the approach is not appropriate for the description of molecules with large amplitude motions (*e.g.*, the inversion motion of ammonia). Second, the singularity of the (ro)vibrational Hamiltonian hinders the convergence of vibrational energy levels significantly sampling the singular region of the Hamiltonian, *e.g.,* linear geometries. As the coordinates are coupled in the singular region, the treatment of the singularity is difficult on a direct product grid or basis.

Apart from these limitations, due to an ideal combination of the discrete variable representation, Hermite polynomials, the Eckart–Watson Hamiltonian, and iterative eigensolver techniques the DEWE program is very efficient for solving the nuclear motion problem of semi-rigid molecules. If very accurate energy levels and wave functions of medium-sized molecules are required it might be competitive with tailor-made computer codes. At present, finite computational resources allow the computation of a large number of well-converged vibrational energy levels and wave functions of semi-rigid five-atomic molecules (Chapter 7),[36] and according to our preliminary tests it is very likely that semi-rigid six-atomic molecules can be handled in the very near future using DEWE.

In order to surmount the limitations of DEWE, while keeping the universal context of the treatment, one has to go back to the roots of internal coordinate

(ro)vibrational Hamiltonians (Chapter 3). In an early stage of the derivation there are general formulae of the internal coordinate (ro)vibrational Hamiltonians, given in Eqs. (3.6) and (3.10), which are valid for any choice of body-fixed frames and internal coordinates. These forms contain the universal quantities $\mathbf{g}$, $\mathbf{G}$, and $U$.

Based on this observation, I have developed an algorithm and implemented it in a computer code called GENIUSH. The name refers to the main characteristics of the program, General (ro)vibrational code with Numerical, Internal-coordinate, User-Specified Hamiltonians. GENIUSH is written using universal quantities $\mathbf{g}$, $\mathbf{G}$, and $U$, the forms of the vibrational Hamiltonians given in Eqs. (3.9) and (3.11), a discrete variable representation, and sophisticated Lanczos eigensolver techniques (Chapter 6). The actual choice of the body-fixed frame and internal coordinates is carried by the actual values of the $\mathbf{g}$, $\mathbf{G}$, and $U$ quantities at the grid points, which are computed by the program automatically (Chapter 5).[34]

There have been previous attempts to write such a black-box-type vibrational program.[29,31,33] The present one provides numerically exact results without any need to introduce of approximations in the Hamiltonian by a truncated power series expansion. Inclusion of any representation of the PES is straightforward and numerically exact due to the favorable properties of DVR.

Due to the numerical construction of the quantities $\mathbf{g}$, $\mathbf{G}$, and $U$, the numerical stability and accuracy of the approach must be carefully tested (Section 5.4). Otherwise, a numerical instability of a few $\mathrm{cm}^{-1}$ can appear in the results, while an accuracy of $< 0.01$ $\mathrm{cm}^{-1}$ is often expected by high-resolution molecular spectroscopy. In GENIUSH both the "rearranged" and the Podolsky forms of the vibrational Hamiltonian, Eqs. (3.9) and (3.11), are implemented. The "Podolsky form" has more favorable properties from a numerical mathematics aspect, as it requires only first derivatives of the Cartesian coordinates in the body-fixed frame in terms of internal coordinates, whereas the "rearranged form" requires first, second, and third derivatives of these coordinates (Section 5.2.1).

The GENIUSH program does not contain any inherent limitations for the number of nuclei or the number of active internal degrees of freedom. As the body-fixed frame and internal coordinates are chosen and defined by the user, upon an appro-

priate choice of these coordinates wide amplitude motions over multiple minima of the PES can be described efficiently (Section 5.4.2). Due to the universal context of the treatment, reduced-dimensional vibrational models can also be defined, thus allowing an approximate quantum mechanical description of large molecules otherwise intractable by quantum mechanical methods (Section 5.4).

GENIUSH is free of most of the deficiencies observed for DEWE, while working within a universal context. Limitations on the wide-amplitude motions present in DEWE are eliminated in GENIUSH if an appropriate set of coordinates is chosen. Furthermore, the problem of singularity can be handled more easily in GENIUSH as compared to DEWE.

To be able to compute a large number of vibrational energy levels and wave functions using either DEWE or GENIUSH sophisticated Lanczos eigensolver techniques must have been adapted. For the computation of a few hundreds of vibrational energy levels of 4–5 atomic molecules the usage of thick-restart Lanczos method, periodic reorthogonalization and the shift-fold spectral transformation technique (SF-PerRo-TRLM) was suggested, which is a simple but efficient choice (Chapter 6).

There is a common drawback characterizing DEWE and GENIUSH. Due to the usage of a direct-product grid, the grid size increases exponentially with the number of vibrational degrees of freedom. The possibility of constructing reduced-dimensional models in GENIUSH remedies this problem to some extent by reducing the number of active vibrational degrees of freedom, which is a meaningful approximation especially for tightly bound intermolecular complexes. However, the ideal solution would be the usage of contraction techniques.[145] A pilot version of a code using a two-stage contraction has been written.

Besides these methodological developments, I have produced new physical and chemical results[34,36,66,67,68,69,70,95,121] using the programs developed. Some of these results were discussed in this doctoral thesis and are summarized in what follows.

Well-converged ZPVEs and VBOs of $^{12}CH_4$ and one of its isotopologues, $^{12}CH_2D_2$, were computed using DEWE and the T8 force field[79] up to 5500 $cm^{-1}$ and 3500 $cm^{-1}$, respectively. These are the best converged benchmark-quality results at present available for these molecules. Additionally, for $^{12}CH_2D_2$ the presented en-

ergy levels are the first numerically exact energy levels, *i.e.*, without introducing any approximations in the treatment. Furthermore, a misassignment of two vibrational energy levels of $^{12}CH_4$ published in all previous theoretical works were pointed out and corrected by us (Chapter 7).

I contributed to the experimental identification of newly prepared reactive species, *t*-HCOH (and *t*-HCOD), and six isotopologues of NCCO by computing their very accurate vibrational energy levels and approximate intensities using DEWE and *ab initio* quartic force and first-order dipole fields. Besides the computation of vibrational energy levels, the corresponding wave functions were characterized by using the NMD assignment scheme (Chapter 8). These results are not discussed here due to the limited size of this thesis. Details on the vibrational calculations performed by us as well as electronic structure calculations and the experiments performed by other groups are described in detail in Refs. 66 and 68.

I performed an NMD analysis for these newly prepared as well as for other better known molecules.[69,121] For triatomic $H_2{}^{16}O$, the assignment of fundamentals and the lowest-lying vibrational levels is unambiguous, as there is always a single harmonic oscillator wave function which is dominant in an exact wave function (Section 8.1). In contrast to this, for several four-atomic molecules there is a strong mixing of harmonic oscillator wave functions already for the fundamentals (Section 8.2). This fact makes the assignment of the mixing fundamentals difficult or somewhat ambiguous, which raises the question of the mathematically strict definition of a fundamental vibration (Chapter 8).

The first well-converged and numerically exact ZPVE and the VBOs up to $\sim$ 6000 cm$^{-1}$ were computed for $^{14}NH_3$ using GENIUSH and the "refined" PES published in Ref. 76. Besides the full-dimensional numerically exact vibrational computations, I have studied the accuracy of reduced-dimensional vibrational models on the inversion splitting of ammonia.

Finally, in Chapter 9 of my doctoral thesis preliminary results and promising ideas on possible further applications of the computer codes developed during my doctoral research are presented. In Section 9.1, I presented the ZPVEs of several molecules computed with DEWE using *ab initio* quartic force fields expressed in

internal coordinates as well as VPT2 (including the $G_0$ term) results using the program ANHARM[127,128] and the corresponding quartic force field expressed in normal coordinates. Interestingly, VPT2[$G_0$] often gives exceedingly accurate results as verified by the variational ZPVEs. VPT2 calculations require negligible computer resources, thus these results are particularly encouraging. The excellent agreement between VPT2 and variationally computed ZPVEs is due to an advantageous cancelation of errors introduced by the truncation in the perturbational treatment and the potential.

In Section 9.2 I describe in some detail that the computation of quantum mechanical cumulative reaction probabilities within Miller's trace formalism and thus rate coefficients of bimolecular reactions requires only straightforward modifications in the GENIUSH code. Similarities of variational algorithms computing (ro)vibrational energy levels and quantum cumulative reaction probabilities indicates that theoretical molecular spectroscopy and quantum reaction kinetics are related fields of physical chemistry.

# Chapter 11

# Appendix A: Computation of the extrapotential term

Logarithmic derivatives can be determined very efficiently by using Gauss elimination,[31] $k = 1, 2, \ldots, D+2$,

$$g_{ij}^{(k+1)} := g_{ij}^{(k)} - \frac{g_{ik}^{(k)}}{g_{kk}^{(k)}} g_{kj}^{(k)}, \quad i = 1, 2, \ldots, D+3, j = k+1, \ldots, D+3 \tag{A-1}$$

and $\mathbf{g}^{(1)} = \mathbf{g}$. In the course of the Gauss elimination steps derivatives of $\ln \tilde{g}$ and $\ln \tilde{G}$ are computed iteratively, as

$$\frac{\partial \ln \tilde{g}}{\partial q_m} = \frac{\partial}{\partial q_m} \ln \prod_{k=1}^{D+3} g_{kk}^{(k)} = \frac{\partial}{\partial q_m} \sum_{k=1}^{D+3} \ln g_{kk}^{(k)} = \sum_{k=1}^{D+3} \frac{1}{g_{kk}^{(k)}} \frac{\partial g_{kk}^{(k)}}{\partial q_m} \tag{A-2}$$

$$\frac{\partial^2 \ln \tilde{g}}{\partial q_n \partial q_m} = \frac{\partial}{\partial q_n} \sum_{k=1}^{D+3} \frac{1}{g_{kk}^{(k)}} \frac{\partial g_{kk}^{(k)}}{\partial q_m} = \sum_{k=1}^{D+3} \left[ \frac{1}{g_{kk}^{(k)}} \frac{\partial^2 g_{kk}^{(k)}}{\partial q_n \partial q_m} - \frac{1}{\left( g_{kk}^{(k)} \right)^2} \frac{\partial g_{kk}^{(k)}}{\partial q_n} \frac{\partial g_{kk}^{(k)}}{\partial q_m} \right]. \tag{A-3}$$

In the $k$th step of the Gauss elimination, the $\frac{\partial \mathbf{g}^{(k+1)}}{\partial q_m}$ and $\frac{\partial^2 \mathbf{g}^{(k+1)}}{\partial q_n \partial q_m}$ matrices are computed by using the elements of $\frac{\partial \mathbf{g}^{(k)}}{\partial q_m}$, $\frac{\partial^2 \mathbf{g}^{(k)}}{\partial q_n \partial q_m}$ matrices. In the $k$th step the $(k+1)$th elements of the expressions in Eqs. (A-2) and (A-3) are evaluated. In each elimination step always only the $k$th and $(k+1)$th derivative matrices are stored, so the procedure has only a modest memory requirement.

$$\frac{\partial g_{ij}^{(k+1)}}{\partial q_m} = \frac{\partial g_{ij}^{(k)}}{\partial q_m} - \frac{\partial g_{ik}^{(k)}}{\partial q_m}\frac{g_{kj}^{(k)}}{g_{kk}^{(k)}} + \frac{g_{ik}^{(k)}}{\left(g_{kk}^{(k)}\right)^2}\frac{\partial g_{kk}^{(k)}}{\partial q_m}g_{kj}^{(k)} - \frac{g_{ik}^{(k)}}{g_{kk}^{(k)}}\frac{\partial g_{kj}^{(k)}}{\partial q_m} \tag{A-4}$$

$$\begin{aligned}\frac{\partial^2 g_{ij}^{(k+1)}}{\partial q_n \partial q_m} = {} & \frac{\partial^2 g_{ij}^{(k)}}{\partial q_n \partial q_m} - \frac{\partial^2 g_{ik}^{(k)}}{\partial q_n \partial q_m}\frac{g_{kj}^{(k)}}{g_{kk}^{(k)}} + \frac{\partial g_{ik}^{(k)}}{\partial q_m}\frac{\partial g_{kk}^{(k)}}{\partial q_n}\frac{g_{kj}^{(k)}}{\left(g_{kk}^{(k)}\right)^2} - \frac{\partial g_{ik}^{(k)}}{\partial q_m}\frac{1}{g_{kk}^{(k)}}\frac{\partial g_{kj}^{(k)}}{\partial q_n} + \\ & + \frac{\partial g_{ik}^{(k)}}{\partial q_n}\frac{g_{kj}^{(k)}}{\left(g_{kk}^{(k)}\right)^2}\frac{\partial g_{kk}^{(k)}}{\partial q_m} - 2\frac{g_{ik}^{(k)}}{\left(g_{kk}^{(k)}\right)^3}\frac{\partial g_{kk}^{(k)}}{\partial q_n}\frac{\partial g_{kk}^{(k)}}{\partial q_m}g_{kj}^{(k)} + \frac{g_{ik}^{(k)}}{\left(g_{kk}^{(k)}\right)^2}\frac{\partial^2 g_{kk}^{(k)}}{\partial q_n \partial q_m}g_{kj}^{(k)} + \\ & + \frac{g_{ik}^{k}}{\left(g_{kk}^{(k)}\right)^2}\frac{\partial g_{kk}^{(k)}}{\partial q_m}\frac{\partial g_{kj}^{(k)}}{\partial q_n} - \frac{\partial g_{ik}^{(k)}}{\partial q_n}\frac{1}{g_{kk}^{(k)}}\frac{\partial g_{kj}^{(k)}}{\partial q_m} + \frac{g_{ik}^{(k)}}{\left(g_{kk}^{(k)}\right)^2}\frac{\partial g_{kk}^{(k)}}{\partial q_n}\frac{\partial g_{kj}^{(k)}}{\partial q_m} - \frac{g_{ik}^{(k)}}{g_{kk}^{(k)}}\frac{\partial^2 g_{kj}^{(k)}}{\partial q_n \partial q_m},\end{aligned} \tag{A-5}$$

where $i = 1, 2, \ldots, D+3$, $j = k+1, \ldots, D+3$, and $n, m = 1, 2, \ldots, D$. In some cases the form Eq. (3.13) is more favorable to use (see reduced dimensional models). The quantities $\frac{\partial \ln \tilde{G}}{\partial q_m}$ and $\frac{\partial^2 \ln \tilde{G}}{\partial q_n \partial q_m}$ are evaluated similarly to the procedure described in Eqs. (A-1)–(A-5).

Next, derivatives $\frac{\partial \mathbf{G}}{\partial q_m}$, and if Eq. (3.13) is used, also $\frac{\partial^2 \mathbf{G}}{\partial q_n \partial q_m}$ must be considered. Exploiting the relationship $\mathbf{G} = \mathbf{g}^{-1} \in \mathcal{R}^{(D+3)\times(D+3)}$, the missing derivatives can be expressed as

$$\frac{\partial \mathbf{G}}{\partial q_m} = -\mathbf{G}\frac{\partial \mathbf{g}}{\partial q_m}\mathbf{G} \tag{A-6}$$

$$\frac{\partial^2 \mathbf{G}}{\partial q_n \partial q_m} = \mathbf{G}\frac{\partial \mathbf{g}}{\partial q_n}\mathbf{G}\frac{\partial \mathbf{g}}{\partial q_m}\mathbf{G} + \mathbf{G}\frac{\partial \mathbf{g}}{\partial q_m}\mathbf{G}\frac{\partial \mathbf{g}}{\partial q_n}\mathbf{G} - \mathbf{G}\frac{\partial^2 \mathbf{g}}{\partial q_n \partial q_m}\mathbf{G}. \tag{A-7}$$

Then the matrices $\frac{\partial \mathbf{g}}{\partial q_m}$ and $\frac{\partial^2 \mathbf{g}}{\partial q_n \partial q_m}$ also involved in the above formulae are left to be considered.

$$\frac{\partial g_{kl}}{\partial q_m} = \sum_{i=1}^{N} m_i \sum_a \left( \frac{\partial t_{iak}}{\partial q_m} t_{ial} + t_{iak} \frac{\partial t_{ial}}{\partial q_m} \right) \tag{A-8}$$

$$\frac{\partial^2 g_{kl}}{\partial q_n \partial q_m} = \sum_{i=1}^{N} m_i \sum_a \left( \frac{\partial^2 t_{iak}}{\partial q_n \partial q_m} t_{ial} + \frac{\partial t_{iak}}{\partial q_n} \frac{\partial t_{ial}}{\partial q_m} + \frac{\partial t_{iak}}{\partial q_m} \frac{\partial t_{ial}}{\partial q_n} + t_{iak} \frac{\partial^2 t_{ial}}{\partial q_n \partial q_m} \right), \tag{A-9}$$

where $n, m = 1, 2, \ldots, D$ and $k, l = 1, 2, \ldots, D+3$.

Now, all the terms in the kinetic energy operator are expressed in terms of $\mathbf{t}_{im}$, $\frac{\partial \mathbf{t}_{im}}{\partial q_l}$, $\frac{\partial^2 \mathbf{t}_{im}}{\partial q_k \partial q_l}$, $i = 1, 2, \ldots, N$, $m = 1, 2, \ldots, D+3$, $k, l = 1, 2, \ldots, D$ ($\mathbf{t}$-vector formalism). For the vibrational part, *i.e.*, $k, l, m = 1, 2, \ldots, D$, the $\mathbf{t}$-vectors and their derivatives are

$$\mathbf{t}_{im} = \frac{\partial \mathbf{x_i}}{\partial q_m} \tag{A-10}$$

$$\frac{\partial \mathbf{t}_{im}}{\partial q_l} = \frac{\partial^2 \mathbf{x_i}}{\partial q_l \partial q_m} \tag{A-11}$$

$$\frac{\partial^2 \mathbf{t}_{im}}{\partial q_k \partial q_l} = \frac{\partial^3 \mathbf{x_i}}{\partial q_k \partial q_l \partial q_m} \tag{A-12}$$

whereas for the rotational part, $m = D+1, D+2, D+3$, $k, l = 1, 2, \ldots, D$ they are

$$\mathbf{t}_{im} = \mathbf{e}_m \times \mathbf{x_i} \tag{A-13}$$

$$\frac{\partial \mathbf{t}_{im}}{\partial q_l} = \mathbf{e}_m \times \frac{\partial \mathbf{x_i}}{\partial q_l} \tag{A-14}$$

$$\frac{\partial^2 \mathbf{t}_{im}}{\partial q_k \partial q_l} = \mathbf{e}_m \times \frac{\partial^2 \mathbf{x_i}}{\partial q_k \partial q_l}, \tag{A-15}$$

where $\mathbf{x}_i = (x_{ix}, x_{iy}, x_{iz})$ are the Cartesian coordinates in the body-fixed frame. First, second and third derivatives, $\frac{\partial x_{ia}}{\partial q_m}$, $\frac{\partial^2 x_{ia}}{\partial q_l \partial q_m}$ and $\frac{\partial^3 x_{ia}}{\partial q_k \partial q_l \partial q_m}$ are determined numerically or analytically.

Let us first consider the numerical procedure. The procedure evaluating numerical derivatives uses an expression (a subroutine) which provides the Cartesian

coordinates in the body-fixed frame, $x_{ia}$, in terms of the internal coordinates, $q_m$ ($m = 1, 2, \ldots, D$). Primarily, the central difference formula is used to compute the numerical derivatives.

In the case of numerical differentiation the accuracy is a central question. For instance, if the terms in Eq. (3.12) were directly computed by means of inserting their arguments in the finite difference formulae, numerical instabilities or limited accuracy of the results might arise. In GENIUSH, the flexible type declaration of Fortran 90 is employed; thus, the accuracy of the numerical representation of the variables involved in the computation of $\frac{\partial x_{ia}}{\partial q_m}$, $\frac{\partial^2 x_{ia}}{\partial q_l \partial q_m}$, and $\frac{\partial^3 x_{ia}}{\partial q_k \partial q_l \partial q_m}$ can be easily increased to the required level. In this work $< 0.01$ cm$^{-1}$ was the prescribed accuracy of the computed eigenvalues. The step of differentiation and the number representation were chosen accordingly, typically $10^{-5}$ and $\sim 33$ digits (similar to quadruple precision) turned out to be safe and appropriate choices.

Although the numerical derivative routines provide a perfectly black-box treatment of the actual choice of internal coordinates and the body-fixed frame, they are generally slower than their analytic counterparts. Due to efficiency reasons, first, second, and third analytic derivatives of Cartesian coordinates in the body-fixed frame in terms of internal coordinates are also implemented in GENIUSH for the case of an arbitrary Z-matrix and the $xxy$ frame. The analytic derivative part of the program relies on the chain rule, and it is based on the collection of derivative subroutines of several elementary functions (product, ratio, sine, cosine, etc.), providing a modular and easily expandable structure.

# References

[1]Born, M.; Oppenheimer, J. R. *Ann. Phys. (Leipzig)* **1927**, *84*, 457.

[2]Born, M.; Huang, K. *Dynamical Theory of Crystal Lattices;* Oxford Univ. Press: New York, 1954.

[3]Sutcliffe, B. T.; Tennyson, J. *Int. J. Quant. Chem.* **1991**, *39*, 183.

[4]Handy, N. C. *Mol. Phys.* **1987**, *61*, 207.

[5]Császár, A. G.; Handy, N. C. *J. Chem. Phys.* **1995**, *102*, 3962.

[6]Czakó, G.; Furtenbacher, T.; Császár, A. G.; Szalay, V. *Mol. Phys.* **2004**, *102*, 2411.

[7]Furtenbacher, T.; Czakó, G.; Sutcliffe, B. T.; Császár, A. G.; Szalay, V. *J. Mol. Struct.* **2006**, *780–781*, 283.

[8]Tennyson, J.; Kostin, M. A.; Barletta, P.; Harris, G. J.; Ramanlal, J.; Polyansky, O. L.; Zobov, N. F. *Comp. Phys. Comm.* **2004**, *163*, 85.

[9]Polyansky, O. L.; Császár, A. G.; Shirin, S. V.; Zobov, N. F.; Barletta, P.; Tennyson, J.; Schwenke, D. W.; Knowles, P. J. *Science* **2003**, *299*, 539.

[10]Bramley, M. J.; Carrington Jr., T. *J. Chem. Phys.* **1993**, *99*, 8519.

[11]Kozin, I. N.; Law, M. M.; Tennyson, J.; Hutson, J. M. *Comp. Phys. Comm.* **2004**, *163*, 117.

[12]Mladenović, M. *J. Chem. Phys.* **2000**, *112*, 1070.

[13]Wang, X.-G.; Carrington Jr., T. *J. Chem. Phys.* **2004**, *121*, 2937.

[14]Watson, J. K. G. *Mol. Phys.* **1968**, *15*, 479.

[15]Watson, J. K. G. *Mol. Phys.* **1970**, *19*, 465.

[16]Searles, D.; von Nagy-Felsobuki, E. *Ab Initio Variational Calculations of Molecular Vibration-Rotation Spectra, Lecture Notes in Chemistry No. 61;* Springer-Verlag: Berlin, 1993.

[17]Christiansen, O. *Phys. Chem. Chem. Phys.* **2007**, *9*, 2942.

[18]Whitehead, R. J.; Handy, N. C. *Mol. Phys.* **1975**, *55*, 456.

[19]Dunn, K. M.; Boggs, J. E.; Pulay, P. *J. Chem. Phys.* **1986**, *85*, 5838.

[20]Dunn, K. M.; Boggs, J. E.; Pulay, P. *J. Chem. Phys.* **1987**, *86*, 5088.

[21]Jung, J. O.; Gerber, R. B. *J. Chem. Phys.* **1996**, *105*, 10332.

[22]Bowman, J. M.; Carter, S.; Huang, X. C. *Int. Rev. Phys. Chem.* **2003**, *22*, 533.

[23]Yonehara, T.; Yamamoto, T.; Kato, S. *Chem. Phys. Lett.* **2004**, *393*, 98.

[24]Rauhut, G. *J. Chem. Phys.* **2004**, *121*, 9313.

[25]Mátyus, E.; Czakó, G.; Sutcliffe, B. T.; Császár, A. G. *J. Chem. Phys.* **2007**, *127*, 084102.

[26]Meyer, R.; Gunthard, H. H. *J. Chem. Phys.* **1969**, *50*, 353.

[27]Watson, J. K. G. *J. Mol. Spectry.* **2004**, *228*, 645.

[28]Makarewicz, J. *The calculation of rotation-vibration energies for molecules with large amplitude vibrations, in Computational Molecular Spectroscopy, Part 3, Chapter 12, Eds. P. Jensen and P. R. Bunker.;* Wiley: Chichester, 2000.

[29]Luckhaus, D. *J. Chem. Phys.* **2000**, *113*, 1329.

[30]Luckhaus, D. *J. Chem. Phys.* **2003**, *118*, 8797.

[31]Lauvergnat, D.; Nauts, A. *J. Chem. Phys.* **2002**, *116*, 8560.

[32]Lauvergnat, D.; Baloitcha, E.; Dive, G.; Desouter-Lecomte, M. *Chem. Phys.* **2006**, *326*, 500.

[33]Yurchenko, S. N.; Thiel, W.; Jensen, P. *J. Mol. Spectry.* **2007**, *245*, 126.

[34]Mátyus, E.; Czakó, G.; Császár, A. G. *J. Chem. Phys.* **2009**, *130*, 134112.

[35]Barletta, P.; Shirin, S. V.; Zobov, N. F.; Polyansky, O. L.; Tennyson, J.; Valeev, E. F.; Császár, A. G. *J. Chem. Phys.* **2006**, *125*, 204307.

[36]Mátyus, E.; Šimunek, J.; Császár, A. G. *J. Chem. Phys.* **2009**, *submitted for publication.*

[37]Sørensen, G. O. *in Topics in Current Chemistry, Ed. M. J. S. Dewar et al., Vol. 82, 99;* Springer-Verlag: Heidelberg, 1979.

[38]Littlejohn, R. G.; Reinsch, M. *Rev. Mod. Phys.* **1997**, *69*, 213.

[39]Sutcliffe, B. T. *Coordinate Systems and Transformations in Handbook of Molecular Physics and Quantum Chemistry, Vol. 1, Part 6, Ch. 31, p. 485-500;* John Wiley & Sons, Ltd: Chichester, 2003.

[40]Sutcliffe, B. T. *Molecular Hamiltonians in Handbook of Molecular Physics and Quantum Chemistry, Vol. 1, Part 6, Ch. 32, p. 501-525;* John Wiley & Sons, Ltd: Chichester, 2003.

[41]Eckart, C. *Phys. Rev.* **1935**, *47*, 552.

[42]Wilson, E. B.; Decius, D. C.; Cross, P. C. *Molecular Vibration;* McGraw Hill: New York, 1955.

[43]Lopata, A.; Kiss, A. I. *Computers & Chemistry* **1979**, *3*, 107.

[44]Simons, G.; Paar, R. G.; Finlan, J. M. *J. Chem. Phys.* **1973**, *59*, 3229.

[45]INTDER2000 is a general program developed by Wesley D. Allen and co-workers which performs various vibrational analyses and higher-order nonlinear transformations among force field representations.

[46]Allen, W. D.; Császár, A. G. *J. Chem. Phys.* **1993**, *59*, 2983.

[47]Allen, W. D.; Császár, A. G.; Szalay, V.; Mills, I. M. *Mol. Phys.* **1996**, *89*, 1213.

[48]Smith, F. T. *Phys. Rev. Lett.* **1980**, *45*, 1157.

[49]Yurchenko, S. N.; Zheng, J.; Lin, H.; Jensen, P.; Thiel, W. *J. Chem. Phys.* **2005**, *123*, 134308.

[50]Harris, D. O.; Engerholm, G. G.; Gwinn, W. D. *J. Chem. Phys.* **1965**, *43*, 1515.

[51]Dickinson, A. S.; Certain, P. R. *J. Chem. Phys.* **1968**, *49*, 4209.

[52]Szalay, V. *J. Chem. Phys.* **1993**, *99*, 1978.

[53]Szalay, V.; Czakó, G.; Nagy, Á.; Furtenbacher, T.; Császár, A. G. *J. Chem. Phys.* **2003**, *119*, 10512.

[54]Echave, J.; Clary, D. C. *Chem. Phys. Lett.* **1992**, *190*, 225.

[55]Wei, H.; Carrington Jr., T. *J. Chem. Phys.* **1992**, *97*, 3029.

[56]Lanczos, C. *J. Res. Natl. Bur. Stand.* **1950**, *45*, 255.

[57]Cullum, J. K.; Willoughby, R. A. *Lanczos Algorithms for Large Symmetric Eigenvalue Computations;* Birkhauser: Boston, 1985.

[58]Saad, Y. *Iterative Methods for Sparse Linear Systems;* Society for Industrial and Applied Mathematics: Philadelphia, PA, 2003.

[59]Podolsky, B. *Phys. Rev.* **1928**, *32*, 812.

[60]Xie, J. K.; Tennyson, J. *Mol. Phys.* **2002**, *100*, 1623.

[61]Xie, J. K.; Tennyson, J. *Mol. Phys.* **2002**, *100*, 1615.

[62]Mladenović, M. *Spectrochim. Acta* **2002**, *58A*, 795.

[63]Wang, X.-G.; Carrington Jr., T. *J. Chem. Phys.* **2008**, *129*, 234102.

[64]Yu, H.-G. *J. Chem. Phys.* **2004**, *121*, 6334.

[65]Császár, A. G.; Czakó, G.; Furtenbacher, T.; Mátyus, E. *Ann. Rep. Comp. Chem.* **2007**, *3*, 155.

[66]Schreiner, P. R.; Reisenauer, H. P.; Pickard, F. C.; Simmonett, A. C.; Allen, W. D.; Mátyus, E.; Császár, A. G. *Nature* **2008**, *453*, 906.

[67]Czakó, G.; Mátyus, E.; Simmonett, A. C.; Császár, A. G.; Schaefer III, H. F.; Allen, W. D. *J. Comp. Theor. Chem.* **2008**, *4*, 1220.

[68]Schreiner, P. R.; Reisenauer, H. P.; Mátyus, E.; Császár, A. G.; Simmonett, A. C.; Allen, W. D. *J. Phys. Chem. A* **2009**, *to be submitted.*

[69]Allen, W. D.; Bing, Y.; Kozin, I.; Mátyus, E.; Czakó, G.; Császár, A. G. *J. Phys. Chem. A* **2009**, *in preparation.*

[70]Fábri, C.; Furtenbacher, T.; Mihály, B.; Zoltáni, T.; Mátyus, E.; Nemes, L.; Császár, A. G. *J. Mol. Spectry.* **2009**, *in preparation.*

[71]`www.openmp.org`.

[72]Polo, S. R. *J. Chem. Phys.* **1956**, *24*, 1133.

[73]Léonard, C.; Handy, N. C.; Carter, S.; Bowman, J. M. *Spectrochim. Acta* **2002**, *58A*, 825.

[74]Rajamaki, T.; Miani, A.; .; Halonen, L. *J. Chem. Phys.* **2003**, *118*, 6358.

[75]Rajamaki, T.; Kállay, M.; Noga, J.; Valiron, P.; Halonen, L. *Mol. Phys.* **2004**, *102*, 2297.

[76]Yurchenko, S. N.; Zheng, J.; Lin, H.; Jensen, P.; Thiel, W. *J. Chem. Phys.* **2005**, *123*, 134308.

[77]Császár, A. G.; Allen, W. D.; Schaefer, III, H. F. *J. Chem. Phys.* **1998**, *108*, 9751.

[78]Klopper, W.; Samson, C. C. M.; Tarczay, G.; Császár, A. G. *J. Comp. Chem.* **2001**, *22*, 1306.

[79]Schwenke, D. W.; Partridge, H. *Spectrochim. Acta* **2001**, *57A*, 887.

[80]Henderson, J. R.; Tennyson, J. *Chem. Phys. Lett.* **1990**, *173*, 133.

[81]Yu, H.-G.; Nyman, G. *Chem. Phys. Lett.* **1998**, *298*, 27.

[82]Ericsson, T.; Ruhe, A. *Mat. Comput.* **1980**, *35*, 1251.

[83]Kono, H. *Chem. Phys. Lett.* **1993**, *214*, 137.

[84]Wyatt, R. E. *Phys. Rev. E* **1995**, *51*, 3643.

[85]Wang, L.-W.; Zunger, A. *J. Chem. Phys.* **1994**, *100*, 2394.

[86]Farkas, I. J.; Derényi, I.; Barabási, A.-L.; Vicsek, T. *Phys. Rev. E* **2001**, *64*, 026704.

[87]Yu, H.-G.; Nyman, G. *J. Chem. Phys.* **1999**, *110*, 7233.

[88]Yu, H.-G. *J. Chem. Phys.* **2001**, *114*, 2967.

[89]Tal-Ezer, H.; Kosloff, R. *J. Chem. Phys.* **1984**, *81*, 3967.

[90]Huang, S.-W.; Carrington Jr., T. *J. Chem. Phys.* **2000**, *112*, 8765.

[91]Poirier, B.; Carrington Jr., T. *J. Chem. Phys.* **2001**, *114*, 9254.

[92]Tomov, S.; Langou, J.; Dongarra, J.; Canning, A.; Wang, L.-W. *Int. J. Computational Science and Engineering* **2006**, *2*, 205.

[93]Simon, H. D. *Math. Comp.* **1984**, *42*, 115.

[94]Wang, X.-G.; Carrington Jr., T. *J. Chem. Phys.* **2002**, *117*, 6923.

[95]Czakó, G.; Mátyus, E.; Császár, A. G. *J. Phys. Chem. A* **2009**, *submitted for publication.*

[96]Wu, K.; Simon, H. D. Lawrence Berkeley National Laboratory Report No. 41412, 1998.

[97]Goloub, G. H.; Loan, C. F. V. *Matrix Computations;* Johns Hopkins University Press, 1996.

[98]Grcar, J. *Analyses of the Lanczos Algorithm and of the Approximation Problem in Richardson's Method, PhD. Thesis;* University of Illinois, 1981.

[99]Wu, K.; Canning, A.; Wang, L.-W. *J. Comput. Phys.* **1999**, *154*, 156.

[100]Wu, K.; Simon, H. D. *SIAM J. Matrix Anal. Appl.* **2000**, *22*, 602.

[101]Wang, X.-G.; Carrington Jr., T. *J. Chem. Phys.* **2001**, *114*, 1473.

[102]Wang, X.-G.; Carrington Jr., T. *J. Chem. Phys.* **2003**, *119*, 101.

[103]Bowman, J. M.; Carrington Jr., T.; Meyer, H.-D. *J. Chem. Phys.* **2008**, *106*, 2145.

[104]Wang, X.-G.; Sibert III, E. L. *J. Chem. Phys.* **1999**, *111*, 4510.

[105]Duncan, J. L.; Law, M. M. *Spectrochim. Acta* **1997**, *53A*, 1445.

[106]Halonen, L. *J. Chem. Phys.* **1997**, *106*, 831.

[107]Venuti, E.; Halonen, L.; Della Valle, R. G. *J. Chem. Phys.* **1999**, *110*, 7339.

[108]Carter, S.; Shinder, H. M.; Bowman, J. M. *J. Chem. Phys.* **1999**, *110*, 8417.

[109]Carter, S.; Bowman, J. M. *J. Phys. Chem. A* **2000**, *104*, 2355.

[110]Lee, T. J.; Martin, J. M. L.; Taylor, P. R. *J. Chem. Phys.* **1995**, *102*, 102.

[111]Chakraborty, A.; Truhlar, D. G.; Bowman, J. M.; Carter, S. *J. Chem. Phys.* **2004**, *121*, 2017.

[112]Marquardt, R.; Quack, M. *J. Chem. Phys.* **1998**, *109*, 10628.

[113]Marquardt, R.; Quack, M. *J. Phys. Chem. A* **2004**, *108*, 3166.

[114]Schwenke, D. W.; Partridge, H. *Spectrochim. Acta* **2002**, *58A*, 849.

[115]Oyanagi, C.; Yagi, K.; Taketsugu, T.; Hirao, K. *J. Chem. Phys.* **2006**, *124*, 064311.

[116]Hilico, J.-C.; Robert, O.; Loete, M.; Toumi, S.; Pine, A. S.; Brown, L. R. *J. Mol. Spectry.* **2001**, *208*, 1.

[117]Georges, R.; Herman, M.; Hilico, J.-C.; Robert, O. *J. Mol. Spectry.* **1998**, *187*, 13.

[118]Venuti, E.; Halonen, L.; Valle, R. G. D. *J. Chem. Phys.* **1999**, *110*, 7339.

[119]Ulenikov, O. N.; Bekhtereva, E. S.; Grebneva, S. V.; Hollenstein, H.; Quack, M. *Phys. Chem. Chem. Phys.* **2005**, *7*, 1142.

[120]Bunker, P. R.; Jensen, P. *Molecular Symmetry and Spectroscopy;* NRC Research Press: Ottawa, 1998.

[121]Mátyus, E.; Fábri, C.; Czakó, G.; Allen, W. D.; Császár, A. G. *J. Mol. Spectry.* **2009**, *to be submitted.*

[122]Tajti, A.; Szalay, P. G.; Császár, A. G.; Kállay, M.; Gauss, J.; Valeev, E. F.; Flowers, B. A.; Vázquez, J.; Stanton, J. F. *J. Chem. Phys.* **2004**, *121*, 11599.

[123]Papoušek, D.; Aliev, M. R. *Molecular vibrational rotational spectra;* Academia: Prague, 1982.

[124]Suhm, M. A.; Watts, R. O. *Phys. Rep.* **1991**, *204*, 293.

[125]McCoy, A. B. *Chem. Phys. Lett.* **2000**, *321*, 71.

[126]Allen, W. D.; Schuurman, M. S.; Schaefer III, H. F. unpublished results.

[127]ANHARM is a FORTRAN program for VPT2 analysis written by Y. Yamaguchi and H. F. Schaefer, Center for Computational Chemistry, University of Georgia, Athens, GA.

[128]See the program descriptions in K. Sarka and J. Demaison, in *Computational Molecular Spectroscopy*, edited by P. Jensen and P. R. Bunker (Wiley, Chichester, 2000), p. 255.

[129]Mills, I. M.; Császár, A. G. *Spectrochim. Acta* **1997**, *53*, 1101.

[130]Martin, J. M. L.; Francois, J.-P.; Gijbels, R. *J. Mol. Spectry.* **1995**, *169*, 445.

[131]Császár, A. G.; Leininger, M. L.; Szalay, V. *J. Chem. Phys.* **2003**, *118*, 10631.

[132]Martin, J. M. L.; Taylor, P. R.; Lee, T. J. *Chem. Phys. Lett.* **1993**, *205*, 535.

[133]Martin, J. M. L.; Lee, T. J.; Taylor, P. R. *J. Mol. Spectry.* **1993**, *160*, 105.

[134]Schuurman, M. S.; Allen, W. D.; Schaefer III, H. F. *J. Comp. Chem.* **2005**, *26*, 1106.

[135]Martin, J. M. L.; Lee, T. J.; Taylor, P. R. *J. Chem. Phys.* **1998**, *108*, 676.

[136]Seideman, T.; Miller, W. H. *J. Chem. Phys.* **1992**, *96*, 4412.

[137]Seideman, T.; Miller, W. H. *J. Chem. Phys.* **1992**, *97*, 2499.

[138]Manolopoulos, D. E. *J. Chem. Phys.* **2002**, *117*, 9552.

[139]Gonzalez-Lezana, T.; Rackham, E. J.; Manolopoulos, D. E. *J. Chem. Phys.* **2004**, *120*, 2247.

[140]Silva, B. C.; Barletta, P.; Munro, J. J.; Tennyson, J. *J. Chem. Phys.* **2008**, *128*, 244312.

[141]Manthe, U.; Seideman, T.; Miller, W. H. *J. Chem. Phys.* **1993**, *99*, 10078.

[142]Sorensen, D. S.; Lehoucq, R.; Vu, P.; Yang, C.

[143]Frayssé, V.; Giraud, L.; Grattan, S.; Langou, J.

[144]Császár, A. G.; Handy, N. C. *Mol. Phys.* **1995**, *86*, 959.

[145]Wang, X.-G.; Carrington Jr., T. *J. Chem. Phys.* **2008**, *129*, 234102.

# Abstract

During my doctoral research I have developed variational algorithms and computer codes for the computation of highly accurate vibrational energy levels and wave function for $N$-atomic molecules with arbitrary bonding arrangements.

I have developed a computer program called DEWE which is based on the Discrete variable representation of the Eckart-Watson Hamiltonian(s) with the numerically Exact inclusion of the actual representation of the potential energy surface and by using sophisticated iterative eigensolver techniques. The DEWE program is very efficient for semi-rigid species, but fails in the description of flexible systems with large-amplitude motions.

In order to be able to describe either semi-rigid or flexible molecules, I have developed a computer code called GENIUSH, which is a General (ro)vibrational code with Numerical, Internal-coordinate, User-Specified Hamiltonians applicable either for full- or reduced vibrational dimensionality models. In GENIUSH, similarly to DEWE, the inclusion of the potential energy is numerically exact and sophisticated iterative eigensolver techniques are used for the computation of vibrational energy levels and wave functions.

For the characterization of vibrational energy levels and wave functions I have introduced the normal mode decomposition technique (NMD), which allows the assignment of variational vibrational levels based on harmonic oscillator wave functions. I have pointed out that the assignment of fundamental vibrations might be ambiguous already for four-atomic molecules.

I have computed the zero-point vibrational energy (ZPVE) and band origins of $t$-HCOH (and $t$-HCOD), HNCO (and DNCO), six isotopologues of NCCO, $^{14}NH_3$, $^{12}CH_4$ (and $^{12}CH_2D_2$) using the DEWE or GENIUSH programs. Additionally, I have computed the variational ZPVEs of 23 three to four-atomic species, and compared the variational results with ZPVEs obtained within the second-order perturbational theoretical treatment.

Finally, I have shown that the GENIUSH program originally written for the computation of (ro)vibrational energy levels and wave functions can be straightforwardly modified to compute rate constants of bimolecular reactions.

# Összefoglalás

Doktori kutatásaim során $N$-atomos molekulák rezgési energiaszintjeinek és hullámfüggvényeinek számítására alkalmas variációs programok fejlesztésével foglalkoztam. Kifejlesztettem egy félmerev molekulák számítására alkalmas programot, amely a DEWE nevet kapta. A DEWE program az Eckart–Watson Hamilton-operátor Diszkrét változójú reprezentációján alapul. Az algoritmus lehetővé teszi tetszőleges potenciális energia felület numerikusan Egzakt figyelembe vételét. Az energiaszintek és hullámfüggvények számítása egy hatékony iteratív sajátértékmegoldóval történik. A DEWE program nagyon hatékony félmerev molekulák számítására, nem vizsgálhatóak azonban nagyamplitúdójú mozgásokkal rendelkező flexibilis rendszerek.

Kifejlesztettem egy a molekula flexibilitásától függetlenül jól alkalmazható programot, amely a GENIUSH nevet kapta. A GENIUSH egy általánosan alkalmazható program, amely automatikusan számítja a felhasználó által definiált belső koordinátákhoz tartozó Hamilton-operátort teljes vagy redukált rezgési dimenzióban. A GENIUSH programban is a potenciális energia numerikusan egzaktul figyelembe vehető, és az energiaszinteket és hullámfüggvényeket egy hatékony iteratív sajátértékmegoldóval számítjuk.

A rezgési energiaszintek és hullámfüggvények jellemzésére bevezettem egy asszignációs eljárást, amely az NMD (normal mode decomposition) nevet kapta. Az NMD eljárás segítségével rámutattam arra, hogy az “alaprezgések” fogalma egyes négyatomos molekulák esetén nem egyértelmű, szigorú matematikai értelemben.

A DEWE és GENIUSH programokkal a rezgési zérusponti energiát és számos rezgési szintet számítottam a $t$-HCOH (és $t$-HCOD), a HNCO (és DNCO), az NCCO hat izotopológja, az $^{14}NH_3$ valamint a $^{12}CH_4$ (és $^{12}CH_2D_2$) esetére. Ezen kívül kiszámítottam 23 különböző 3–4 atomos speciesz variációs rezgési zérusponti energiáját, és ezt összehasonlítottam a másodrendű perturbációszámítás keretein belül számítható zérusponti energia értékekkel.

Végezetül rámutattam, hogy a GENIUSH program, amelyet eredetileg rezgési(-forgási) energiaszintek és hullámfüggvények számítására fejlesztettem ki, könnyen módosítható bimolekuláris reakciósebességi együtthatók számítására.